ABRASIVE WEAR RESISTANCE OF RUTHENIUM ALUMINIDE INTERMETALLIC AND FERRITIC STEELS CONTAINING A SIGMA INTERMETALLIC PHASE.

BY M.NGAKANE

A THESIS SUBMITTED TO THE UNIVERSITY OF CAPE TOWN IN FULFILMENT OF THE DEGREE OF MASTER OF SCIENCE IN APPLIED SCIENCE.

DEPARTMENT OF MATERIALS ENGINEERING
UNIVERSITY OF CAPE TOWN
JANUARY 1998

ABSTRACT

The abrasive wear resistance of ruthenium aluminide intermetallic and ferritic steel containing an iron-chrome sigma intermetallic phase have been investigated in this study. A medium carbon wear resistant steel (MCV) was used in the study to facilitate comparison between wear resistances in the materials of interest.

Specimens of ruthenium aluminide, MCV and ferritic stainless steels containing a sigma phase were produced. The MCV steel was quenched and tempered to match the bulk hardness of the as-received ruthenium aluminide. Five different grades of thermomechanically worked ferritic steels specimens were heat treated to produce different volume fractions of sigma phase. The mechanical properties of the specimens were investigated by compression testing and microhardness measurements. Abrasion testing was carried out on a pin on belt abrasion apparatus. The surface response of the specimens to abrasive wear was characterised by optical and scanning electron microscopy. Microhardness of the specimens were measured with a digital microhardness machine.

The wear resistance of ruthenium aluminide was found to be higher than all materials tested in this project. The wear resistance in some of the ferritic steels containing sigma phase was comparable to that of the wear resistant medium carbon steel. The surfaces of the specimens were shown to work-harden during the abrasion process. The corresponding work-hardening results showed that ruthenium aluminide had the highest work-hardening rate. It can be concluded that the work-hardening ability of the test materials correlates with their respective wear resistance properties.

ACKNOWLEDGEMENTS

My grateful acknowledgement to the following:

Dr C. Lang - For her encouragement and guidance in this project

Prof C Allen - For his assistance in the final stages of the project

Mr B Greeves and J Petersen - For their assistance in photography

Mintek (through Dr M Cortie) for financial support and providing experimental material for this project.

To all staff and students in the Materials Engineering Department who may in one way or the other have offered their help.

Dedicated to my Family for their support and patience.

TABLE OF CONTENTS

CHAPTER 1: INTRODUCTION

Intermetallic materials present a major challenge to conventional engineering materials because of their good specific properties, and have been extensively studied for structural and high temperature applications. An understanding of the wear behaviour of intermetallics constitutes an integral part of the knowledge necessary for their commercial application. It is in this context that a study of the abrasive wear response of ruthenium aluminide intermetallic and ferritic steels containing a sigma intermetallic phase has been undertaken in this project

Abrasive wear can be severe, acting alone or in combination with other wear types. In industries such mining and agriculture abrasive wear accounts for approximately 50 % of the damage observed in the working tools. In order to reduce the effects of abrasive wear, given the economic implications of replacing worn components, numerous studies have been undertaken and different materials have been tested in order to select materials which are wear resistant in abrasive environments. In this context, the present project investigates the abrasive wear behaviour of two potentially wear resistant materials: ruthenium aluminide and ferritic steels containing the sigma phase.

Ruthenium aluminide and sigma are intermetallic compounds formed by metal elements. In spite of the excellent properties that intermetallics can possess, such as low specific gravities, high melting points, high strengths, high stiffness and oxidation resistance at elevated temperatures, the use of these materials in high technology industries such as aerospace and aircraft industries has been limited because of their room temperature brittleness. However, the high hardness and strength of intermetallics may confer useful wear resistance.

The wear behaviour of ruthenium aluminide is of interest because there is local abundance of ruthenium, which occurs as a by-product of platinum benefaction in South Africa. There could also be economic spin-offs if ruthenium aluminide proves a suitable material for engineering applications.

South Africa is a major stainless steels producer because of the advantage of its mineral wealth. Ferritic steels are relatively cheaper than their competitors in the stainless steels group; the iron-chrome sigma intermetallic which occurs in ferritic steels is however a source of concern because of the brittleness associated with this phase. This has serious consequences in critical applications such as nuclear plants where ferritic stainless steels are often used. It is therefore of interest to investigate the role played by this phase in the abrasive wear behaviour of the ferritic steels, as this may open other avenues in which the sigma prone ferritic steels can be applied.

This work is an attempt to assess the abrasive wear of ruthenium aluminide compared to a commercial wear resistant material of similar hardness. Further, the influence of the hard sigma intermetallic phase on the abrasive wear behaviour of ferritic stainless steels is also assessed. A series of heat treatments was carried out in order to produce a variation in the volume fraction of sigma phase, with a view to determining the optimum volume fraction for abrasive wear resistance.

Chapter 2 presents a survey of the literature pertaining to wear, particularly abrasive wear; and intermetallic materials, with the emphasis on ruthenium aluminide and sigma phase. The materials and experimental procedures used in this study are described in Chapter 3. The results obtained are presented in Chapter 4, and discussed in Chapter 5. Finally, conclusions are drawn regarding the use of the materials studied in applications requiring wear resistance.

CHAPTER 2: LITERATURE SURVEY

Since the aim of the present work is to investigate the abrasive behaviour of materials containing an intermetallic phase, the literature survey consists of two sections: abrasive wear and intermetallic materials. The study of abrasive wear is part of a larger concept known as tribology, which is essentially the study of friction, lubrication and wear of materials. The tribosystem is a collective term for all elements which are relevant to the characterisation of a wear problem, including the environment and the materials involved.

Engineering materials may suffer from one or more modes of wear; these may include the following:

Adhesive wear: occurs when asperities between two surfaces adhere to one another leading to material transfer or loss from either surfaces [1, 2, 104].

Fretting Wear: occurs when there is a very low amplitude vibratory motion between two surfaces under load such as in bolted parts [3].

Corrosive Wear: occurs when there are chemical or electrochemical reactions between a surface and its environment [4, 104].

Erosive Wear: occurs when there is a high velocity contact between a solid surface and fluids such gas, wind and liquid. Examples of this type of wear include: cavitation, liquid impingement and impact erosion [4, 5, 6].

Fatigue Wear: occurs when subsurface microcracks are subjected to cyclic loading leading to the failure of the material by fracture [7].

Sliding Wear: occurs when two bodies are in contact and are also in relative motion; sliding wear may be of adhesive or abrasive nature [8].

Abrasive wear is a process by which one surface is worn by hard asperities of another surface with which it is in contact and relative motion [9, 104].

2.1 Abrasive Wear

Abrasive wear essentially involves the rubbing together of two surfaces under a load. One of the two surfaces under consideration must be relatively rough and harder compared to the other. Under such conditions the rough and harder surface will be responsible for most of the abrasive wear. It is important to note that, the involvement of rough and hard surface in not only a necessary condition, but that it is an important characteristic that distinguishes abrasive wear from other forms of sliding wear in the removal of material from a surface undergoing abrasion [10].

During the process of abrasive wear, the surface may respond by plastic deformation or microchips may be produced due to the cutting effect of the abrasive or fracturing may occur in the case of brittle materials.

Dowson argued that wear in general can be classified according to its effects on materials; alternatively the classification can be based on the physical nature of the underlying processes [10]. There are two broad categories of abrasive wear: two-body and three-body abrasive wear

Two-body Abrasion

Two-body abrasion occurs as a result of two surfaces in relative motion. The important condition in this type of wear is that the two surfaces must be significantly dissimilar in their hardness. The harder surface must also be relatively rough in order to produce ploughing and cutting of material from the less hard surface [2]. Depending on the wear conditions two-body abrasion can be further defined as mild or severe; this is discussed later in section 2.1.1. In some situations two-body abrasion can be clearly distinguished from three-body abrasion, but this is not always the case.

Three -body abrasion

Three-body abrasion occurs when a relatively harder body is trapped between the rubbing surfaces. Depending on the nature of the harder body, and the processes it may experience, its hardness can be greater than one of the surfaces or both. The general mechanism of material removal in this type of wear involves ploughing or gouging of the surface. Rock crushers, ball mills, sandblasting equipment and sand conveyors are some examples where three-body abrasive wear is experienced. The trapped particles may also be derived from the presence of air-borne dust. Corrosion products can also contribute to enhanced abrasion by trapped particles. It is also possible that wear debris produced during adhesive wear may be subsequently work-hardened by the rubbing motion and later result in abrasion of one of the surfaces. Another process may involve embedding of the abrasive particles in the softer of the surfaces, so that further motion between the two surfaces results in the harder surface being abraded [2].

2.1.1 Parameters That Influence Abrasive Wear

There are many factors that influence abrasive wear of materials [11,12]. These parameters are grouped together collectively as the tribosystem. Some of these parameters, and their interrelationships, are discussed below.

Properties of an Abrasive

Size

Abrasive papers are commonly used to simulate size effect in abrasive wear processes. It was found that the greater the grit size the higher the wear rate of the material [13]. Other workers [14, 15] came to a similar conclusion, but considered the grit size effect in terms of the material's wear resistance. It has been established that not all abrasive particles in contact with the surface being abraded contribute towards the volume wear observed on it. The number of abrasive particles responsible for the wear process was found to be less

in coarse grit size abrasive papers than in fine grit size abrasive papers [14]. It was therefore inferred that the real contact area is influenced by the abrasive particle size, where the contact area is greater for finer grit size paper [16].

Coarse particles under high load often fracture. This follows after the fracture stress of the abrasive particles has been exceeded. The fracturing of the abrasive particles contributes to producing fresh angular edges that can cut small chips from the surface. This can result in an increase of the wear rate in the abraded material. The fracture stress in coarse grit abrasive papers is exceeded much faster than in fine grit abrasive papers. This is to be expected because the load is borne by fewer particles in coarse grit abrasive papers, resulting in high local stresses experienced by the abrasive particles. This argument supports observations that the wear rate generally decreases with decreasing abrasive particle size [15, 16].

Shape and Orientation

High wear rates can result when microchips are cut from the surface by abrasive particles under load. The rate at which the surface will be worn is dependent on the number of favourably oriented abrasives that can cut chips from the surface. The conditions for cutting to occur were placed in perspective by Sedriks and Mulhearn [17, 18] when they defined a critical attack angle to be the angle formed between the leading face of an abrasive and the surface being abraded. They suggested that below this critical angle no cutting will occur. When this condition holds, the abrasives plough the surface; in this case wear debris is produce by the combined effect of the hard abrasive and a fatigue failure mechanism. Further work on commercial abrasive papers has supported the observation that debris material produced does not occur only by microchip cutting [16]. It was argued that this was because the shape of a large number of abrasive particles on abrasive papers is such that their resultant attack angles are less than the critical attack angle for cutting. Moore [19] argued that the importance of the shape of the particle is in the formation of the cross-sectional area during abrasion. He further argued that a high

wear rate in the material will be caused by the reduction of the cone angle of the pyramid or decrease in the radius of the spherical abrasives. He suggested that the wear rate in such instances can be determined by taking the ratio of the grooves' cross-sectional area and the projected area of contact. If the ratio is high, the wear rate will increase proportionately. The relation of geometrical aspects to abrasion rate has also been supported by other workers[20].

Surface Characteristics of the Abraded Material

Surfaces of materials are never completely smooth even after fine metallographic finish. Although instruments such as the Talysurf may be used to determine the smoothness of surfaces, Barwell [21] has argued that high resolution microscopes are necessary to reveal the true nature of the material surface. The characteristics of the surface features are important in determining the behaviour of the material in an abrasive environment.

Near Surface Microstructure.

The microstructure of the near surface region gives an indication of the properties on which the wear resistance of the material is dependent. The microstructure itself is dependent on factors such as chemical composition, production history of the component and its response to other elements in the tribosystem. An important factor is the crystal structure of the near surface region that experiences the immediate effect of the abrasive particles.

The interaction between the environmental elements and the surface of the material may give rise to the formation of oxide films on the topmost part of the surface. The presence of an oxide layer in many cases reduces the contact between asperities of materials. Since wear is dependent on the dynamics of asperity contact, oxide layers formed may contribute to reducing the rate of wear on the surface. These oxides are easily formed in metals since they are sensitive and reactive to the environment.

It is argued that these surface layers form an integral part of the microstructure. The exact nature of these layers is still a subject of research. Zum Gahr [22] has presented an example of the cross-sectional microstructure that can be expected from the surface to the middle of the material, as shown in Figure 2. 1.

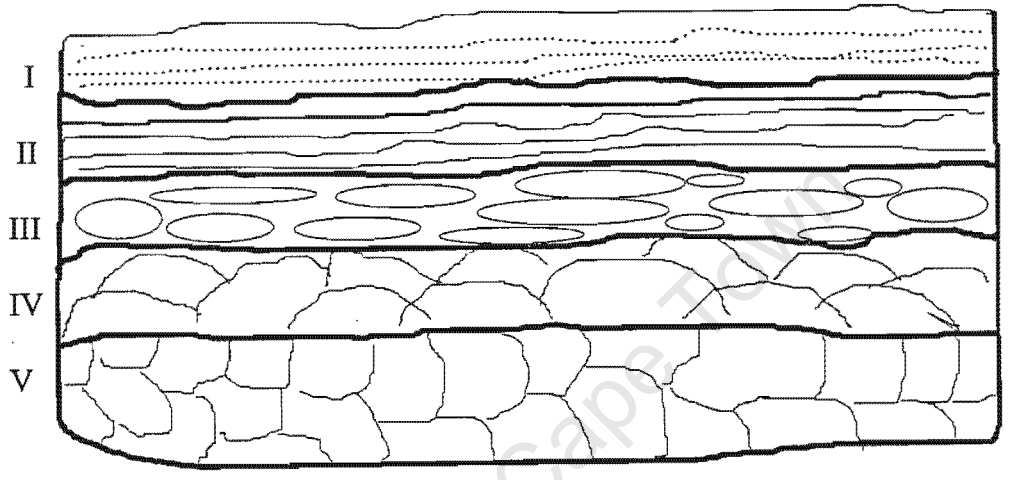

Figure 2. 1. Schematic cross-section of the surface microstructure (After Zum Gahr [22]).

Region I represents the topmost contamination layer. Region II is the adsorption layer, region III is the reaction layer. Region IV is the defect or worked layer and region V is the bulk microstructure. It is estimated that the width of regions I, II and III combined are of the magnitude $10^{-2}\mu m$. It has been argued that the first three regions are crucial to wear resistance in the material. They may act as lubricants in dry sliding wear conditions. Archard and Hirst [23] suggested that the wear rate will change with time during the early stages of rubbing as the structure of the surface layers changes. They also suggested that wear rate becomes constant as the layers reach their equilibrium. The layers in most cases are oxides and they can be present even after cleaning by machining or grinding.

It has also been argued that, if an oxide layer is removed from a metallic surface on which it has formed under ordinary atmospheric conditions, the surface will almost instantaneously be covered by a new monomolecular oxide layer [3].

The strength of the surface microstructure approximates a simple estimation of the wear resistance of the material. Surface strength measurement is often represented in physical terms by hardness values. In this regard the microstructures that yield high hardness values provide better wear resistance to the material.

Hardness

When an abrasive's hardness is greater than the intrinsic hardness of the abraded material, wear resistance of the abraded material is approximately proportional to its hardness [24]. The direct proportionality between wear resistance and hardness also holds in materials subjected to metallurgical processes prior to testing. However it is argued that hardness values alone are inadequate for comparing wear resistance between different materials [21]. In spite of this fact Kruschov [25] reported a linear relation between hardness and relative wear resistance for commercially pure metals in the annealed state as shown in Figure 2. 2. Metals such as lead (Pb), Tin (Sn), copper (Cu) and nickel (Ni) whose hardness varied with impurity content still fell on the same line as their respective 'pure' partners. Similar results were obtained for steels with varying carbon content. Work-hardening the material prior to the test was reported to have no effect on their relative wear resistance [25, 10].

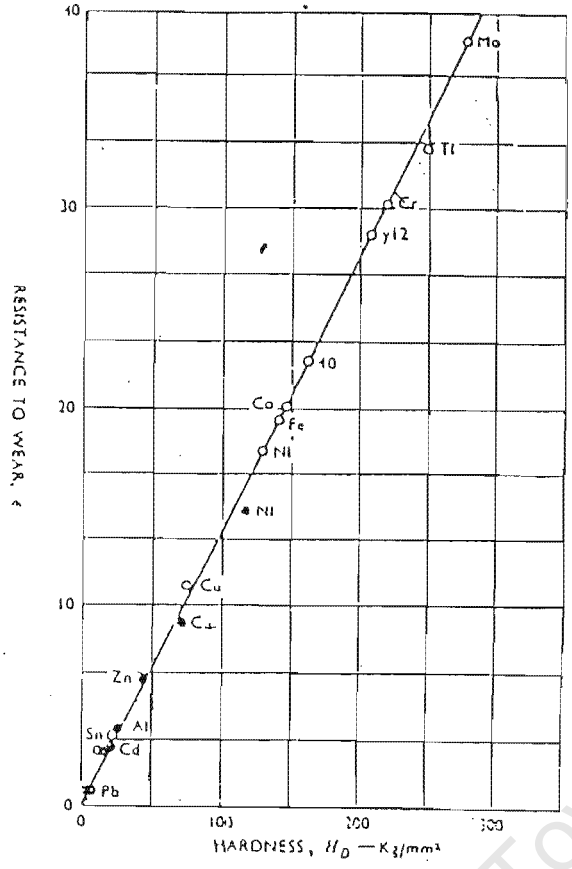

Figure 2. 2. Relative wear resistance and hardness for different annealed metals (After Kruschov [25]).

Oberle [26] contends that the high hardness sought to increase wear resistance in a material proportionally increases the elastic deformation that such a material can tolerate. To estimate the elastic limit of strain in different materials, a ratio of hardness to the elastic modulus was suggested for convenience. This ratio, which Orbele called the 'Modell' when multiplied by 10^6, indicates the depth of indentation penetration that a material can sustain without exceeding its elastic limit. High Modell materials have the ability to absorb energy elastically and prevent load from building up. Low Modell materials deform plastically much faster; bearing metals have been made out of the low Modell alloys for their advantage in being easy to reshape in service in the case that misalignment occurs. The Modell concept divides materials into two broad categories of low wear (high Modell) and high wear (low Modell) using their bulk hardnesses. It was argued that the high Modell values improves the wear resistance of high melting point materials.

In addition to the intrinsic hardness of the abraded material, the hardness achieved during the abrasion process plays an important role in wear resistance. The applicability of this principle is demonstrated in Figure 2. 3 [27]. Wear plotted against the original bulk hardness produced a wide scatter of results, whereas wear plotted against the work-hardened hardness falls within a comparatively narrow band. Steels with a high final hardness exhibit little wear even if their initial hardness had been low.

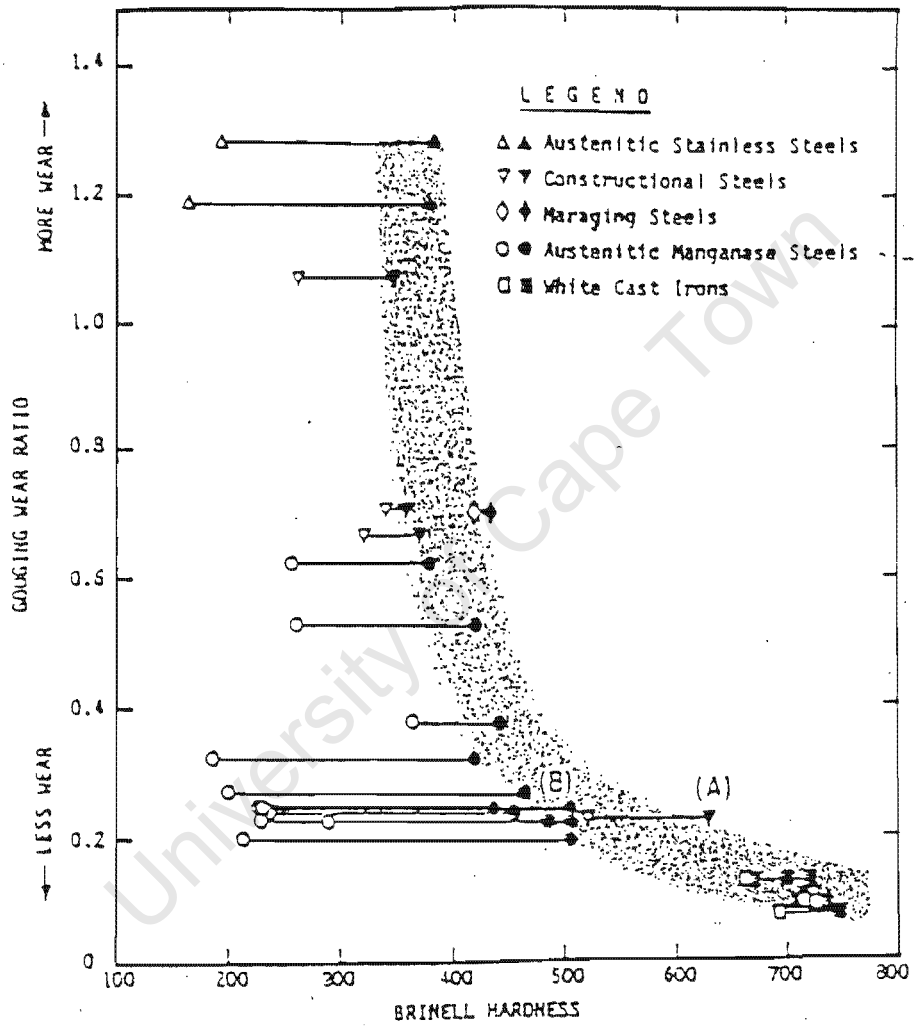

Figure 2. 3. Gouging wear ratio against the hardness of various materials. Open data points represent original bulk hardness and full points represent work hardened hardness (After Borik [27]).

Work-hardenability

Hardening of a material provides a better resistance to wear, but the process of work-hardening is also important during the abrasion process [14, 21, 25]. The significance of the work hardening in wear resistant materials was emphasised by Ball [28] in his work on the design of wear resistant materials. He suggested that the process of wear that results in the damage of the material at the surface occurs when the critical fracture strain is reached. During this process other sections of the same material are at different levels of strain as shown in Figure 2. 4.

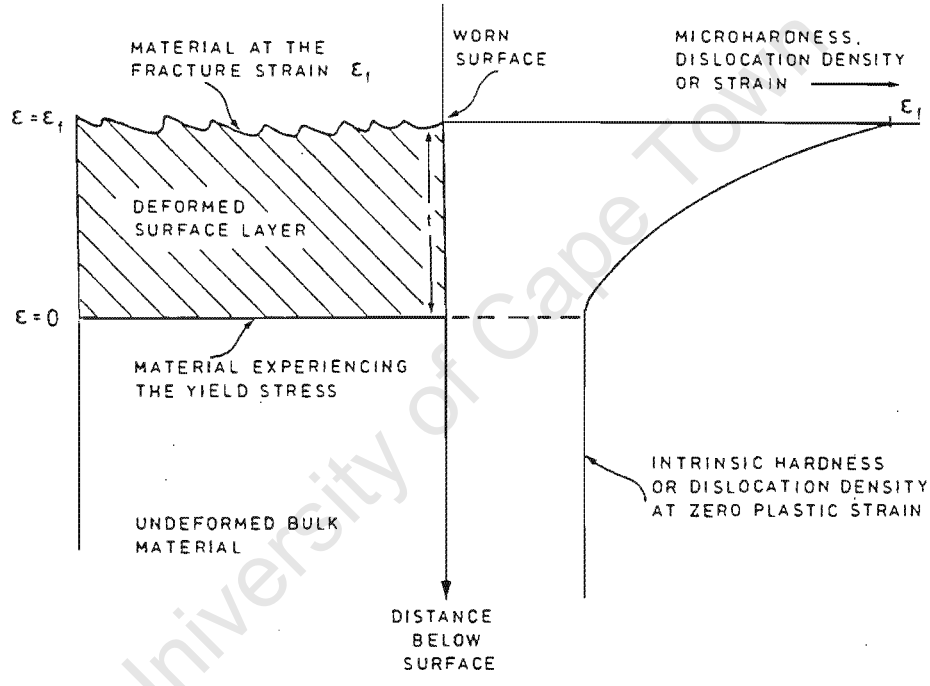

Figure 2. 4. Schematic illustration of the deformed surface layer of an abraded or eroded material (After Ball [28]).

For a wear resistant material a microstructure that never accumulates critical fracture strain under the imposed abrasive stress is ideal. Alternatively the microstructure should be such that the critical strain is slow to accumulate [28]. Materials with three different yield strengths were considered against a hypothetical stress distribution frequency of abrasive or erosive strikes as shown in Figure 2. 5.

Materials with yield stress coinciding with their ultimate strength are susceptible to sudden fracture and are therefore not suitable for high stress designs. Such a material is represented by curve number I in Figure 2. 5. It will be noted that in spite of the mean applied stress being much less than its yield stress, this factor is overridden by the fracture susceptibility. Very ductile materials represented by curve II absorb much higher strains before the critical strain is reached. The disadvantage of such materials is the low yield stress and the low stress that causes the material to fracture. Ideal materials will be those represented by curve III where the work-hardening is high. The first abrasive or erosive strike causes plastic deformation but for the following strike to result in any damage the stress will have to be higher [28].

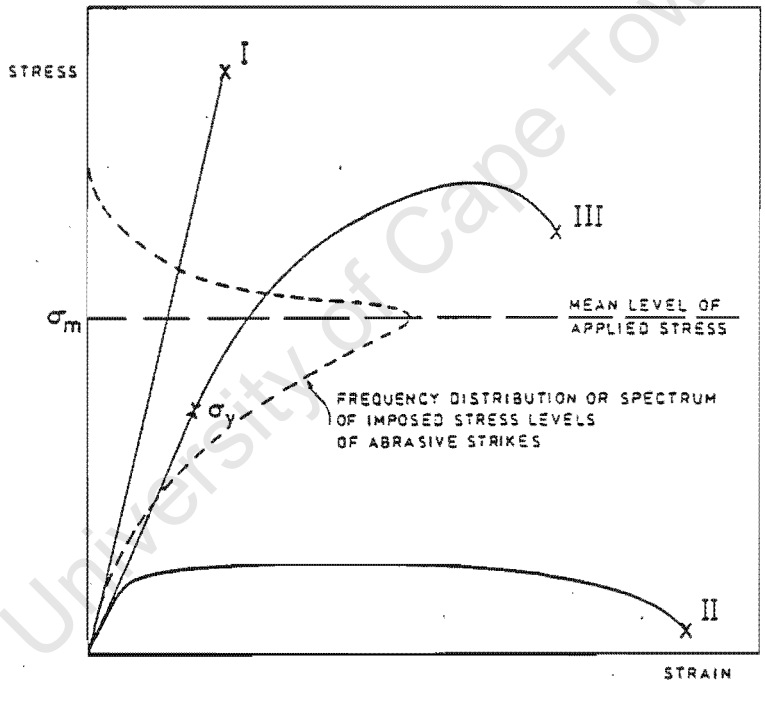

Figure 2. 5. Hypothetical stress-strain curves for the wear of three classes of materials superimposed upon the stress distribution frequency (After Ball [28]).

As the work-hardening increases in the abraded material the fracture toughness decreases. It was reported that there are exceptional cases where the wear rate increases with increasing hardness. Such an anomaly was suggested to be due to a decrease in fracture toughness which occurs as a result of the change in conditions of the tribosystem such as

thermal and mechanical hardening processes [29]. This observation was supported by Ball [28] who suggested that there is no simple and direct relation between wear resistance of the material and physical properties such as fracture toughness, yield strength, ultimate tensile strength and elongation. Work-hardening in the material can be affected by the crystal structure, presence of impurities, thermal effects and microstructural effects such as recovery and recrystallisation [30].

Relative Hardness of the Abrasive and the Abraded material.

The relative hardness of an abrasive and the maximum hardness of the surface that experiences abrasion allows a definition of two processes, namely, hard abrasive condition and soft abrasive condition. These two conditions are discussed below. The hardness of the abrasive in three-body abrasion determines whether it will be present as a loose particle or it will be embedded in the softer of the rubbing surfaces, this will in turn influence the abrasive condition [2].

A process is defined as hard abrasive when the hardness of an abrasive exceeds the maximum hardness of the wearing material. This maximum hardness in the wearing material may be attained during the wear process, but due to the random distribution of contacting particles the surface hardness is unlikely to be uniform. Therefore the maximum hardness becomes more important as a parameter than the overall strength attained by the whole effective surface [30]. A study by Richardson showed that the hard abrasive condition is related to the average maximum hardness of the wearing surface [14].

The process of soft abrasion occurs when the maximum hardness of the wearing material or its constituents is equal to or slightly exceeds the hardness of an abrasive. This occurs when the bulk hardness or maximum hardness is approximately 0.8 times or more than the hardness of an abrasive [14]. Materials that have comparable bulk hardness to the abrasive particles' hardness work harden slowly. The relative wear resistance on a soft abrasive is greater than on hard abrasive.

Eyre suggested [6] that wear resistance of materials on any abrasive will rapidly increase when the ratio of the material's hardness to the abrasive's hardness is greater than 0.5. When this critical value is attained transition in wear loss may occur as illustrated in Figure 2. 6.

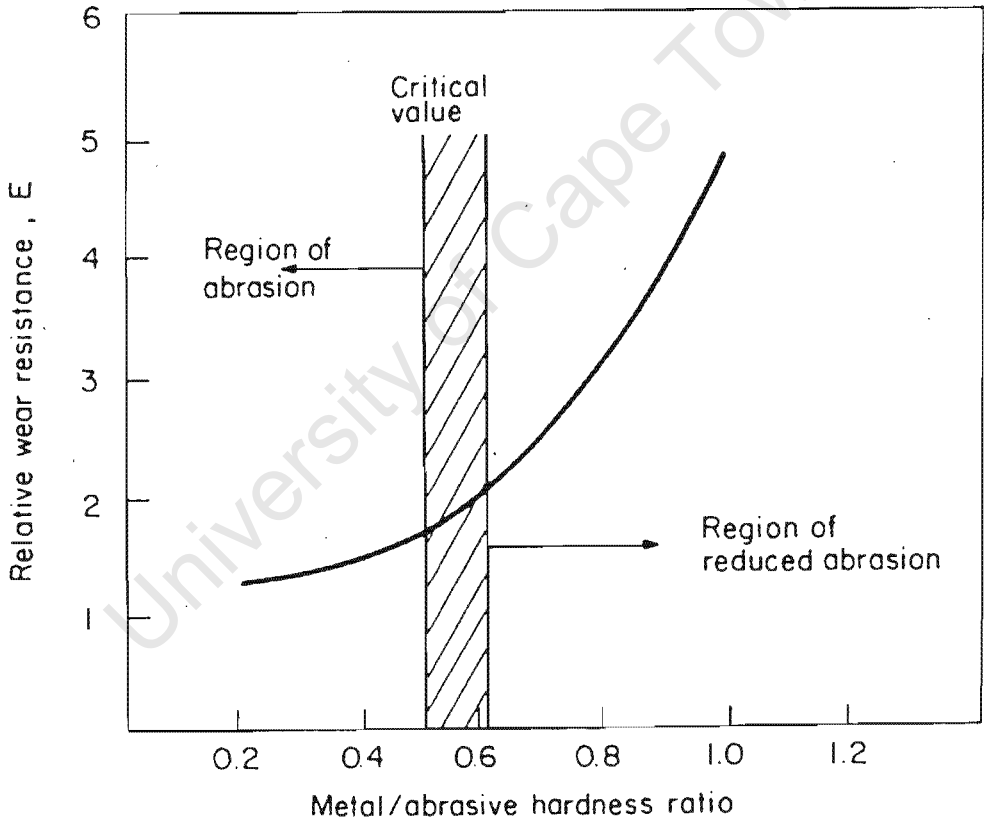

Figure 2. 6. Relative wear resistance against the (metal/abrasive) hardness ratio (After Eyre [6]).

Influence of Temperature on the Abraded Surface

Temperature effects on the surface of the material may result in microstructural changes depending on the nature of the material being abraded. This makes the temperature under which abrasion occurs an important parameter. For instance temperature change has an effect on the rate of oxidation and the types of oxide formed on the surface. The nature and properties of the oxides formed are important to the wear resistance of the exposed surface. Oxides such as formed in the presence of aluminium and chromium can be beneficial under suitable conditions, as they can offer protection due to their impervious properties.

The role played by temperature has been illustrated in an experiment involving the tribology of cobalt in vacuum. It was found that the wear rate in cobalt at 350°C was a hundred times greater than at 280°C, as shown in Figure 2. 7. The temperature contribution was attributed to both ambient and frictional heating. It was found that the temperature changes observed were independent of the speed of the abrasion test [3]. The increase in temperature expands the true area of contact by multiplying the number of asperities. This condition holds where temperature dominates over other effects or in their absence. If the true area of contact is larger and the hardness of the abrading surface is lower the wear rate will be higher than if the conditions were reversed [3].

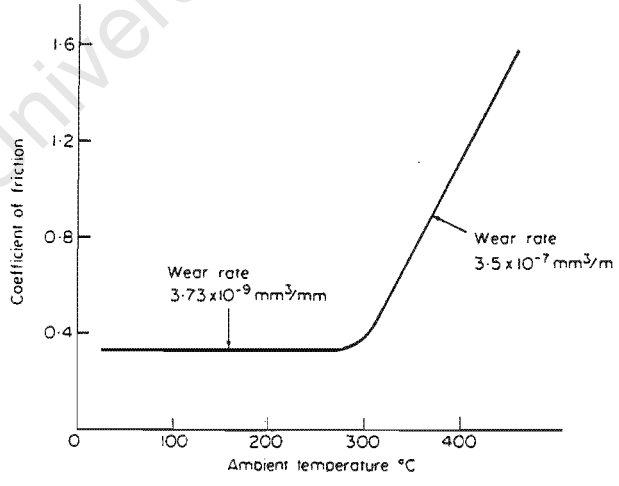

Figure 2. 7. The friction coefficient vs Ambient temperature. Wear rates are indicated by the values of the slopes (After Halling [3]).

In metal to metal wear, a transition from adhesive to abrasive wear may be observed due to asperity welding. The effect of temperature is pronounced in soft, low melting point bearing alloys in metal to metal wear. Bowden and Tabor [31] compared the influence melting point has on wear behaviour; their results showed that the low melting point materials exhibit higher wear loss than the high melting point materials. However it was reported that welding that occurs in low melting metals are easily broken during the abrasion motion resulting in these metals suffering less damage [26]. Conversely higher melting point materials such as ferritic steels suffer more damage from the welding process, due to the high pressures and extensive areas over which welds are formed [26].

The temperature attained on the surface during abrasive wear may be affected by the thermal conductivity of the material under a load. Richardson [30] suggested that high temperatures at the surface are proportional to the size of asperities and are localised. He further suggested that such a condition may exist even during slow abrasion. This implies that frictional heating is induced by the rubbing motion of the asperities. Bowden and Tabor [32] suggested that heating generates hot spots on the surface, which in turn increases the reactivity of the surface, and of the wear fragments, with the environment [32]. The rapid heating and cooling of the hot spots during the wear process can introduce phase changes that can influence the rate of wear in the material. The phase change process requires a sufficiently high temperature for interdiffusion; at such temperatures alloy formation at the interface may also occur. At very high speeds of several hundred meters per second the melting temperature of the metal can be reached; the onset of the melting is often accompanied by the low friction and wear [32].

Richardson [30] found that steels he had tested had a diverse response to the temperature and there was no significant thermal hardening or softening resulting from the rubbing action. He concluded that if the recrystallisation of a material is above the ambient test temperature, frictional heating at moderate sliding speeds will not affect the abrasive wear considerably.

Effect of Load on the Abrasive and the Abrading Surface.

The size effect of the abrasive particles on the rate of wear is dependent on the applied load. The wear rate increases proportionately with increasing load with a few exceptions [23]; this increase may in turn bring about other effects such as a rise in temperature due to frictional heating.

Mild wear is characterised by low loads, low speeds, fine wear debris. In metals there is little contact between asperities on the surface due to protective films on the surface [31]. These films can be reformed as the new surface of the metal is exposed by the rubbing process [24].

A transition may occur from mild to severe wear when the load is increased; this occurs when the ratio of the load to the apparent area of contact is approximately one third of the hardness of the softer material [3]. The transition is attributed to the interaction of the plastic zones below the contacting asperities as illustrated in Figure 2. 8. Surface A is assumed relatively harder than surface B such that at the contact points surface B yields plastically resulting in the creation of plastic deformed regions represented by the dark ellipsoidal regions. These regions are isolated in mild wear because of the lighter loads involved. Deformation of surface structure is comparatively less than in severe wear. The subsurface damage is confined to regions closer to the surface.

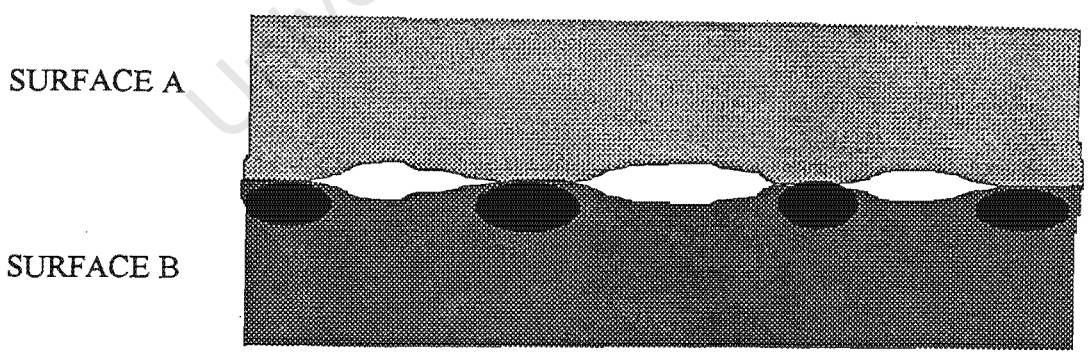

Figure 2. 8. The schematic cross-section of surfaces of two specimens touching at their asperities. The ellipsoid regions represent the plastically deformed areas below the of contact.

Severe wear is marked by large wear debris, roughened abraded surfaces, an increase in the amount of asperity contact and an enlargement of their area of contact [32]. During the 'running in period' in machines severe wear may be observed, but this may change to mild wear as the surface become smooth. The transition to mild wear can also be improved if the temperature generated by frictional losses promotes the formation of stable protective oxide film on the surface.

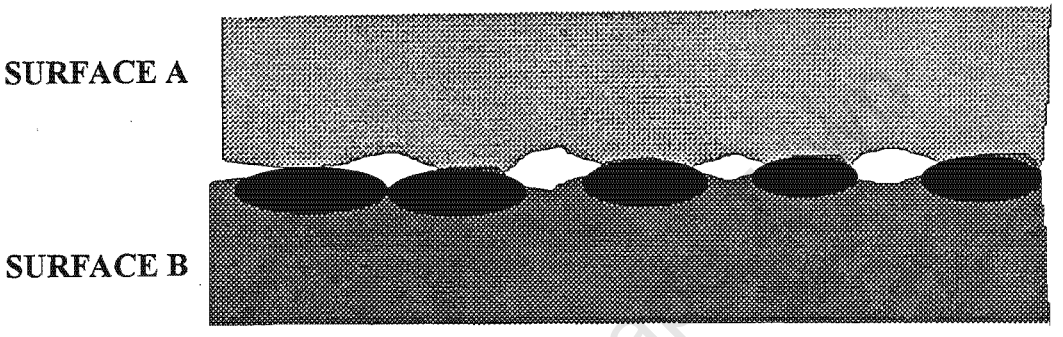

Figure 2. 9. The cross-section of specimens making contact at asperities. The increase in size of the contacting points results in the overlapping between some of the plastic regions. The ellipsoidal regions represent the plastic deformed areas below the points of contact.

Figure 2. 9 shows severe wear, in which the number and the size of some of the area of contact has increased as a result of the higher loads which press the two surfaces closer together. There is also some interaction between some of the adjacent deformation regions below the points of contact. The crystal structure of the surface layer becomes heavily distorted during the severe wear process.

Archard and Hirst [23] plotted the wear rate against load from their initial wear against time graphs. Their result for ferritic stainless steel rubbing on hardened tool steel were presented graphically as shown in Figure 2. 10 to illustrate the transition that occurs with the increase in load. From the graph it is clear that at higher loads the wear rate is increased, as indicated by a clear transition to a steeper slope. There are examples where this transition is not as simple as observed in Figure 2. 10. Conditions have been reported where the surface may exhibit a combination of mild and severe wear instead of their sequential occurrence. Such an example is the wear rate of the 70/30 brass against load shown in Figure 2. 11 [23]. The test was conducted against hardened tool steel as in the previous example. The region between A and B indicates the loads that produced a combination effect of mild and severe wear.

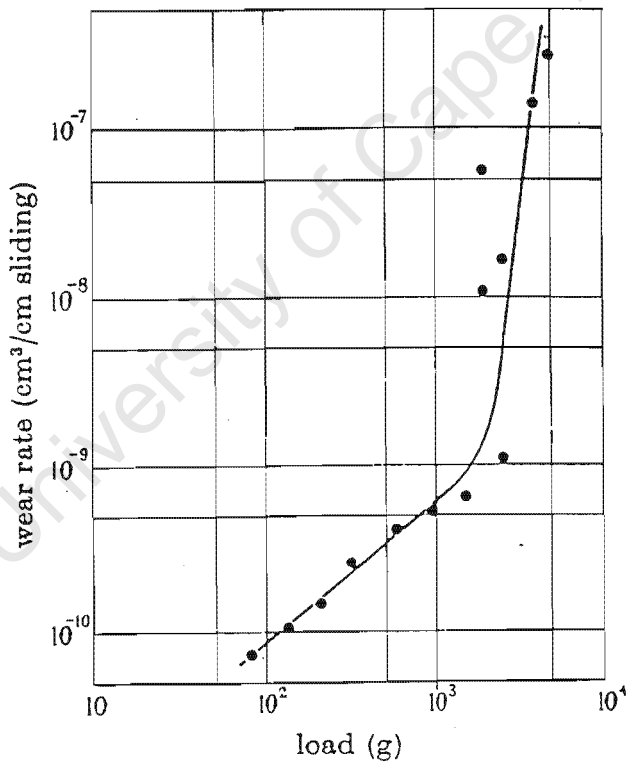

Figure 2. 10. Logarithmic graph of wear against load for ferritic stainless steel (After Archard and Hirst [23]).

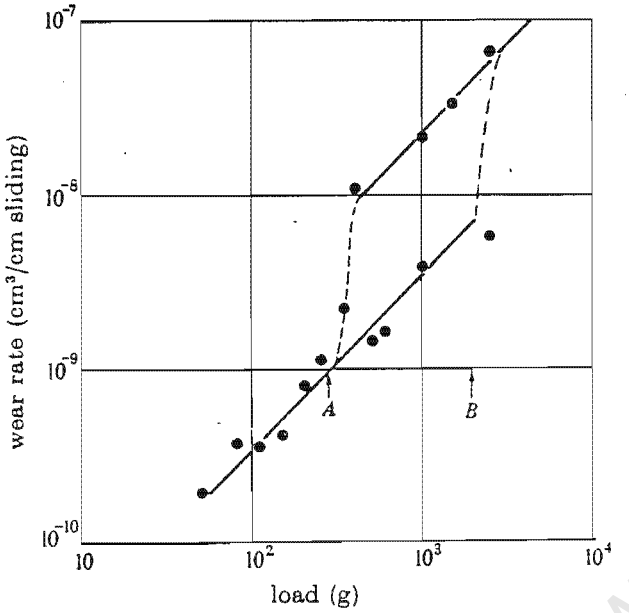

Figure 2. 11. Logarithmic graph of wear against load for 70/30 brass (After Archard and Hirst [23]).

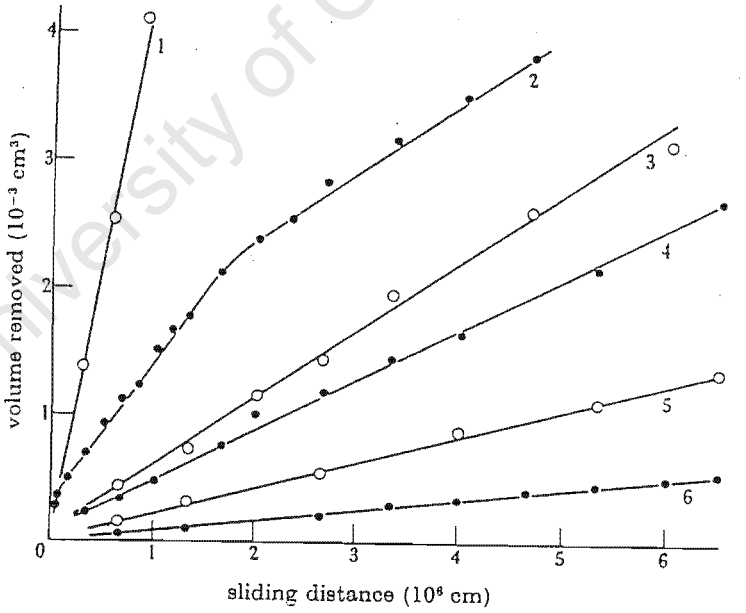

Figure 2. 12. Wear against sliding distance for ferritic stainless steel at different loads (After Archard and Hirst [23]).

In Figure 2. 12, curves 1 to 6 present the result for ferritic steel rubbed on hardened tool steel. The loads used were 2000g, 1500g, 930g, 580g, 330g, and 80g respectively. The volume wear loss during abrasive wear shows a proportional increase with the applied load over the same distance [23].

2.1.2 Mathematical Models Of Abrasive Wear

In abrasive wear, the interaction between different parameters leading to abrasion is often complicated; but some parameters may be neglected in order to simplify the model solution to abrasive wear in laboratory simulations. The close agreement between some models and the experimental data has contributed to identifying some of the main parameters common to many abrasive wear situations. Models of abrasive wear are based on the features produced by different mechanisms such as ploughing, cutting and cracking. These mechanisms occur on a microscale but have effects on a macro level. In general ploughing and cutting occur in predominantly ductile materials and microfracture in predominantly brittle materials.

Abrasive Wear In Brittle Materials

Fracture is the dominant mode of abrasive wear in brittle materials [33,34]. Abrasive wear involves indentation and scratching by abrasive particles under load; fracture may be initiated by this indentation process or may develop from pre-existing flaws. Lawn and Wilshaw [33] investigated the stress distribution in brittle materials due to indentation by indenters of various shapes. Figure 2. 13 shows how cracks are induced by a sharp indenter. The point of contact in this case is at a single point with the assumption that the contact is perfectly elastic. This ideal condition of contact is never observed because inelastic (plastic) deformation occurs to relieve the stress concentration. The sharp indenter then introduce a small area of plastic deformation immediately below this region (Figure 2. 13 (i)); a flaw will occur and later develop into a crack (Figure 2. 13 (ii) and (iii)).

The resulting crack will run preferentially along the contact axis provided there are no other defects that can act as crack initiation points. On unloading the material, the median vent closes up but does not completely heal (Figure 2. 13 (iv)). A further reduction of the load results in the development of lateral cracks indicated (by c-c) in Figure 2. 13 (v). When the load is completely removed the lateral cracks initiated continue growing until they intersect with surface as illustrated in Figure 2. 13 (vi). The process of reopening the median vent and the formation of the lateral cracks is repeated when the material is re-loaded [33].

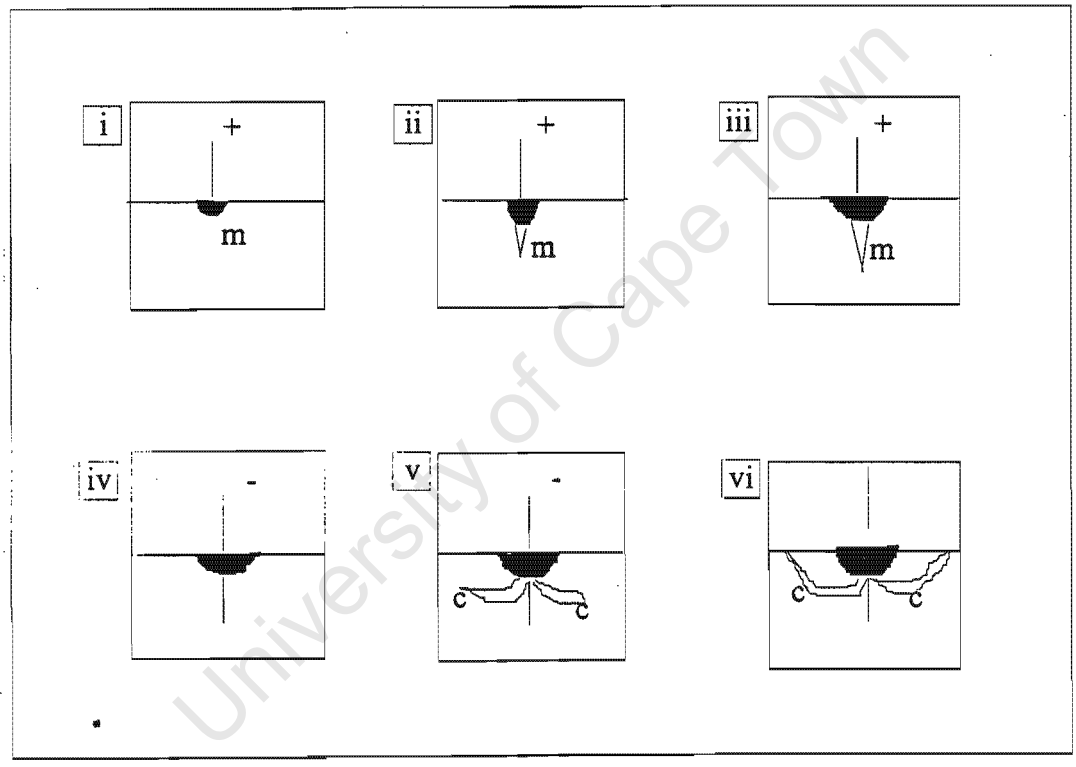

Figure 2. 13. Schematic illustration of a crack induced by the deformation associated with a point indentation from a sharp indenter (After Lawn and Wilshaw[33]).

The volume wear loss by brittle fracture can be estimated by using two equations involving the wear rate per unit abrasion distance. Hutchings derivation of equations 1 and 2 is based on the removal of material by lateral cracks when a sharp indenter slides over the surface and forms a plastic groove as in Figure 2. 14 [35].

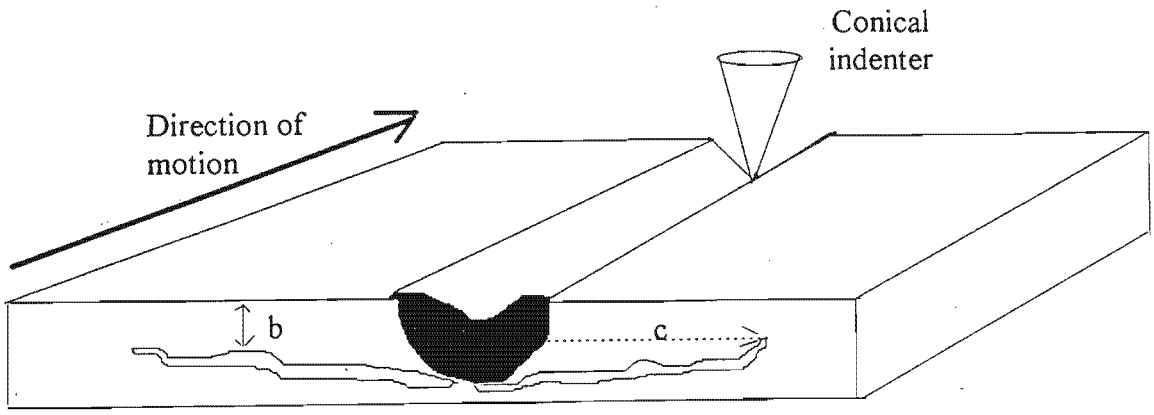

Figure 2. 14. A schematic representation of the point indenter and the lateral cracks it forms as it carves a groove over the surface of the material (After Hutchings [35]).

The dark shaded region represents the plastically deformed region from which lateral cracks initiate after the indenter has passed. The length and depth below the surface of the cracks is represented by "c" and "b". These cracks contribute to the total wear debris produced [35]. The total wear loss is represented in terms of the wear rate per unit sliding distance and is given by the following equations:

$$Q = \alpha_1 . N . \frac{(E/H) . w^{\frac{9}{8}}}{K_c^{\frac{1}{2}} . H^{\frac{1}{2}}} \qquad \textbf{Equation 1}$$

Where Q = the wear rate per unit sliding distance
α_1 = a material-independent constant
N = number of particles making contact with the surface
K_c = the fracture toughness of the material whose surface is abraded
E = the Young modulus of the material
H = hardness of the material
w = normal load on each particle

Equation 1 was derived from combining the crack length "c" which is a function of E, H, w, K_c and the crack depth "b" beneath the surface which is dependent on E, H w. Another equation with the same practical meaning but arrived at differently is equation 2:

$$Q = \alpha_2 . N \frac{w^{\frac{5}{4}}}{K_c^{\frac{3}{4}} . H^{\frac{5}{8}}}$$ **Equation 2**

The symbols for equation 1 have the same meaning as in equation 2. The two equations differ only in the ratio E/H which is the brittle index value; this ratio does not vary greatly between hard brittle solids [35].

The normal load on each particle in both equations is greater than 1. For N particles over an apparent area of contact A, the total normal load will be Nw. If it is assumed that the particles have the same linear dimension d then N is proportional to $Ad^{-1/2}$ resulting in the modification of equation 2 to:

$$Q = \alpha_3 \frac{W^{\frac{5}{4}} . d^{\frac{1}{2}}}{A^{\frac{1}{4}} . K_c^{\frac{3}{4}} . H^{\frac{1}{2}}}$$ **Equation 3**

Where W = a fixed load distributed over each particle as "w"

A = apparent contact area

The product of fracture toughness and the hardness of the worn material are the two important mechanical properties common to equation 1 to 3 quantifying the wear rate experienced by a brittle solid during the process of abrasive wear. It has been argued that exponents for the fracture toughness and the hardness in these mathematical models are determined by amongst other parameters the mode of material removal in brittle solids [36].

Abrasive Wear in Ductile Materials

Abrasive Wear by cutting and ploughing

Cutting and ploughing are the dominant modes of abrasive wear in ductile materials such as metals. The cracking mode may occur in ductile materials but is overshadowed by the other two modes to an extent where it can be considered negligible.

Sedriks and Mulhearn [17] showed that when a chip is cut from a material surface of non work-hardening material the cross-sectional area of the resultant groove formed is given by equation 4; providing the geometry and the orientation of the abrasive is known.

$$A = \frac{W}{c.p}\left(\frac{1+\mu.\tan b}{\mu-\tan b}\right) \qquad \textbf{Equation 4}$$

Where W = applied load
p = yield pressure of workpiece material
μ = coefficient of friction between the contacting surfaces
b = rake angle = a-90° (a = attack angle)
c = constant

When an abrasive does not cut a chip but only scratches the surface, the cross-sectional area of the groove is represented by equation 5.

$$A = \frac{\mu'.W}{c.s.\cot a + c.p} \qquad \textbf{Equation 5}$$

Where μ = coefficient of friction
s = shear strength of the material

A plot of the groove cross-sectional area against the attack angle for the conditions represented in equations 3 and 4 gives the minimum attack angle at which a chip will be cut. This value is determined by the intersection of the two graphs as shown in Figure 2. 15.

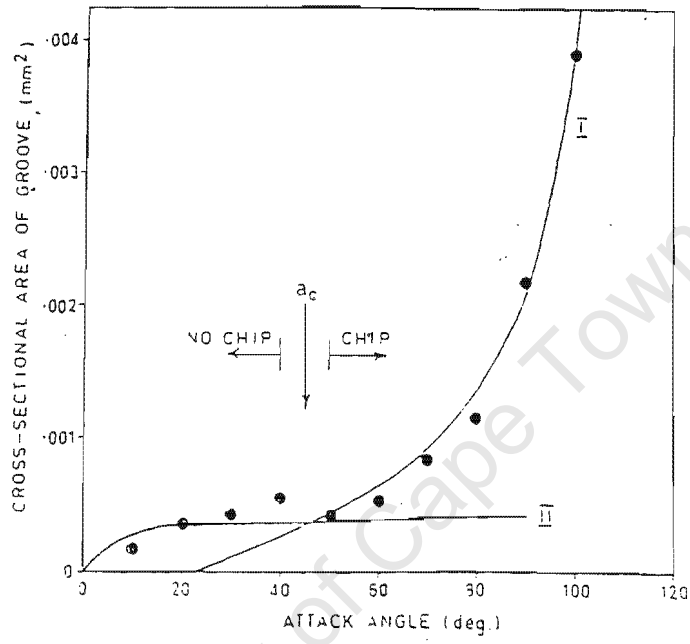

Figure 2. 15. The cross-sectional area vs attack angle for equation 3 and 4. Graph I represent equation 3 and graph II represent equation 4 (After Sedriks et al [17]).

The point a_c is the critical attack angle at which a chip will be cut from the surface. The approach represented in Figure 2. 15 essentially divides the abrasive particles into two groups; one which has the correct minimum attack angle for cutting chips and the other which only carves scratches because the attack angle is less than the minimum.

It has also been suggested that the transition from ploughing to chip formation occurs when the critical depth of penetration by an indenter of a known radius is exceeded [22]. The value that marks the start of the transition is give by:

$$\frac{h_c}{R} = \frac{1}{2}\left(1 - \frac{2.\tau}{p_y}\right)$$ **Equation 6**

Where h_c = critical depth of indentation

p_y = the yield stress of the material

R = radius of the indenter

τ = shear strength in the contact area

The ratio of abrasive particles that cut chips to those that merely rub grooves was estimated by Mulhearn and Samuels for abrasives that are bound to the abrasive paper. The results they obtained are represented in Figure 2. 16. They found that for their case study of bonded silicon carbide abrasive there is a well defined critical attack angle above which a chip was cut. They also found that the critical attack angle was independent of the indenting load [16]. Hutchings [35] suggested that the attack angle is a function of the Young's Modulus and Hardness of the surface (i.e. $\frac{E}{H_s}$). Using this ratio the critical attack angle for many metals can be estimated to be approximately between 30° and 90°. When the $\frac{E}{H_s}$ ratio is below the critical value of the material, ploughing will dominate over cutting mode of abrasive wear. The opposite will hold if the ratio is equal or exceeds the critical value of the material under consideration.

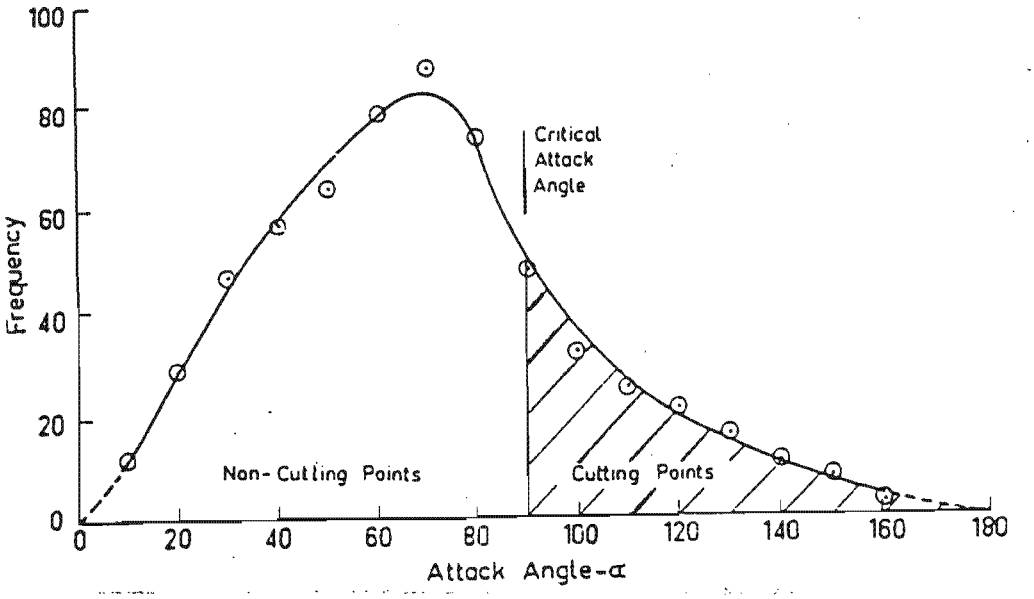

Figure 2. 16. The distribution frequency vs the attack angle(After Mulhearn and Samuels [16]).

The shaded area of the graph in Figure 2. 16 represents the distribution frequency of the attack angles that are equal and greater than the critical attack angle. For such angles the wear loss by debris formation is higher. The unshaded area represents the conditions when the attack angles of the abrasives are lower and chips are not formed but the surface is grooved.

Hutchings [35] considered the removal of material from ductile material by a moving conical indenter. It is assumed that only a certain proportion of the groove is removed as wear debris; the rest of the displaced material is piled on the sides of the grooves formed [35]. Figure 2.17 represents the schematic of the conditions assumed; the material is assumed to be abraded purely by plastic deformation.

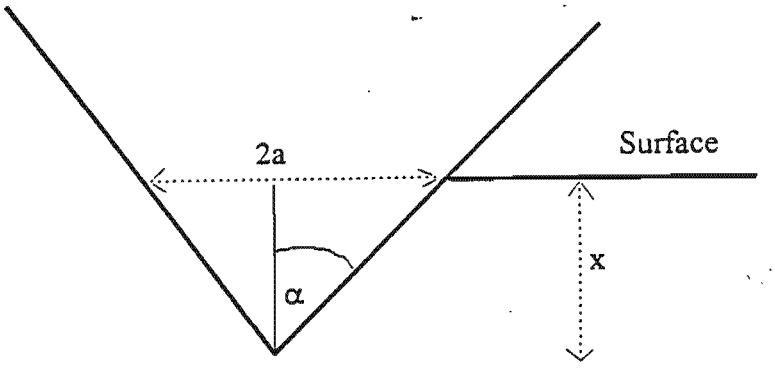

Figure 2. 17. A cross-section view of a sharp cone indenter (After Hutchings [35]).

The normal load on the indenter as it moves through the material is given by

$$w = P.\frac{\pi.R^2}{2} = \frac{1}{2}P.\pi.x^2\tan^2\alpha \qquad \textbf{Equation 7}$$

Where w = the normal load supported by the indenter
P = the stress acting over the area of contact
R = the radius of the indenter
x = depth of the groove formed by the indenter.

The volume removed from the groove without being detached from the surface can be estimated by equation 8. When a known fraction of the groove material is removed as wear debris equation 9 is used to predict the volume wear produced by one particle per unit sliding distance.

$$dV = \ell.a.x = \ell.x^2.\tan\alpha \qquad \textbf{Equation 8}$$

$$q = \eta.x^2.\tan\alpha = \frac{2\eta.w}{\pi.P.\tan\alpha} \qquad \textbf{Equation 9}$$

Where dV = the volume removed as wear debris
ℓ = the sliding distance by the indenter
q = volume wear loss per unit sliding distance by one indenter

2.1.3 Abrasive Wear Of Inhomogeneous Materials

Abrasive wear models based on inhomogeneous (or multiphase) materials have been developed in order to improve the performance of materials under abrasion. The descriptive terminology of multiphase material differs from one author to the other; in this project for purposes of simplification, the term composite will be adopted to describe both inhomogeneous materials produced by transformation/precipitation and artificially produced composites.

Composite materials are essentially constituted by distinct individual phases with different properties. The combination of the individual phases to form a composite can occur as a result of common equilibrium transformation or precipitation mechanisms in a particular system. Composites can also be artificially produced by mixing a harder reinforcing phase with a softer matrix such that in the final product the harder phase is embedded in the softer matrix. The reinforcing phase in artificially produced composites is commonly in the form of particles, whiskers, fibres or weaves [37]. Ideally it is expected that the composite will combine the best and suppress the worst properties of the constituent phases.

Kruschov [38] expressed and showed mathematically that the wear resistance of the composite is a linear function of the product of the volume fraction and the relative wear resistance of the respective constituent phases. In terms of the total wear rate Kruschov in effect expressed what is know as the inverse rule of mixtures (IROM). Garrison [39] argued that this rule is applicable only if the wear rate of the composite is proportional to the load, which he pointed out is true for ductile metal systems. The inverse rule of mixtures was reported to not hold when wear rate of the composite depends on the area of individual constituents and is non-linearly dependent on load as in ceramics [39]. Linear rule of mixtures (LROM) gives improved results compared to the inverse rule of mixtures because it does not emphasise the dominance of one phase [40]. Based on this observation it was reported to be suitable in predicting the wear rate of the composite with phases having similar properties. In spite of the shortcomings in the inverse rule of mixtures, this rule was reported to predict the wear rate of composites better when the constituent phases have different characteristics [40]. For an example the inverse rule of mixtures was applied in the epoxy-CuAl and NiCrBSi-WC systems; it was reported to be accurate when the size of the abrasive grooves is smaller than the microstructure of the reinforcing phase, in the composite, but deviated from the predicted results when pull out of the reinforcing phase occurs during the abrasion process [40].

Axèn and Jacobson [37] introduced the equal wear (EW) and equal-pressure (EP) concepts for models based on two phase composites in order to explain their behaviour in relation to the load distribution. Their assumption for the equal-wear model is that the reinforcing phase carries the maximum possible portion of the load. In such conditions the composite takes full advantage of the hardness of the reinforcing phase and suffers minimum wear (i.e. attains maximum wear resistance). In the equal-pressure model the reinforcing phase carries the minimum portion of the load; this results in higher wear rate (i.e. minimum wear resistance) [37]. The increase in wear rate in the equal-pressure model is attributed to two possible modes of wear in the composite. The first mode is when the reinforcing phase is removed as part of a small wear chip. The second mode is when the matrix strength around the reinforcing particles is weak, thereby exposing the reinforcing phase to fracturing or being pulled loose during the abrasion event [37]. The effect of the wear resistance of the reinforcing phase as its volume fraction increases improves the wear resistance of the composite in the equal-wear conditions. This effect is less in the equal-pressure condition see Figure 2. 18.

As the volume fraction of the reinforcing phase increases the equal-wear condition follows the predictions of the linear rule of mixtures; the equal-pressure conditions of the composite is predicted by the inverse rule of mixture. As can be seen from Figure 2. 18 the magnitude of benefit for the composite in the latter conditions is not optimum compared to the equal-wear conditions. The Al_2O_3-SiC system investigated by Yamada et al [41] agreed well with the model of the linear rule of mixture. The investigators reported an improvement in the wear resistance of the composite with the increase in the volume fraction of the silicon carbide, the harder of the two ceramic phases.

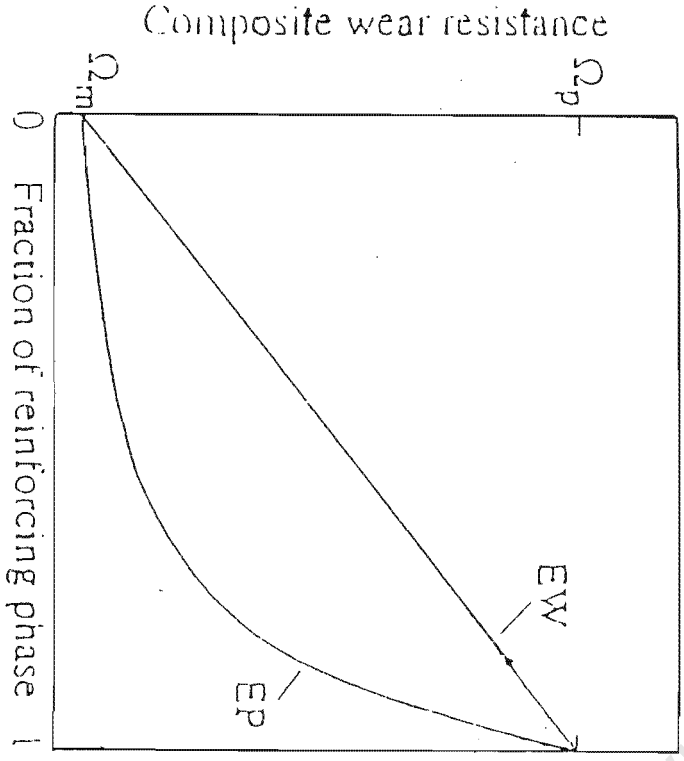

Figure 2. 18. Wear resistance vs fraction of the reinforcing phase. Ω_p ***= wear resistance of reinforcing phase,*** Ω_m ***= wear resistance of matrix(After Axèn and Jacobson [37]).***

In order to evaluate the abrasion behaviour of a composite the following parameters are important : the size (dβ) and volume fraction ($f_{v\beta}$) of the harder reinforcing phase, strength of the interface, total interface area per unit volume($S_{\alpha\beta}$), properties of the matrix and the mean free path (λ)between the harder reinforcing phase, as shown in Figure 2. 19. It must be noted that the mean free path and the total interface area per unit volume are dependent on the size and volume fraction of the reinforcing phase(s) [40].

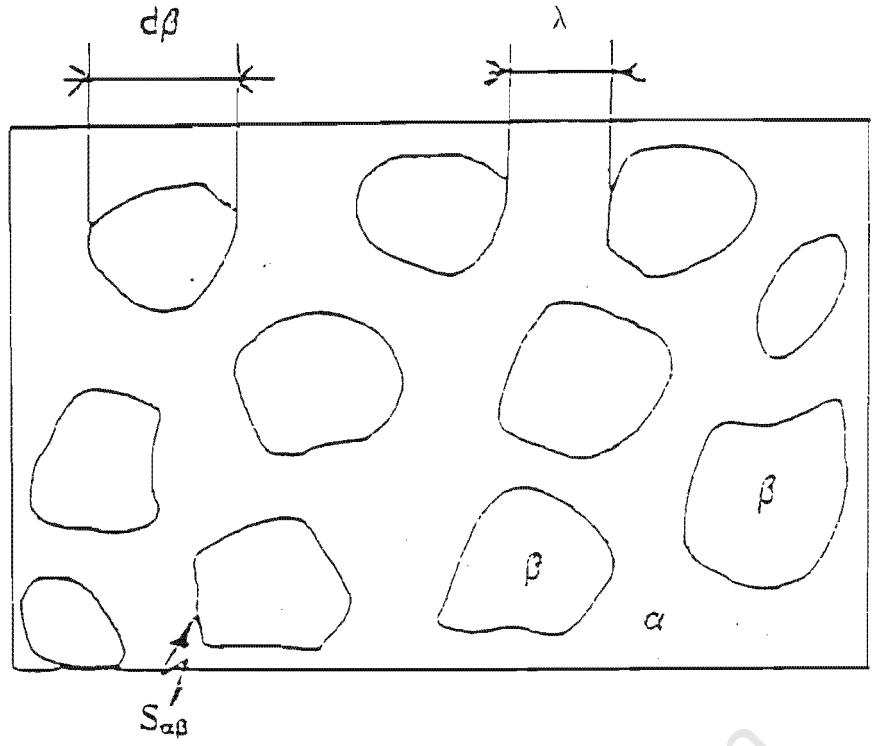

Figure 2. 20. Schematic of the microstructure of an isotropic composite (After Simm and Fretti [40]).

The importance of size and volume fraction of the reinforcing phase was emphasised in the Si3N4-TiC system [36]. In this system it was reported that abrasive wear of the composite was influenced by the grain size of the reinforcing phase (TiC). The abrasive wear resistance of the composite increased as the grain size of TiC was reduced. The volume fraction of TiC particulates was kept below a certain volume fraction for effective resistance against wear.

A different approach in the assessment of abrasive wear of inhomogeneous materials was adopted by Zum Gahr [22] where he considered the hardness ratio of the abrasive to that of the material. The abrasive wear of a homogeneous material was compared to that of an inhomogeneous material. One material contained high volume fraction of carbides in the matrix (inhomogeneous) and the other material had no carbides or the volume fraction was comparatively low to be considered less significant (homogeneous). The graphs of abrasive wear against the hardness ratio he obtained (i.e. abrasive's hardness/material's hardness) are shown in Figure 2. 21.

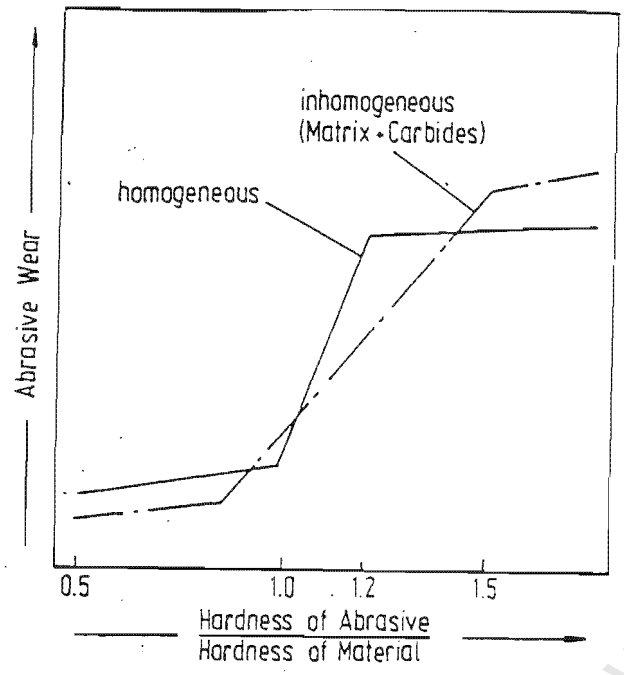

Figure 2. 20. Abrasive wear against hardness ratio.(After Zum Gahr[22])

The graph illustrates the transition from the low wear to higher wear for both homogeneous and inhomogeneous materials. At the intersection of the graphs where the hardness ratio is equal, the two materials have the same hardness provided abrasives of the same type are retained. The matrix of the inhomogeneous material is softer relative to the homogeneous material at the point of intersection; but the overall abrasive wear resistance of the inhomogeneous material is superior.

2.2 Intermetallic Materials

Intermetallics are compounds formed by two metallic elements, and are characterised by order in their crystal structures. The term order defines the tendency of one atom to form a strong bond with that of a different kind. The order in the crystal structure of intermetallic is termed long range order. This type of crystal order involves arrangement of ordered domains of atoms on a scale larger than 10-50 Å [42]. Crystal ordering in certain intermetallics can be maintained until the melting point. Other intermetallics lose the order in the crystal structure when a critical temperature is reached below the melting temperature of the compound. In order to distinguish intermetallics falling in the two groups from each other, Cahn [43] suggested a term "reversibly ordered intermetallic" for intermetallic compounds that undergo a disordering process before their melting point is reached; and the term "intermetallic" to describe the intermetallic compounds that remain ordered until their melting point. The differentiation is technically important but remains difficult to implement as all compounds that fall under the two categories are still referred to as intermetallics. Implementing these terms is also made difficult by the fact that much research work still needs to be covered in the field of these new materials for their classification to be simplified.

Intermetallic compounds are distinguished from the ordered metal alloys by the strong directional bonding between the elements involved [44]. These compounds are stable over a narrow range of composition which lies approximately around the stoichiometric ratio of the elements. Intermetallics have raised much interest as possible structural materials because of their high moduli, yield strengths and melting temperatures. They also possess qualities that makes them suitable for application at elevated temperatures, such as creep and oxidation resistance. Intermetallic compounds have a comparatively low self-diffusion coefficient which account for the good creep resistance in these materials. Creep resistance is also enhanced by the degree of ordering an intermetallic is able to achieve in its structure [44].

Another factor that makes intermetallics attractive is their excellent specific properties (e.g. moduli, yield strengths, etc. per unit mass) when compared to the conventional engineering materials. This is more particularly relevant in aircraft and space industries where the reduction of weight and the maintenance of good structural properties in a material is important. Intermetallic compounds possess an ability to work-harden rapidly compared to the metals from which they are derived [44]. Their major disadvantage is brittleness at room temperature. This brittleness is attributed to a number of factors such as, strong directional bonding, insufficient slip systems and poor grain cohesion [45].

Deformation of any material requires sufficient slip systems for the movement of dislocations, intermetallics are not an exception to this requirement. In terms of the microstructure the dislocations move easily in high symmetry crystals because of the high number of slip systems available, compared to a few that may be present in low symmetry crystals. Therefore the low symmetry associated with the microstructure of some intermetallics limits the amount of deformation they can undergo. This factor contributes to the observed brittleness in intermetallics. However, certain intermetallics with high symmetry crystals remain brittle as a result of poor grain boundary cohesion in the polycrystalline microstructure. An example of the latter case is a compound of nickel aluminide (Ni_3Al) whose single crystal has high ductility but the polycrystalline material of the same compound is brittle. There is a body of theory that supports the notion that intermetallics generally deform at low stresses because of the movement of superdislocations. The dislocations occur in pairs or in units of four that are closely spaced and always move in groups [45, 46]. The lattice structure is preserved by the group movement of these dislocations, this phenomenon is known as lattice dislocation resistance. It has also been argued that lattice dislocation resistance can also be produced by quenching an intermetallic from above its melting point [47]. It is further argued that the lattice dislocation resistance (or surperdislocation movement) has a limiting effect on cross-slip in the crystal structure, thus resulting in the embrittling of the material [45, 46, 47].

In spite of good physical and mechanical properties in the intermetallics compounds, their room temperature brittleness limits their use as structural materials. It was reported that metallurgical processes such as rapid solidification by melt spinning improved ductility in certain intermetallics. Other processes such as thermomechanical grain refinement were also reported to have improved ductility in nickel aluminide (NiAl) [43]. The elongation reported in nickel aluminide was approximately 40 % when the critical grain size is below 20 microns [48]. Alloying with elements such as boron is another method reported to have improved ductility in intermetallics such as ruthenium aluminide and titanium aluminide at room temperature. Intermetallics with crystals belonging to either an ordered fcc (or Ll_2) or ordered bcc (or B2) crystal system have better ductility than intermetallics belonging to other ordered crystal systems [48]. Metallurgical process such as alloying can serve to enhance the ductility they already possess.

A better abrasive wear resistant intermetallic composite consisting of molybdenum-silicide reinforced with niobium (MoSi-Nb) was reported [49, 50]. Following this improvement, it is suggested that further research into abrasive wear behaviour of intermetallics will culminate in the development of good abrasive properties in these compounds. Molybdenum-silicide, it is argued poses a serious challenge to the dominance of cobalt based composites as abrasive wear resistant materials [51]. The results come in support of other independent studies that found that mechanical properties of multiphase materials were better when compared to monolithic intermetallics [52, 51].

It was also reported that bronze is preferred as wear resisting material for journal bearing material under high loads [53]. The bronze owes its wear resistance properties to the presence of delta (δ) intermetallic compound ($Cu_{31}Sn_8$) in the copper-tin system [53]. Another intermetallic cobalt-molybdenide-silicide (Co_3Mo_2Si) of the Laves phase family was reported to prevent other forms of wear at high temperatures such as seizure.

The hardness of the Lave phase is approximately 1,200 HV. The wear resistance of systems that precipitates this phase, such as the Mo-Co-Si ternary system benefit from its high hardness [53].

2.2.1 Ruthenium Aluminide (RuAl)

Ruthenium aluminide is an intermetallic compound formed between ruthenium and aluminium. The formation energy of ruthenium aluminide is approximately 35.8 kcal/mol, this is higher than some of the intermetallics such as nickel aluminide. The crystal structure of this intermetallic is an ordered body centred cubic (i.e. B2 [cP2]); which consists of two interpenetrating simple cubic lattices with one type of an atom at the body-centre of a sublattice of the second type atom [54]. The lattice parameter for the crystal structure is approximately 3.03 Å.

The anti-phase boundary in the B2 intermetallics is created by the dissociation of the <111> superdislocation [55]. It is essentially a region of discontinuity that breaks the order in the crystal lattice structure of the material. The order in intermetallics is broken by the formation of bonds between atoms of the same kind during the growth of adjacent crystals. The existence of an anti-phase boundary improves the cohesive strengths and ductility of an intermetallic [56, 57].

A ruthenium aluminide compound that is close to stoichiometry has an approximate melting temperature of 2060°C with a Young's modulus of 267 GPa. The yield stress of the unalloyed stoichiometric composition of ruthenium aluminide is ~ 1000 MPa; for the same composition but alloyed with boron the yield strength is ~ 2000 MPa. Fleischer [46] reported that the yield strength is also sensitive to the variation of ruthenium content from stoichiometry; it shows an increase with the higher ruthenium content and a decrease when ruthenium content is lower [46]. The specific gravity lies between 7.3 and 8.89 g/m^3 depending on the stoichiometry of ruthenium aluminide compound considered [58].

The oxidation resistance in ruthenium aluminide up to ~ 1200°C is enhanced by minor additions of elements such as chromium and yttrium. It must be noted that the oxidation resistance is also provided by the aluminium in the compound. The hardness of stoichiometric or near-stoichiometric ruthenium aluminide varies between approximately 2.7 and 3.7 GPa at room temperature [57].

2.2.2 The Sigma Phase

Sigma phase is a term which describes certain complex intermetallic compounds formed between transition elements. It is an electron compound formed by bonding between terminal elements. The formation of this phase in many binary systems follows a set of criteria such as : (a) One element must be electronegative and the other electropositive, (b) The atomic radii of the elements must be approximately equal [59], (c) The unit structure formed must belong to the tetragonal crystal system [60, 61, 62], with the lattice parameter ratio (c/a) of approximately 0.52 and (d) The average electron per atom ratio (e/a) of approximately 7 to 7.12 [63]. Examples of the systems capable of forming the sigma phase include Manganese-Vanadium (Mn-V), Cobalt-Vanadium (Co-V), Iron-Chrome (Fe-Cr), Iron -Molybdenum (Fe-Mo) etc. As an intermetallic compound the sigma phase is characterised by room temperature brittleness [64].

Sigma phase in iron chromium steels was first discussed by Bain and Griffiths [65] who referred to it as the 'B' constituent before being later named 'sigma' by other workers. They found sigma to be stable below a temperature of 950°C. This temperature of stability was determined later to be 820°C as shown in the iron-chromium equilibrium phase diagram in Figure 2. 1 [66]. Sigma phase was reported to be the stable low temperature phase in the 50:50 iron-chromium system with less than 10% nickel. The role of sigma in reducing ductility of the steel as a result of its room temperature brittleness is confirmed by a number of workers [67]. However its role in the 475°C embrittlement of ferritic steel is dubious [67,68]. Sigma precipitates very slowly in some iron chromium alloys. This has lead to some workers expressing doubt about its existence; in spite of working with compositions reported to be sigma prone [69].

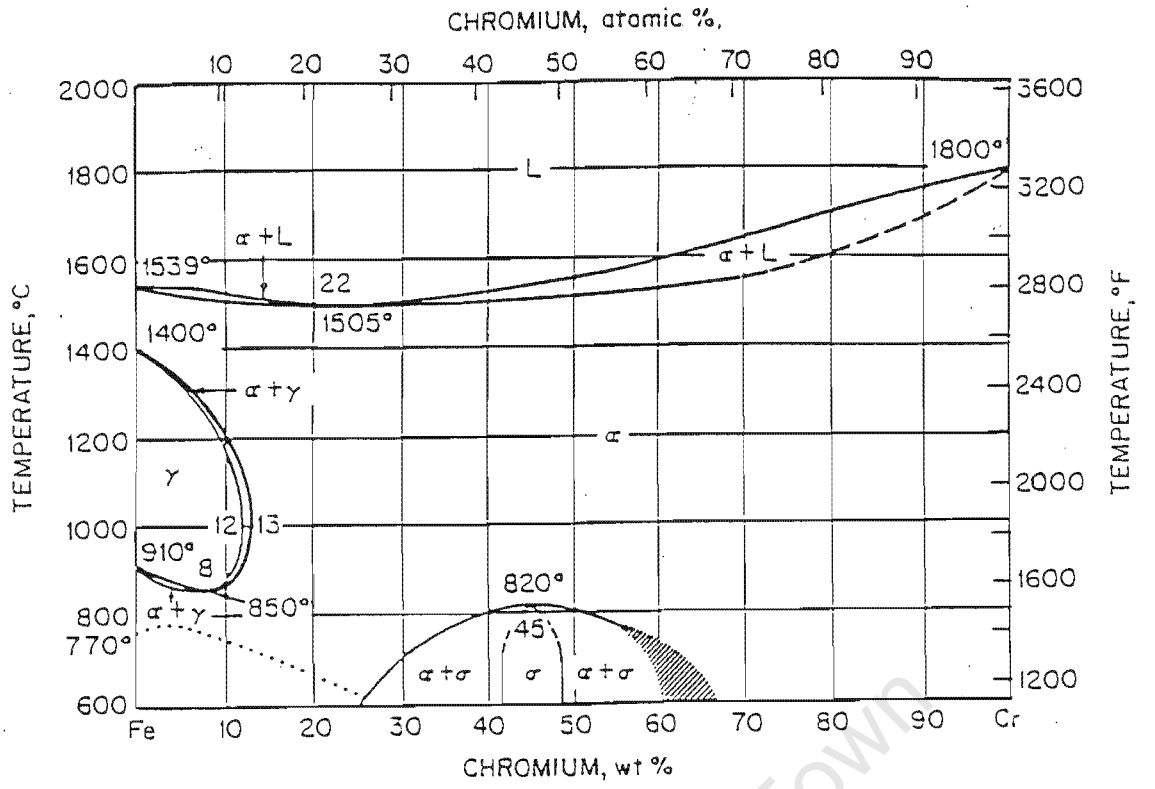

Figure 2. 21. Iron-Chromium equilibrium phase diagram (After Novak [66])

Sigma phase in ferritic stainless steels

Stainless steels are used widely as structural materials because of their advantageous corrosion resistant properties. Chromium contents above 12% provide stainless steels with exceptional oxidation and creep resistance. As a result stainless steels can be used for corrosion resistance and as high temperature creep resisting materials. Without these properties stainless steels could be equalled or exceeded by many other steels in formability and mechanical properties [70]. Within the group of stainless steels competition exists between the ferritic and austenitic grades. In many engineering application ferritic stainless steels are preferred to austenitic grades, because of their relative low cost and improved pitting and crevice corrosion resistance under reducing environments [71]. The competitiveness of ferritic steels against austenitic grades is enhanced by their wide range of yield stresses. Ferritic steels are also easily workable because they possess comparatively low work-hardening rates. Application of ferritic steels has lead to development of new grades within this group.

New definitions are used in order to differentiate between the grades within the ferritic group. The two major grades are the "Ferritic" and "Super ferritic". The latter description refers to the ferritic steels with chromium content of no less than 18%; this is a term recently adopted in the stainless steel industry. Elements such as titanium and niobium are used in stabilising ferritic steels because of their strong ability to form more stable carbonitrides than chromium. The formation of titanium or niobium carbonitrides is beneficial in preventing chromium depletion. Chromium in the stainless steels is important in corrosion protection of the substrate [72, 73]. It is clear from the factors mentioned that developing desired properties in ferritic steel may need a combination of different processes. Thermomechanical and alloying processes are the most important techniques used in improving the service properties in ferritic steel [74,75].

Ferritic stainless steels suffer from a dominant shortcoming in that many are susceptible to the 475°C embrittlement. The cause for this embrittlement was reported to be due to a number of factors, such as precipitation of the inherently brittle carbides and nitrides at grain boundaries. It was also reported that in high chromium steels the embrittlement is aggravated by the presence of the brittle chromium-rich ferrite [64, 76]. Further argument for the embrittlement was suggested as the formation of the sigma phase [77] which occurs in the miscibility gap of the iron-chrome equilibrium phase diagram, shown in Figure 2. 21. However doubt has since been expressed about the role of sigma phase because its embrittlement effect was reported to be sensitive to the heat treatment at temperatures above the "brittle temperature" of the ferritic steels [78, 79]. The view that the embrittlement is caused by the chromium rich ferrite has gained strong support from many workers [80]. None of these factors alone have conclusively accounted for the observed embrittlement [72].

The role played by alloying elements in raising the critical temperature over which sigma is stable was an important observation in the study of the iron-chrome system. It culminated in the development of research interest to improve the understanding of the mode and rate of sigma precipitation [65]. Alloyed steels were reported to have a higher rate of sigma precipitation than pure binary systems [65].

Hall and Algie [81] suggested that sigma's stability temperature and compositional range is increased by addition of certain alloying elements. It was also reported that some alloying elements may show no effect and others may retard the precipitation of the sigma phase [81,82]. Further investigation by other workers reported that austenitic [83] and ferritic microstructures have an influence on the formation of sigma. The rate of precipitation being relatively faster in the latter microstructure [84].

Grain boundaries are preferentially sites for sigma precipitation because they are regions of high energy. The precipitation of this phase at grain boundaries has an effect of lowering the energy of the system. Sigma can also precipitate in the interior of the grains along preferred matrix planes and dislocations [83]. The precipitation kinetics are influenced by processes such as grain refinement [84]. This process effectively reduces the diffusion paths over which elements can traverse to the sites where sigma formation will start. Thermomechanical processes such as hot and cold working influence the rate of sigma phase precipitation in the microstructure [77]. It has also been argued that prior precipitation of titanium carbide and other secondary phases which act as chromium reservoirs can promote the formation of the sigma phase in the steel [84]. The presence of elements such as manganese, vanadium, titanium and niobium were reported to enhance the formation of sigma phase by their ability to stabilise the ferritic microstructure. Care may need to be exercised not to exceed the limits when adding alloying elements. Their excessive concentrations may retard sigma precipitation where it may be needed.

Other elements also identified as promoting the rate of sigma formation are zirconia, nickel, molybdenum and the non-transition elements such as silicon, phosphorus and aluminium [81, 85, 86]. In order to understand how the alloying elements affect the sigma their role was considered in terms of being electronegative or electropositive relative to one another.

A description of this approach is that, an electronegative element withdraws electrons from the sigma phase; and electropositive elements donate electrons to the sigma phase. Silicon, phosphorus and aluminium were used to illustrate this electronic effect. It was reported that additions enhanced the formation of the sigma phase. These elements were also found to increase the ability of sigma phase to accommodate extra electropositive elements such as vanadium and chromium. The electronegative aluminium was reported to retard the sigma formation when added in certain quantities [81, 87]. Therefore the addition of electronegative elements retard the formation sigma phase, except in the case where they are added in careful amounts to allow sigma to accommodate extra electropositive elements.

Shortsleeve and Nicholson [88] in a different study of the effect of alloying elements, used silicon and manganese in ferritic steels to illustrate their influence on the sigma/ferrite boundaries. In terms of the chromium content of the steel, Cook and Jones [89] suggested that heating a steel containing 26 to 71 % chromium at 600°C will result in the formation of sigma. They also carried out work on the phase boundaries of the sigma and ferrite. Edmonds and Honeycombe [90] reported a temperature of 850°C at which they suggested sigma will precipitate. The upper most temperature estimate for the stability of the sigma phase was suggested by Bain and Griffiths to be just below 950°C. Gilman [91] suggested that repetitive recrystallisation in the steel has an effect of reducing the rate of sigma formation.

The effect of sigma phase in the steel is two fold, it can enhance certain properties on one hand and be deleterious on the other. Properties such as toughness, corrosion resistance, electrical conductivity and magnetisation are adversely affected by the presence of the sigma phase [72, 65, 81, 87 92]. However properties such as creep resistance and yield strength were as reported as promising [93].

In spite of the embrittlement associated with sigma at room temperature; hot hardness (creep strength) benefits from the sigma formation. Such strength was observed in engine exhaust valves [84, 91]. The wear resistance in some of sigma prone iron-chrome system was reported to have even performed better than mild steels [93]. A further discussion on the sigma properties was present by Williams and Paxton [68]; who in their work suggested the presence of an alpha-prime phase α' as responsible for the embrittlement of the iron-chrome steel. They suggested that this phase come as result sigma decomposition into alpha and alpha-prime phases (α and α') at temperatures lower than 600°C. Although this is a possibility, the notion of a eutectoid decomposition of sigma they have suggested has not yet received wider support.

The blocky morphology precipitates of sigma phase can prevent crack propagation in the steel [59]; conversely when the sigma precipitates are plate-like the steel becomes susceptible to crack propagation. This is because the sigma platelets are easily traversed by cracks and they may also act as sources for crack initiation [59]. Bain and Griffiths [65] have suggested that cracks observed in the steel in the presence of sigma phase are due to the volume change that occurs during the phase transformation to sigma; they pointed out that the high stiffness and low ductility associated with sigma was responsible for limiting the steel's ability to accommodate the strain imposed by the transformation; other workers have expressed similar views [94].

CHAPTER 3: EXPERIMENTAL PROCEDURES

3.1 Materials

Ruthenium Aluminide

Two small flat discs of 15mm diameter each and one solid cylinder of sintered ruthenium aluminide (RuAl) were obtained from Council for Mineral Technology (Mintek). The discs were prepared for metallography. A cylindrical specimen for compressive tests and a square specimen for abrasive tests were cut from the received cylinder. The dimensions of the compressive test specimen were 5.4 mm in diameter and 8mm in length; the length to diameter ratio was chosen in accordance with the ASTM recommendation to avoid buckling in the specimens during the compressive test [95]. The dimensions of the abrasion test specimen were 10mm x 10mm x 24mm, determined by the size of the specimen bracket on the abrasion apparatus, see Figure 3.1 and Figure 3. 2. Difficulties experienced in machining of the hard and brittle material of the specimens led to spark erosion being employed in specimen preparation.

MCV (A medium carbon proprietary steel)

MCV is a commercially available medium carbon steel which has the nominal composition shown in Table 3. 1. The dominant characteristics of this steel are high strength, toughness, hardenability and ease of machining even when hardened and tempered. The MCV steel was quenched and tempered to a hardness of approximately 310 HV in order to match the hardness of ruthenium aluminide. Compressive test specimens and abrasion test specimens of the same dimensions as the ruthenium aluminide were machined.

Table 3. 1. The nominal composition of the MCV (from data provided by the manufacturers). The balance is iron.

Element	Content (wt %)
CARBON	**0.45/0.50%**
SILICON	**0.25/0.35%**
MANGANESE	**1.00/1.30%**
NICKEL	**0.40/0.75%**
CHROMIUM	**0.40/0.75%**
MOLYBDENUM	**0.20/0.30%**

Ferritic Steels

Three grades of ferritic steels were provided by Mintek with compositions indicated in Table 3. 2. The specimens provided had been subjected to different thermomechanical processes, as shown in Table 3. 3. It must be noted that VF 550 was first reduced from a thickness of 45mm to 12 mm at a temperature of 1100°C by rolling process and was subsequently divided into two halves: VF550 (i and ii) which received further treatment described in Table 3. 3. A portion of VF550 (ii) was cut and given further treatment shown by VF550 (iii) also in Table 3. 3.

Table 3. 2. Chemical composition of ferritic steel specimens, the balance percentage is iron. NB the regions marked with -- indicate concentrations below 0.02 (Data supplied by Mintek[87]).

	Chemical Composition Of the Alloys (wt %)									
Alloys	Cr	Ni	Mo	Si	Nb	Ti	Zr	Al	C	N
VF 245	40.7	5.82	--	--	--	--	--	--	0.016	0.003
VF 550	28.7	--	3.94	0.15	0.25	0.15	-	-	0.007	0.002
VF 660	38.8	2.25	2.03	0.17	--	--	1.00	--	0.008	0.002

Table 3. 3. Summary of thermomechanical history of ferritic steel specimens [87].

Specimens	Thermomechanical History		
	Heat treatment (°C)	Further working	Thickness reduction
VF245	1100	Q + WR (300°C)	24mm to 12mm
VF550 (i)	1100	Q + CR	12mm to 6mm
VF550 (ii)	1100	HR (1100°C)	12mm to 6mm
VF550 (iii)	1100	HR (1100°C)	6mm to 3mm
VF660	1100	HR (1100°C)	45mm to 12mm to 6mm

A systematic program of heat treatments was carried out on all the ferritic steel specimens in order to produce specimens containing a range of volume fraction of sigma phase. Heat treatment was performed on the 10mm x 10mm x 24mm abrasion specimens cut from each specimen provided. The heat treatments were performed in order to identify the heat treatment temperature and time required for precipitation of the sigma phase and to identify optimum heat treatment procedures.

In order to accumulate the large amount of data required, the following procedures were adopted: initial heat treatments for 30 and 60 minutes were conducted at 600°C, 650°C, 700°C, 750°C, 800°C and 850°C. On the basis of the results of these heat treatments, temperatures of 600°C and 650°C were selected for conducting further heat treatments. Sufficient specimens were machined in order to permit twelve fresh specimens to be used for each heat treatment temperature. The duration of these heat treatments varied from 5 minutes to 1 hour (at intervals of 5 minutes).

The heat treatment procedure employed was that: twelve specimens of each grade at a time were simultaneously placed in the furnace at a chosen temperature (600°C or 650°C). A specimen was taken out after every five minutes until all were removed from the furnace. As they were taken out of the furnace they were immediately quenched in

water. Errors inherent in opening the furnace during heat treatment were accepted on the basis that the procedure enabled a large amount of data to be accumulated. Heat treatment times and temperatures determined by this method were treated with caution and used only as indicators of the appropriate heat treatment conditions.

Comment

The initial heat treatments were used to narrow down the temperature range which produced good results in terms of sigma precipitation. Hardness and magnetic tests were performed in order to determine if any transformation to sigma had occurred after the heat treatments. The emphasis in the second set of heat treatments was on the specimens that produced the two phase microstructure of sigma and ferrite.

3.2 Metallography

Ruthenium Aluminide and MCV

Ruthenium aluminide discs and one cylinder of the MCV were hot mounted using IMP clear thermoplastic powder and a Buehler mount press hydraulic jack. Grinding of the specimens was carried out on Knuth Rotor machines with silicon carbide abrasive papers (grit size: 80, 180, 220, 320, 600 and 800 respectively). Diamond impregnated cloths (3μm, 1μm and 1/4 μm respectively) were used to polish the specimens.

The Struers® DP 9 apparatus was used for rotating discs on which the polishing cloths were mounted. Before proceeding with polishing, the specimens were placed in a beaker of alcohol in an ultrasonic bath for cleansing; the same procedure was repeated between the change over from one polishing cloth to another. The reason for this procedure was to improve the quality of the surface finish by preventing the contamination of the polishing cloths. Ruthenium aluminide did not need any etchant to reveal the microstructure; for MCV a 2 % dilute nital solution was used to etch the specimen.

Ferritic Steels

The sequence of grinding and polishing was the same as in ruthenium aluminide and MCV. A dilute oxalic acid solution was prepared by dissolving 8g of oxalic acid pellets in 100ml of distilled water. The solution was used in the electronic etching of the ferritic stainless steel specimens in order to reveal their microstructure. The voltage for the electronic etching was between 3 and 5 volts. Micrographs of the microstructure were taken on the Reichert MeF3A® optical microscope. The micrographs were used in determining the volume fraction of sigma that had precipitated in the specimens. The procedure involved image analysis techniques using the Leitz Focomat V35 photograph enlarger and Joyce Loebl image analyser facilities. The photograph enlarger was used to trace out the microstructure on the micrographs in order to improve the contrast for better volume fraction results on the image analyser. This procedure was employed after etchants such as the solution of hydrochloric acid (75ml) and nitric acid (25ml) were tried without any success for improving the contrast in the microstructure of the ferritic steels.

3.3 Abrasion Testing

Abrasion testing was conducted on a pin on belt apparatus under ambient unlubricated conditions. An 80 grit (~260μm to 270μm in grain size) alumina (Al_2O_3) belt was used as an abrasive counterface against a specimen under load. The testing speed was 0.26 ms^{-1} and the load on the specimens was 3.66 kg or 36.6 N. The starting surface roughness of the specimens before the abrasion test was kept between 2μm and 3μm.

Operation of the Abrasion Testing Apparatus

A specimen of appropriate dimension (i.e. 10mm x 10mm x 24mm) is inserted and firmly locked into a bracket and the surface measuring 10mm x 10mm is placed in contact with the abrasive belt. Weights are placed on the pin directly on top of the bracket holding the specimen (see figure 3.3 and 3.4). When the specimen is firmly positioned against the

abrasive belt the machine is switched on. A motor drives the abrasive belt around continually in one direction; the bracket holding the specimen moves simultaneously across the belt in a perpendicular direction to the motion of the belt (all motions occurring in the same plane) with the exposed face of the specimen firmly on the belt, Figure 3.1 and Figure 3. 2.

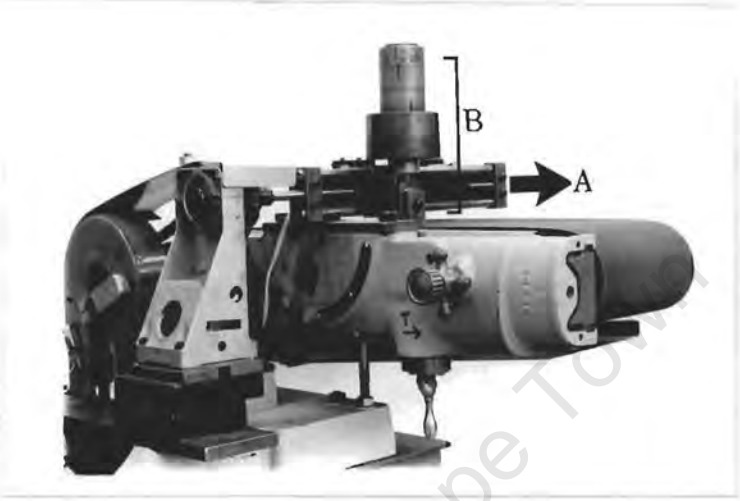

Figure 3.1. Side view of the abrasion apparatus. A = direction of the specimen. B = the weights and the specimen bracket.

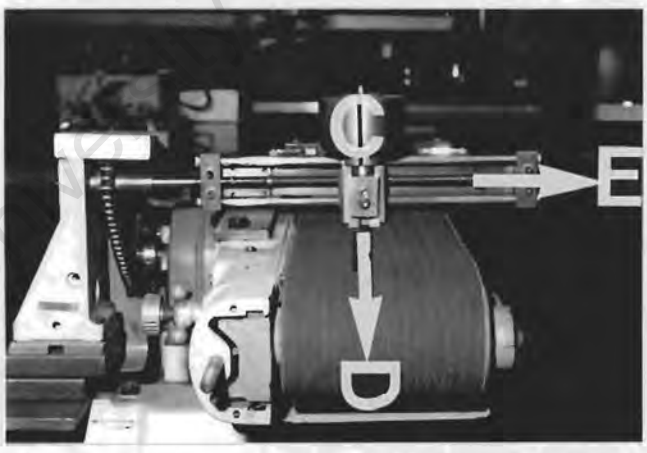

Figure 3. 2. Front view of the abrasion apparatus, C = weights; below the weight is the specimen bracket. D = direction of the abrasive belt. E = the direction of the specimen relative to the abrasive belt.

The test procedure was as follows: the specimens were placed in a beaker of alcohol which in turn was placed in an ultrasonic bath for approximately five minutes; they were subsequently dried and weighed on Sartorius R200D weighing balance before being tested on the abrasion apparatus. After every chosen testing time interval the specimens were placed in a beaker containing alcohol and placed in an ultrasonic bath. Following cleaning and drying mass loss was measured. Micrographs of the surface features were acquired using the Cambridge scanning electron microscope.

The test interval for ruthenium aluminide and MCV specimens was 14 seconds. This rather short time interval was selected because of a lack of information about the response of ruthenium aluminide to abrasive wear, and because of the brittle nature of the material. The short interval would in this case yield more data points than a longer time interval in the event of failure of the specimen. However this approach had a shortcoming in that the specimen was not yet 'run-in' after the first 14 seconds. Tests were carried out for a total of 70 seconds per specimen (i.e. 5 intervals) for both ruthenium aluminide and MCV. The same procedure was used for ferritic steels but at intervals of 28 seconds for each specimen in order to obtain satisfactory running-in. Apparatus set up was such that during each run the test specimen was exposed to a fresh part of the abrasive belt at any particular point.

3.4 Mechanical Testing

Compression tests were carried out on the ESH compression apparatus; the maximum load on the rig was 80 KN. Two MCV specimens were used initially to set up the apparatus for consistent reading. A third and fresh specimen of the MCV was subsequently used in the actual test; ruthenium aluminide was tested under similar conditions to the MCV. The data generated was collected electronically into a computer interfaced to the control panel.

The data obtained was converted into true stress-true strain values which were used in plotting graphs. The work-hardening rate against true strain graphs for both ruthenium aluminide and MCV were obtained from the slopes of their respective true stress-true strain graphs. The formulae used for the true-stress and true-strain are represented by equations 10 (a&b) [96]. Equation 11 was used to calculate the slopes of the true stress-true strain graphs obtained for ruthenium aluminide and the MCV steel [97].

(a) (b)

$$\sigma_t = \sigma_n(1 + \varepsilon_n) \qquad \varepsilon_t = \ln(1 + \varepsilon_n) \qquad \textbf{Equation 10}$$

$$\frac{d\sigma}{d\varepsilon} = \frac{\sum \varepsilon_t . \sigma_t - n\varepsilon_t' . \sigma_t'}{\sum \varepsilon_t^{\,2} - n\varepsilon_t'^{2}} \qquad \textbf{Equation 11}$$

Where: σ_n = Nominal stress

ε_n = Nominal strain

σ_t, σ' = True Stress and the average value of the true stress respectively

ε_t, ε'= True Strain and the average value of the true strain respectively

n = the Number of data points over which the averages are taken.

In order to determine the work hardening induced by the abrasion process in the two specimens, subsurface microhardness measurements were taken on sections through the abrasive test specimens. Taper sections rather than normal sections were produced, in order to obtain a reasonable number of indents in the immediate subsurface region, since this has the effect of magnifying the cross-sectional area. The procedure involved mounting the abraded surfaces on small sloping stages (slope ~5.4°); with a mixture of CIBA-GEIGEY Araldite-M-resin and the HY-956 hardener added in the proportions 5:1. The mounting took 48 hours to be completed. The principles involved are illustrated in Figure 3. 3.

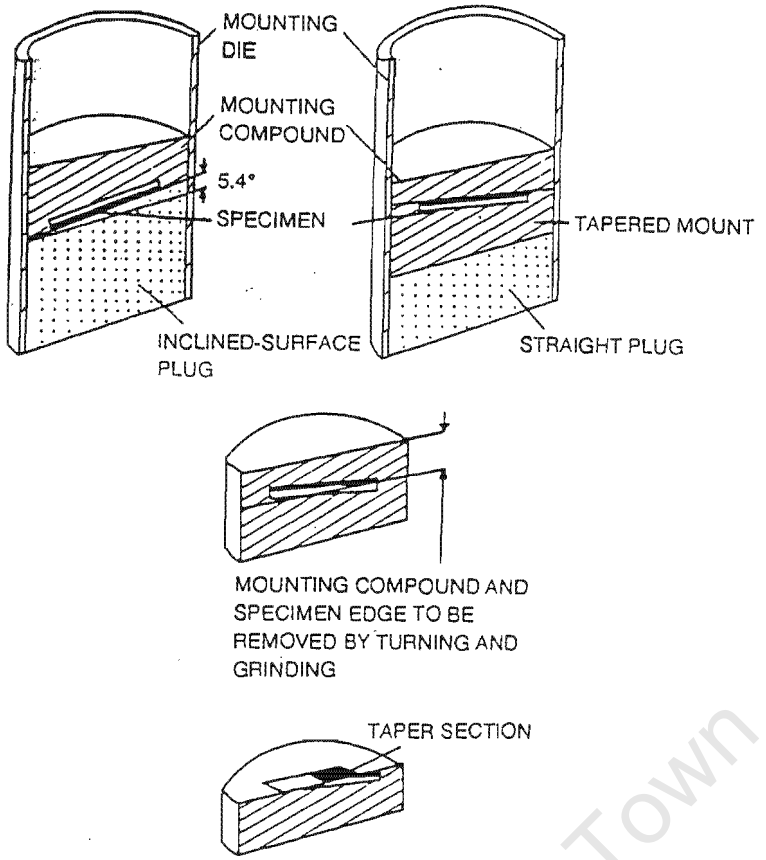

Figure 3. 3. Stage-wise schematic of the process of making a taper section

The exposed tapered surfaces were ground and polished in the same manner as was done in the metallurgical preparations of the microstructure. Microhardness was measured as a function of depth beneath the abraded surface. The microhardness of all specimens (i.e. of ferritic steel, ruthenium aluminide and MCV) were measured using a diamond pyramid indenter and a load of 25gf on the Matsuzawa MXT-α7 digital microhardness tester. The bulk hardness of the specimens were measured using a Vickers diamond pyramid and a load of 20kgf on the ESE WAY (Type SPVR.2.M) hardness tester.

The depth to which the hardness induced by the abrasion process had persisted on the surface, was determined by microhardness measurements on a tapered section of the abraded surface. To determine the depth, a formula: $d = L*\sin\theta$ was used, where L = linear distance measured and θ = the angle of the taper section (5.4°).

CHAPTER 4: RESULTS

4.1 Condition of materials prior to abrasion testing

Ruthenium aluminide was tested in the as-received condition. The MCV steel was quenched and tempered to match the hardness of the ruthenium aluminide as closely as possible. The ferritic steel specimens were heat treated at 600°C for a range of times, in order to produce different volume fractions of the hard sigma phase. Figure 4.1 and Figure 4.2 show the percent sigma volume as a function of heat treatment time.

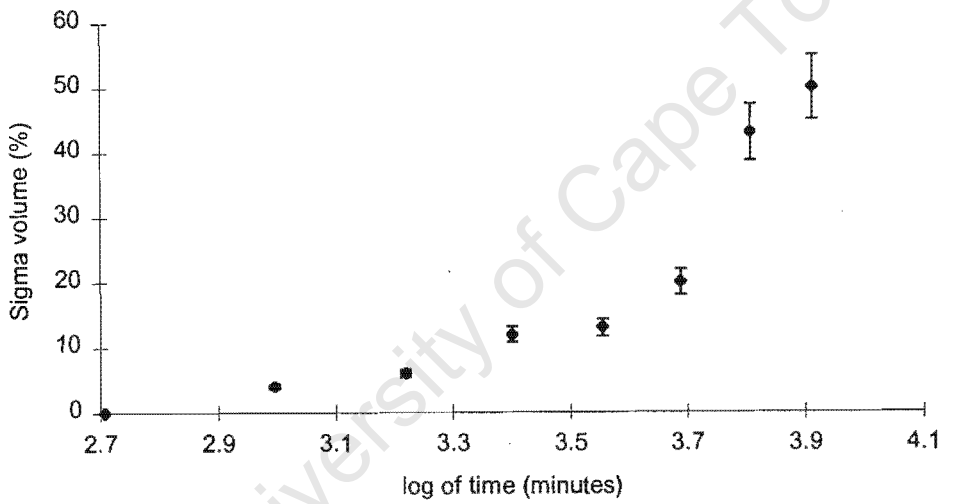

Figure 4.1. Percent sigma volume vs log of heat treatment time at 600°C for VF660 samples.

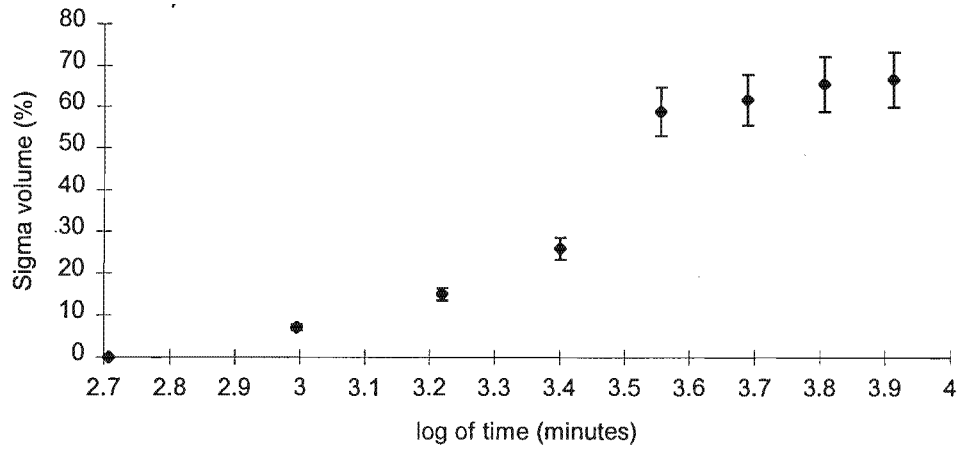

Figure 4.2. Percent sigma volume vs log of heat treatment time at 600°C for VF245 samples.

Ferritic steel specimens which had been heat treated for periods of 5 minutes to 60 minutes were tested for abrasion resistance. Three specimens from each sample (VF660 and VF245) heat treated for 30 minutes and 50 minutes as well as specimens in the as-received condition, were selected to facilitate a comprehensive wear rate comparison within each group. The hardness of specimens prior to abrasion testing is shown in Table 4. 1. The hardness of the ferritic specimens increases with the length of heat treatment time as a result of the increase in sigma volume percent

Table 4. 1. Bulk hardness measurements of the specimens prior to abrasion testing.

	Load = 20kgf							
	RuAl	MCV	VF 660			VF245		
Heat treatment time (minutes)	none	none	none	30	50	none	30	50
Bulk Hardness (HV)	300	310	200	310	364	274	372	412

The microstructures of the test specimens are shown in Figures 4.3 to 4.10. Figure 4.3 is an optical micrograph of ruthenium aluminide showing the presence of the lighter intergranular α-ruthenium phase between the darker ruthenium aluminide grains. The presence of this intergranular ruthenium phase is to be expected since the composition is super-stoichiometric with respect to ruthenium (52% Ru).

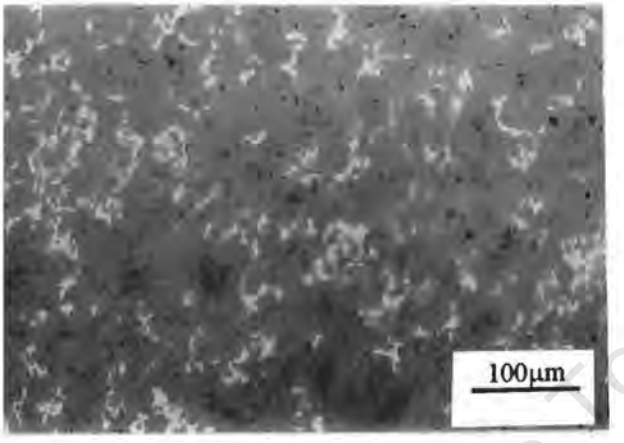

Figure 4.3. Optical micrograph of ruthenium aluminide specimen, showing the presence of intergranular α-ruthenium phase (light phase); the small dark patches are pores that occurred during the sintering process.

In contrast to the ruthenium aluminide, the quenched and tempered MCV has a uniform microstructure of tempered martensite, as shown in Figure 4.4.

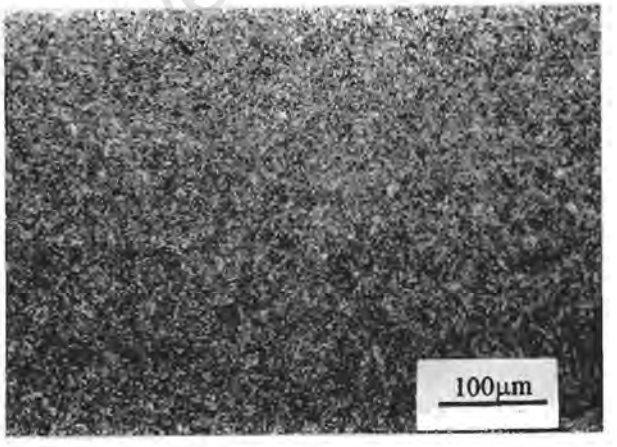

Figure 4.4. Optical micrograph of MCV medium carbon steel, showing a uniform microstructure.

Figures 4.5, 4.6 and 4.7 show the microstructure in VF660 specimens before the abrasion test. Figure 4.5 is an optical micrograph of the as-received specimen showing ferrite grains. Figures 4.6 and 4.7 are the optical micrographs of specimens heat treated for 30 minutes and 50 minutes at 600°C respectively; showing two phase microstructure with different percentage volumes of sigma in a ferrite matrix.

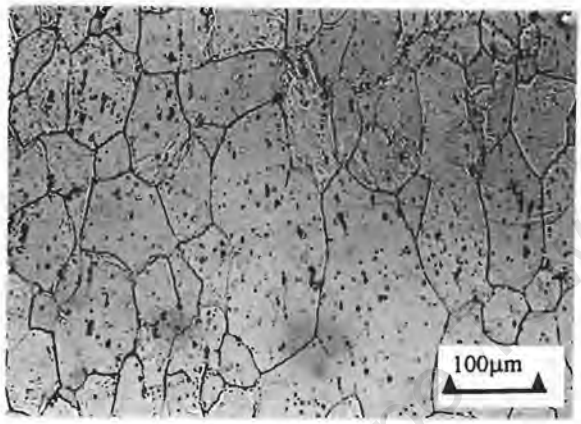

Figure 4.5. Optical micrograph of as-received VF660 specimen, showing ferrite grains.

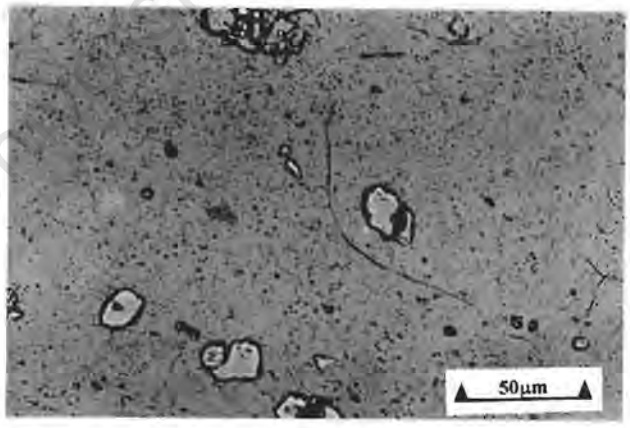

Figure 4.6. Optical micrograph of VF660 specimen after 30 minutes heat treatment at 600 °C, showing small grains of sigma phase in a ferrite matrix.

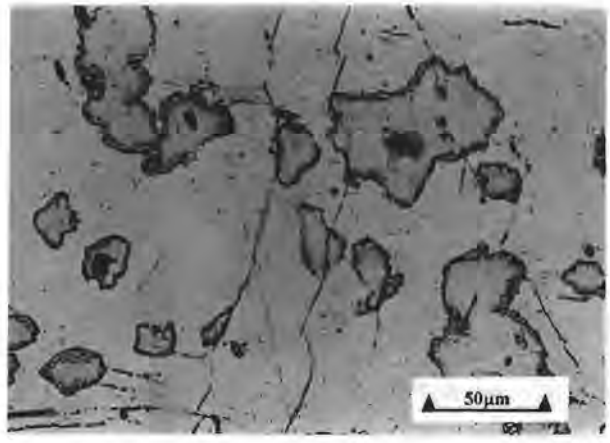

Figure 4.7. Optical micrograph of VF660 specimen after 50 minutes at 600°C, showing bulky sigma grains in a ferrite matrix.

Figures 4.8, 4.9 and 4.10 show the microstructure in VF245 specimens before the abrasion test. The microstructure in the heat treated specimens in VF245 also contained two phases as in VF660 specimens; however the percentage sigma grains in VF245 specimen heat treated for 30 minutes were greater compared to the equivalent specimen in VF660. Sigma grains in the VF245 specimen heat treated for 50 minutes were comparatively more massive with characteristic cracks showing clearly. Figure 4.8 is an optical micrograph of the as-received specimen showing ferrite grains similar as in Figure 4.5.

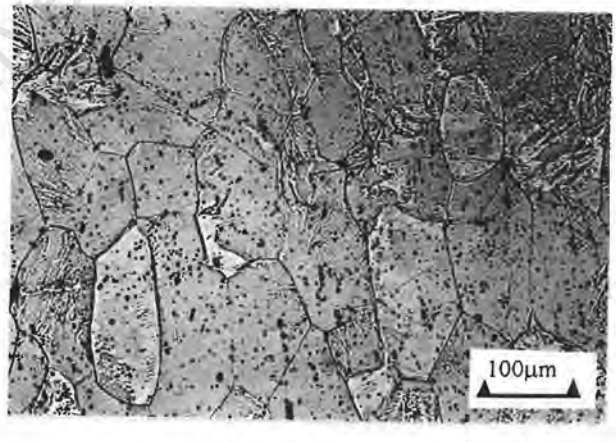

Figure 4.8. Optical micrograph of as-received VF245 specimen, showing ferrite grains.

Figures 4.9 and 4.10 are the optical micrographs of specimens heat treated for 30 minutes and 50 minutes at 600°C respectively; showing a two phase microstructure with different percentage volume of sigma in a ferrite matrix. Figure 4.9 shows the bulky sigma grains in ferrite matrix. Figure 4.10 shows cracks distributed across the sigma grains terminating at sigma-ferrite boundaries in the specimen heat treated for 50 minutes.

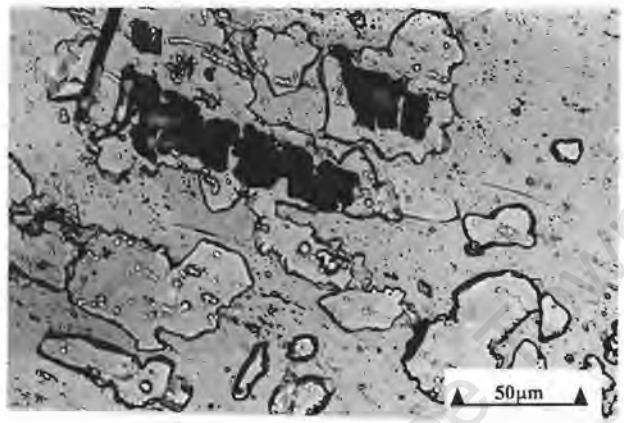

Figure 4.9. Optical micrograph of VF245 specimen after 30 minutes heat treatment at 600 °C, showing bulky sigma grains in ferrite matrix.

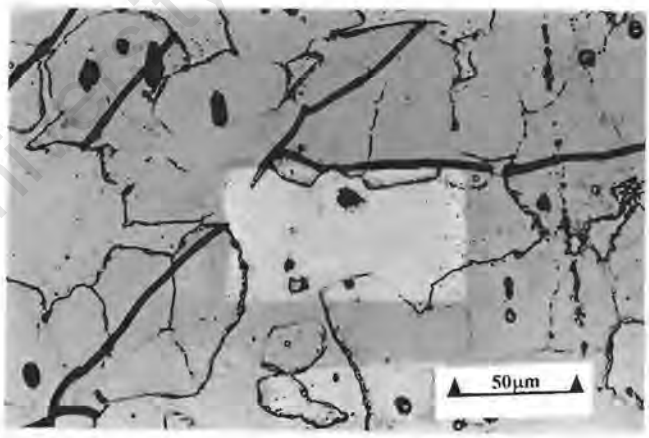

Figure 4.10. Optical micrograph of VF245 specimen after 50 minutes heat treatment at 600 °C, showing cracks distributed across bulky sigma grains in a ferrite matrix.

4.2 Abrasion Testing

Results of abrasion tests are presented as graphs of cumulative mass loss vs abrasion distance. The slope of these graphs thus represents the mass of material removed per unit abrasion distance. The measured cumulative mass loss showed a linear relationship with abrasion distance for all specimens; the slopes were determined using linear regression. Figures 4.11 and 4.12 show abrasion test results for ruthenium aluminide and MCV; the linear wear loss of ruthenium aluminide is observed to be half that of MCV.

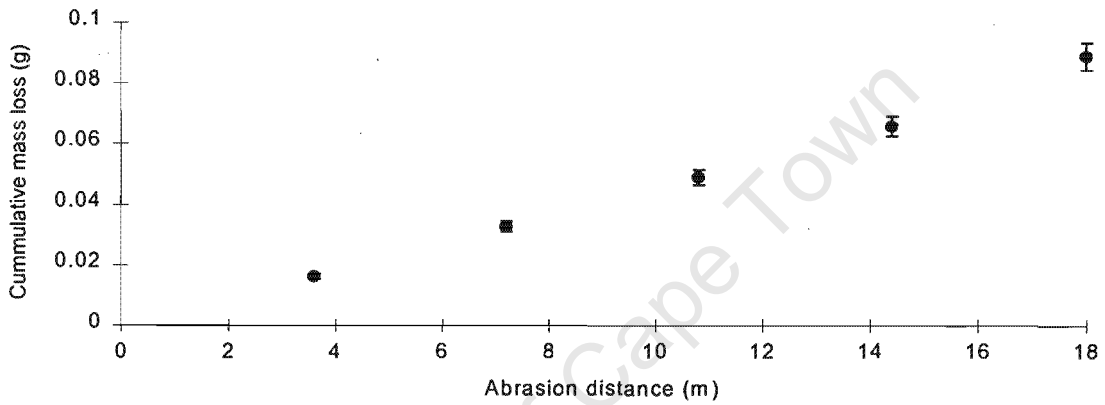

Figure 4.11. Cumulative mass loss vs abrasion distance for ruthenium aluminide, with a slope (or linear wear loss) of 0.005 g/m.

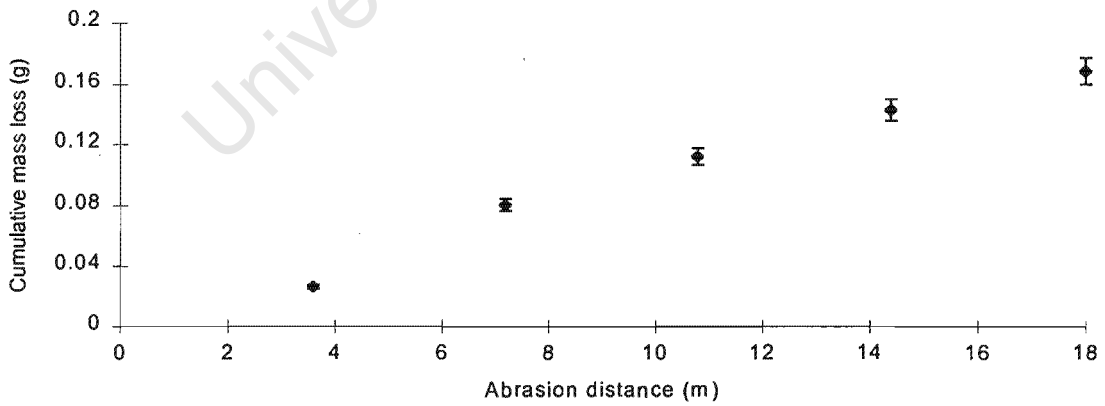

Figure 4.12. Cumulative mass loss vs abrasion distance for MCV, with a slope (or linear wear loss) of 0.010 g/m.

Figure 4.13 shows abrasion test results for the as-received VF660; the linear wear loss is greater than that of both ruthenium aluminide and MCV. Figure 4.14 shows abrasion test results for VF660 after heat treatment for 30 minutes; no change in linear weight loss is observed as a result of heat treatment, suggesting that the amount of the sigma phase present had no effect on the wear resistance.

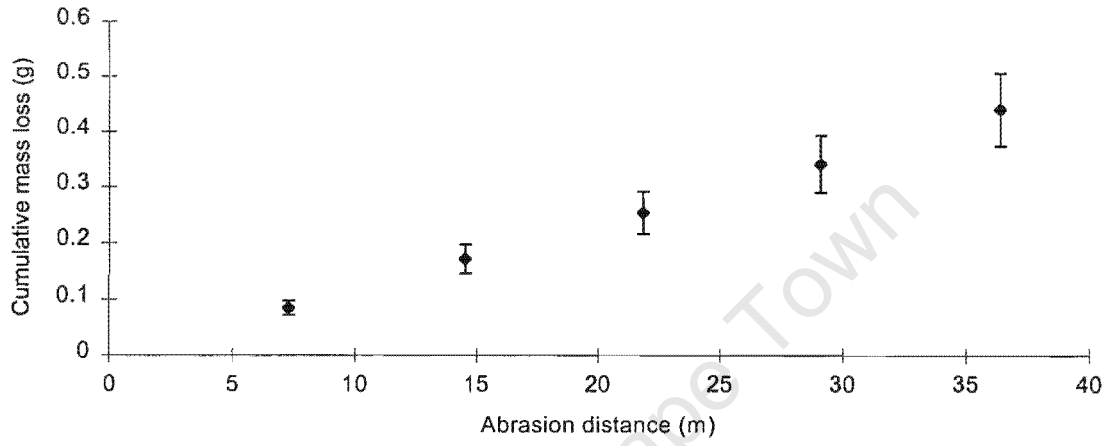

Figure 4. 13. Cumulative mass loss vs abrasion distance for VF660 in the as-received condition, with a slope (or linear wear loss) of 0.012 g/m.

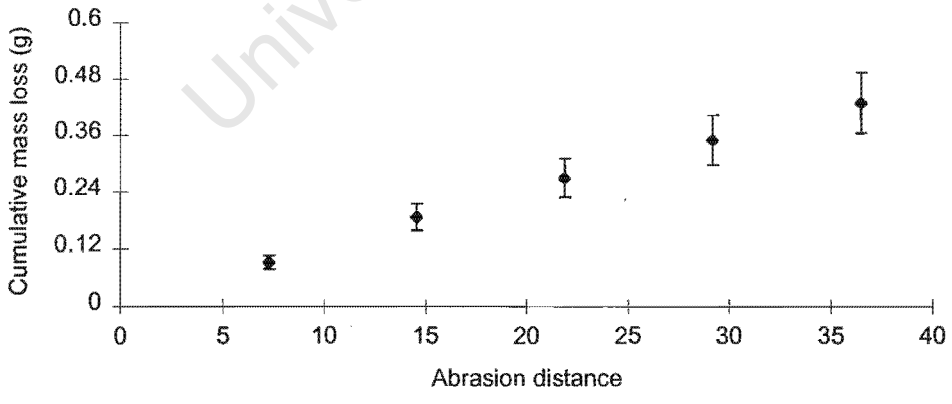

Figure 4. 14. Cumulative mass loss vs abrasion distance for VF660 after 30 minutes heat treatment at 600 °C, with a slope (or linear wear loss) of 0.012 g/m.

Figure 4.15 shows abrasion test results for VF660 specimens heat treated for 50 minutes. Linear wear in this specimen appears slightly reduced relative to specimens in the as-received condition and specimens heat treated for 30 minutes; however, the slope values for all three specimens of VF 660 are similar

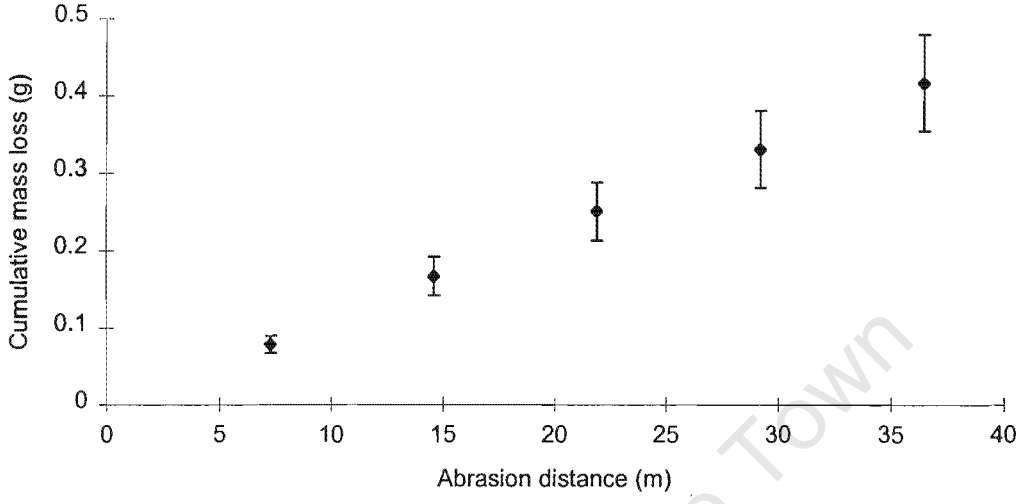

Figure 4.15. Cumulative mass loss vs abrasion distance for VF660 after 50 minutes heat treatment at 600°C, with a slope (or linear wear loss) of 0.011g/m.

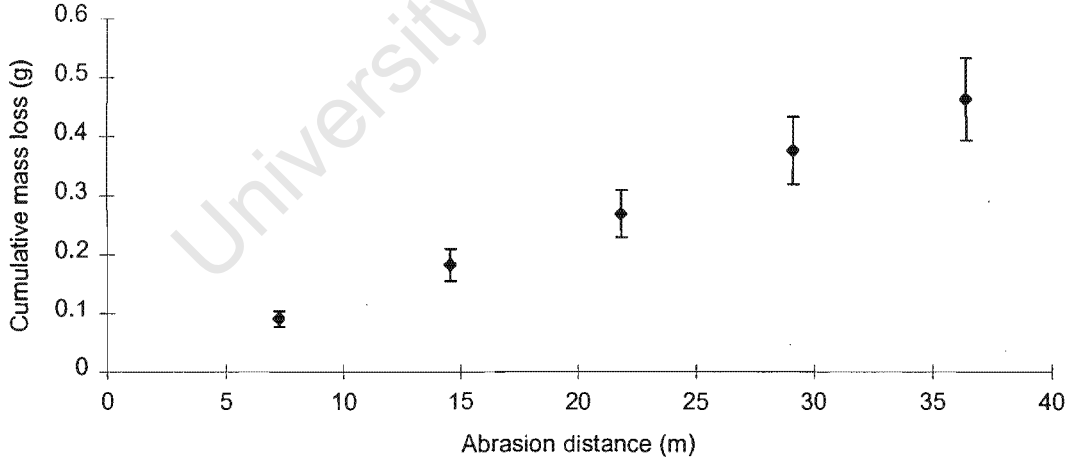

Figure 4.16. Cumulative mass loss vs abrasion distance for VF245 in the as-received condition, with a slope (or linear wear loss) of 0.012 g/m.

Figure 4.16 shows abrasion test results for VF245 in the as-received condition. The linear wear rate is the same as for VF660 in the as-received condition. Figures 4.17 and 4.18 show abrasion test results for VF245 specimen after 30 and 50 minutes heat treatment respectively. After each heat treatment there is a slight reduction in linear wear loss. The linear wear loss in the specimen heat treated for 50 minutes is equal to that of MCV.

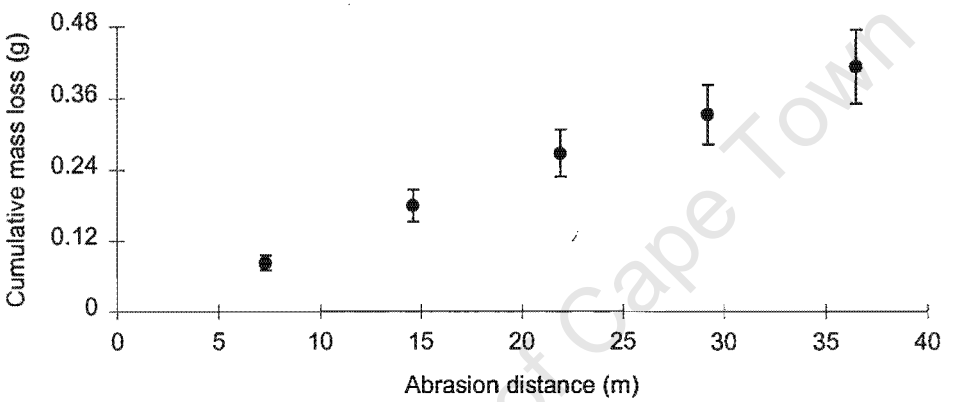

Figure 4.17. Cumulative mass loss vs abrasion distance for VF245 after 30 minutes heat treatment at 600℃, with a slope (or linear wear loss) of 0.011 g/m.

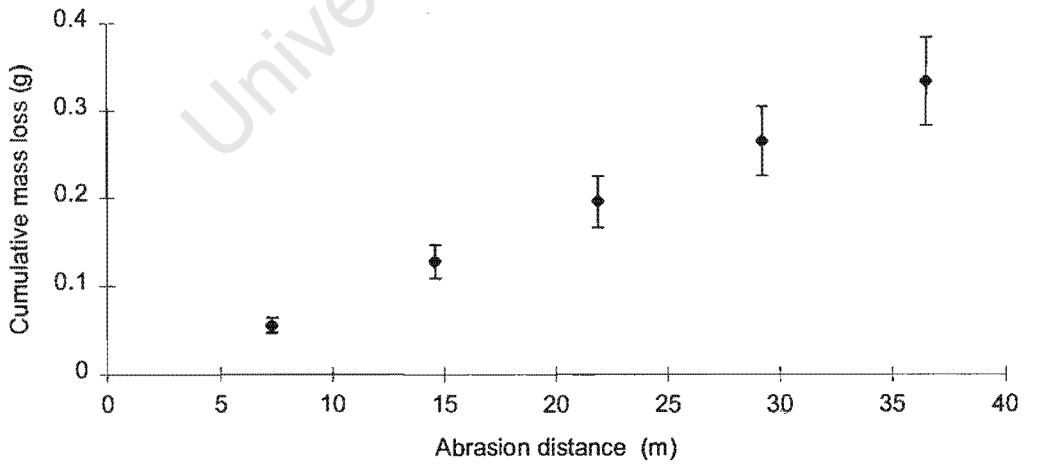

Figure 4.18. Cumulative mass loss vs abrasion distance for VF245 after 50 minutes heat treatment at 600℃, with a slope (or linear wear loss) of 0.010 g/m.

The volume wear rates in the specimens were determined by using the following density values: 7.89 g/cm^3 for ruthenium aluminide, 7.80 g/cm^3 for MCV and 7.7 g/cm^3 for ferritic samples. Figure 4.19 shows the volume wear rates for ruthenium aluminide and MCV. Figures 4.20 and 4.21 show the volume wear rates for the VF660 and VF 245 specimens respectively. Since the densities of the materials are similar, these graphs show the same trends noted for mass loss: ruthenium aluminide has a superior wear resistance to MCV and both ferritic steels; little change in the wear resistance of VF660 results from heat treatment; and VF245 shows a small but consistent decrease in wear rate with increasing heat treatment time.

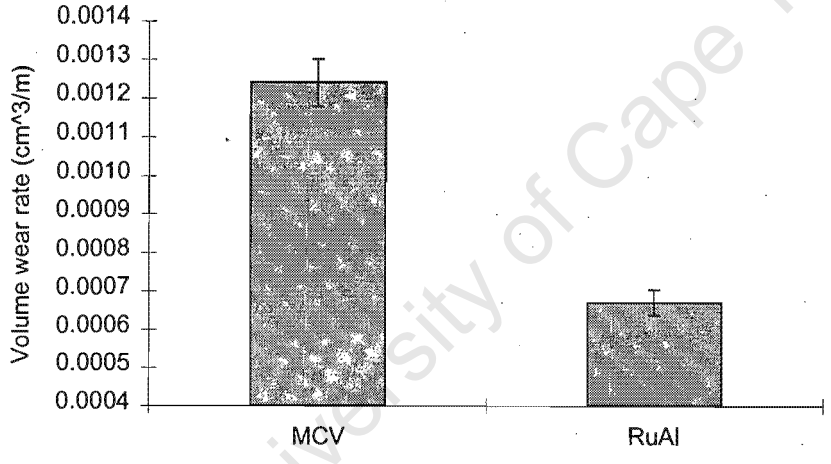

Figure 4. 19. Volume wear rate vs material type. MCV = medium carbon steel, RuAl = Ruthenium aluminide.

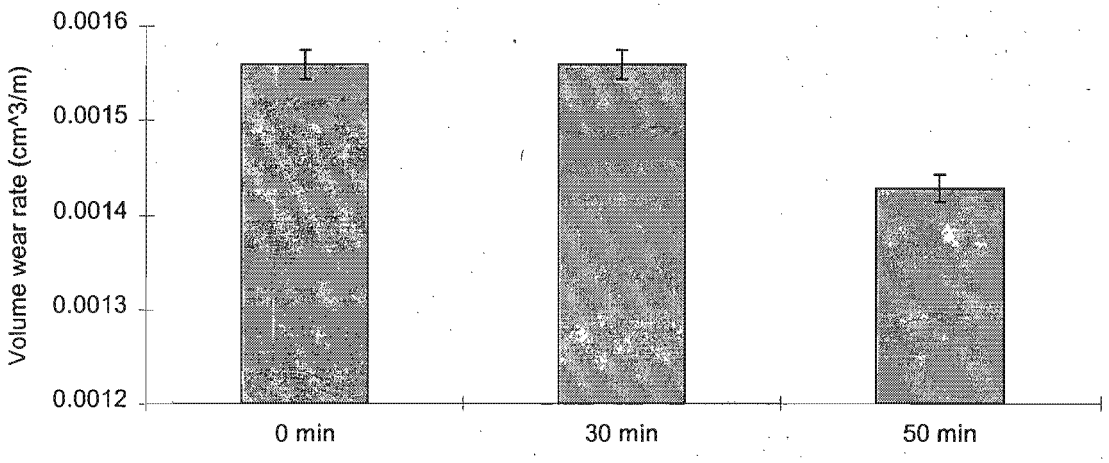

Figure 4. 20. Volume wear rate vs heat treatment time for VF660 samples. 0min = as-received sample (no heat treatment), 30min = 30 minutes , 50min = 50 minutes heat treatments

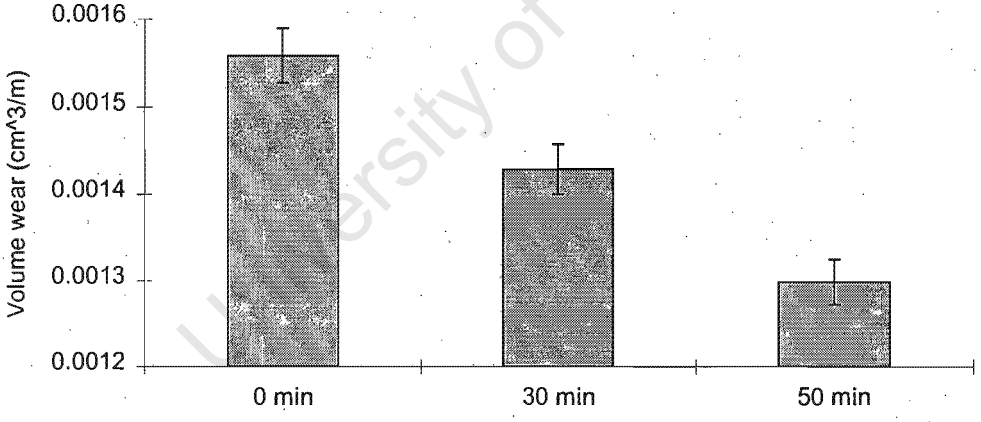

Figure 4. 21. Volume wear rate vs heat treatment time for VF245 samples. 0min = as-received sample (no heat treatment), 30min = 30 minutes , 50 min = 50 minutes heat treatments.

Figure 4.22 shows the graph of wear rate vs percentage sigma volume for VF660. The wear rate is lowest when the percentage sigma is less than 12% or greater than 25%. Figure 4.23 shows the graph of wear rate vs percentage sigma volume for VF245; the wear rate in this group decreases with increasing sigma volume.

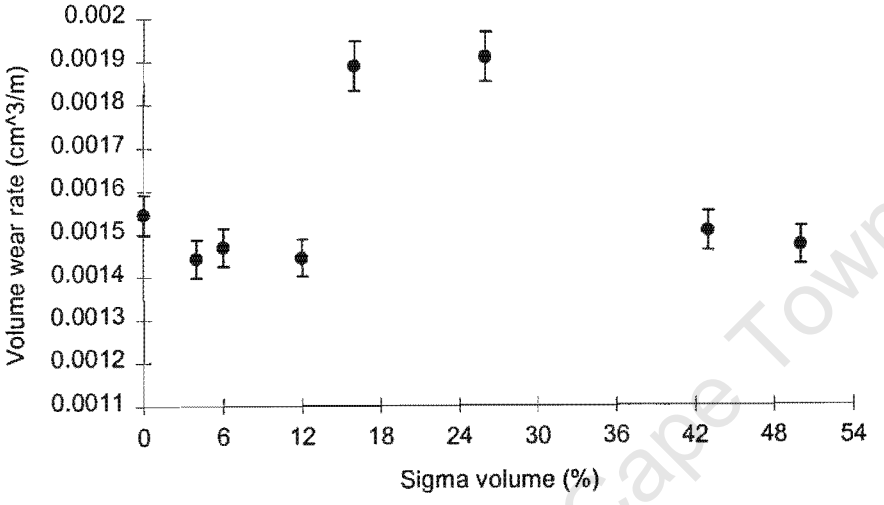

Figure 4.22. Volume wear rate vs percent sigma volume for VF 660 samples.

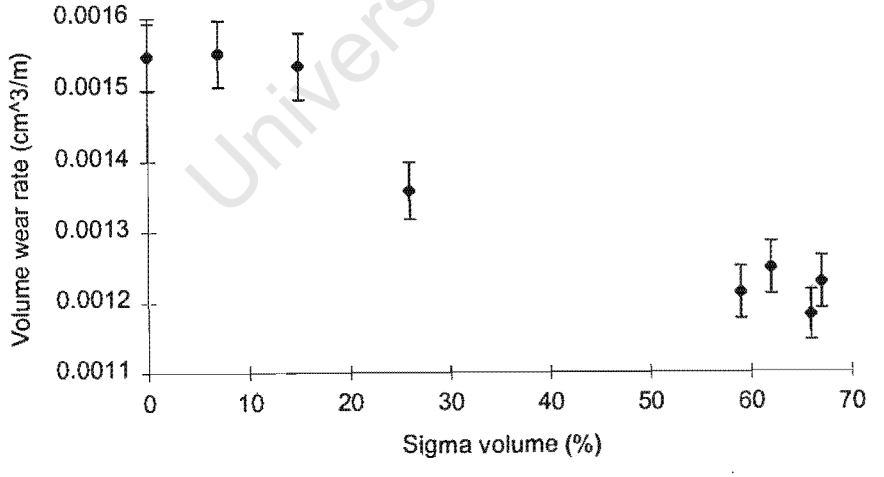

Figure 4.23. Volume wear rate vs percent sigma volume for VF 245 samples.

An overview of volume wear rates for different material types is presented in Figure 4.24. The ferritic specimen used in the comparison was the highest wear resistant in this (ferritic) group. Ruthenium aluminide was the most wear resistant amongst the test materials as indicated by its low volume wear rate.

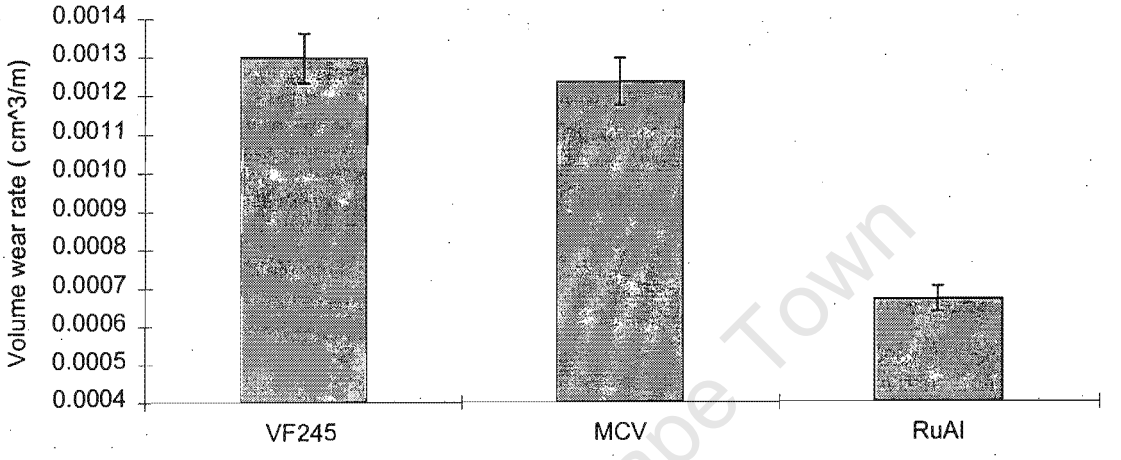

Figure 4. 24. Volume wear rate vs different types of materials. VF245 = The most wear resistant specimen in the ferritic group.

4.3 Condition Of Materials After Abrasion Testing

Subsurface microhardness was measured using a load of 25gf in order to determine if work-hardening had occurred and the depths to which it had persisted in the specimens. Increased microhardness values were observed within depths of 100 microns of the abraded surface, confirming that work-hardening had occurred as a result of abrasion. Figures 4.25 and 4.26 show the microhardness vs depth graphs for ruthenium aluminide and MCV respectively, after 18 meters of abrasion.

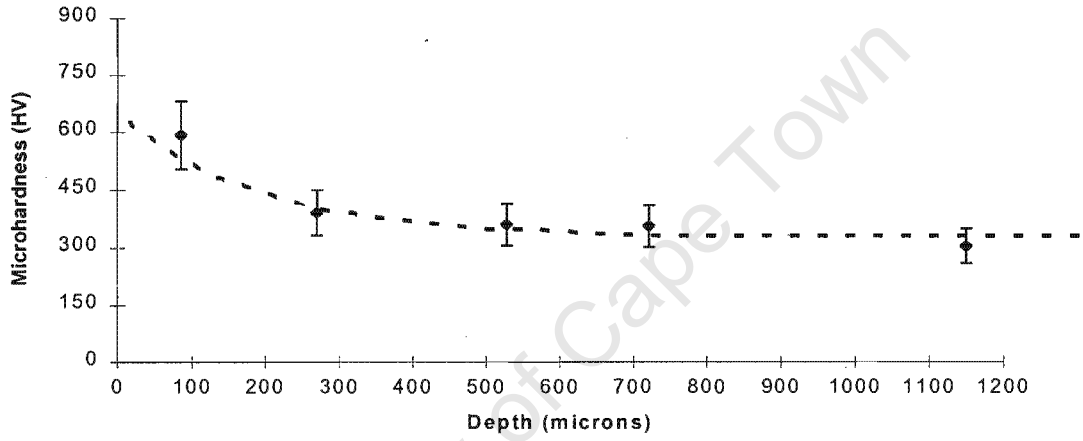

Figure 4.25. Microhardness vs depth graph for ruthenium aluminide after abrasion.

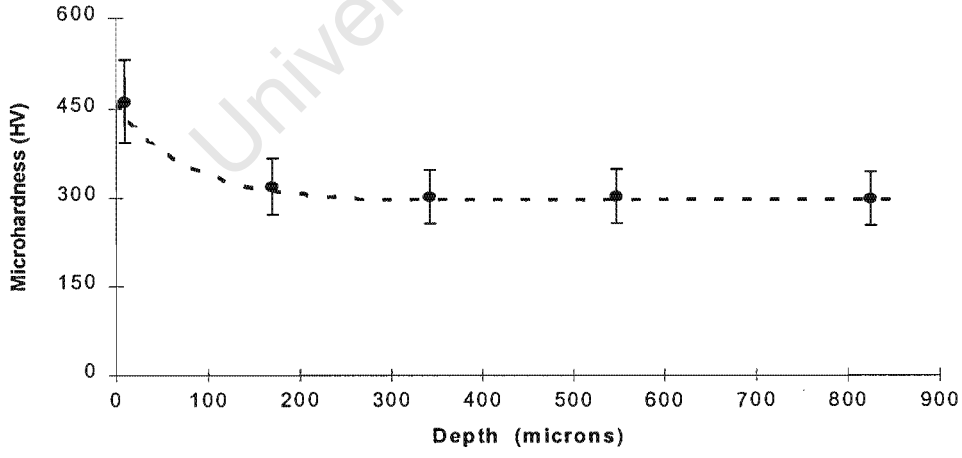

Figure 4.26. Microhardness vs depth graph for MCV after abrasion.

The microhardness graphs of ferritic steel specimens tested in their as received condition showed a similar trend to that shown by ruthenium aluminide and MCV. Figure 4.27 shows microhardness vs depth for VF660 in the as-received condition. Ferritic steel specimens heat treated at 600°C for 30 minutes and 50 minutes consisted of both ferrite and sigma phases. Microhardness measurements, which reflect the hardness of individual phases, show that both ferrite and sigma work-hardened as a result of abrasion. Figures 4.28 and 4.29 show the microhardness vs depth graphs of VF660 with the two phases plotted separately but on the same system of axes for 30 minutes and 50 minutes heat treated specimens respectively.

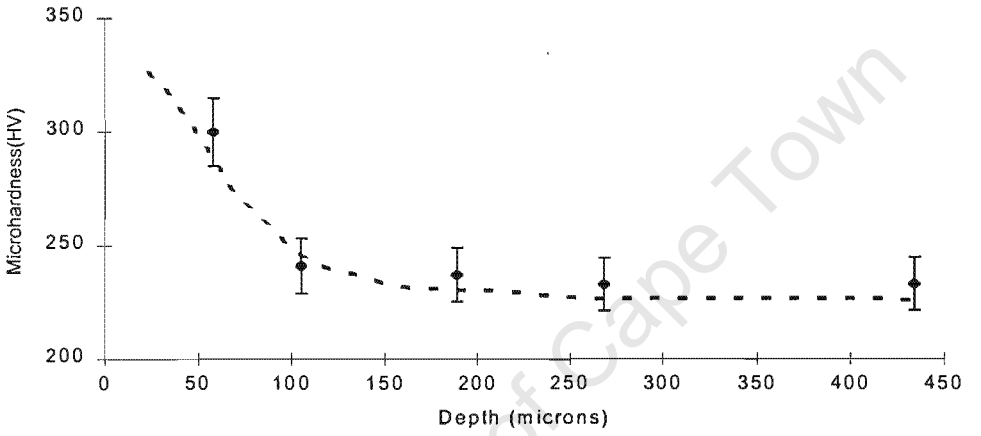

Figure 4.27. Microhardness vs depth graph after abrasion for VF660 specimen in the as-received condition.

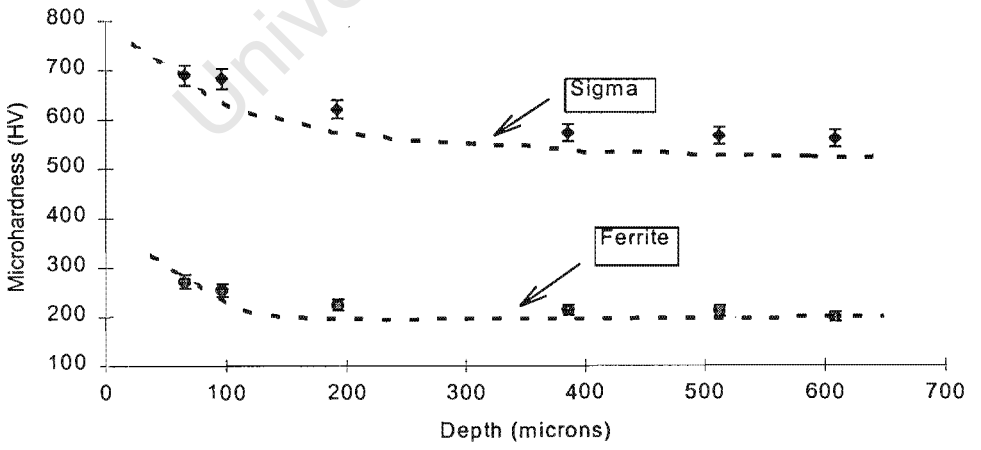

Figure 4. 28. Microhardness vs depth graphs after abrasion for VF660 specimen heat treated for 30 minutes at 600°C.

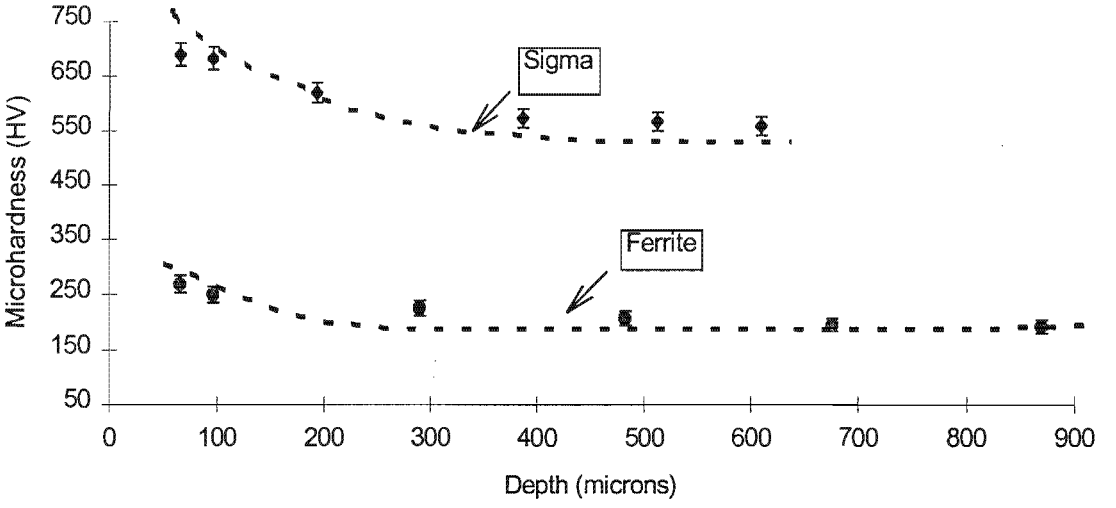

Figure 4.29. Microhardness vs depth graphs after abrasion for VF660 specimen heat treated for 50 minutes at 600°C.

Figure 4.30 shows microhardness vs depth graph for VF245 specimen in the as received condition. Similarly as in 30 minutes and 50 minutes heat treated specimens of VF660 the equivalent specimens of VF245 had two phases with completely different microhardness values. Figures 4.31 and 4.32 show the microhardness vs depth graphs of VF245 with the two phases plotted separately but on the same system of axes for 30 minutes and 50 minutes heat treated specimens respectively.

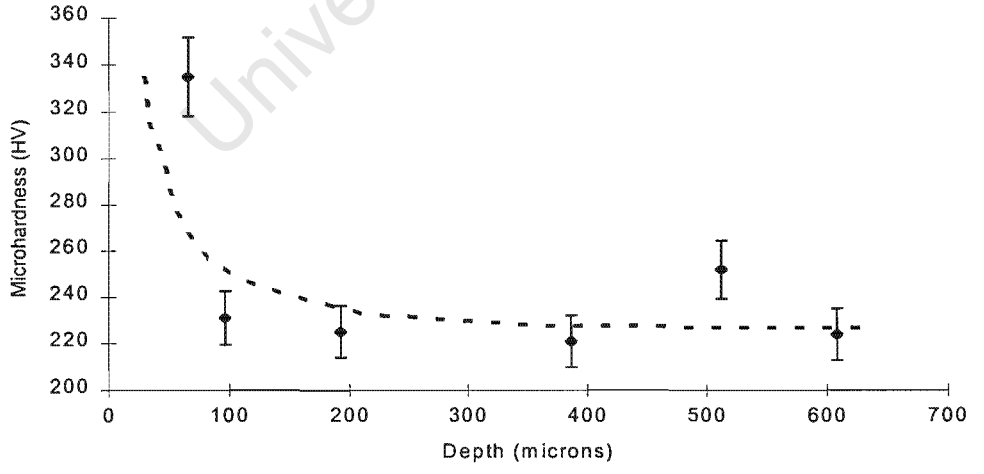

Figure 4.30. Microhardness vs depth graph after abrasion for VF245 in the as-received condition.

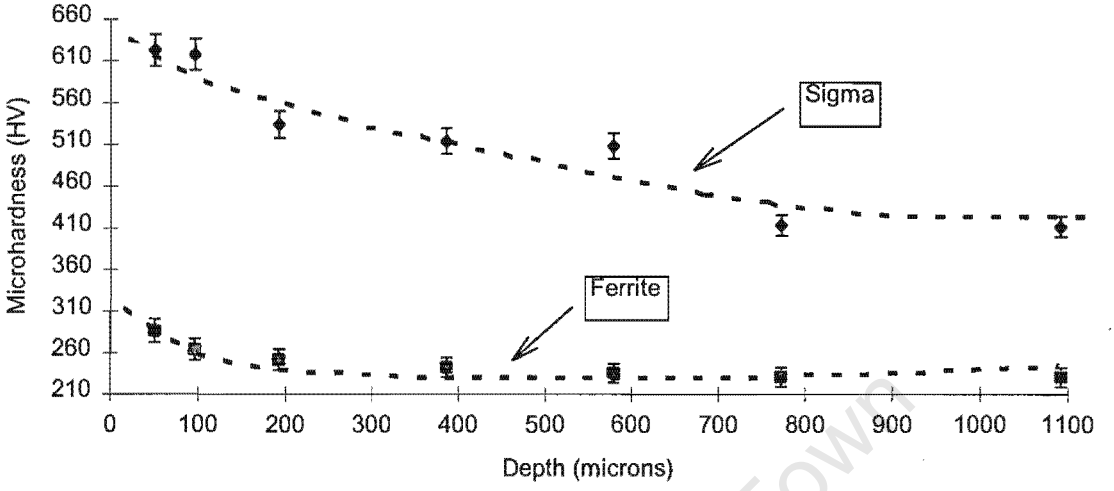

Figure 4.31. Microhardness vs depth graphs after abrasion for VF245 specimen heat treated for 30 minutes at 600 °C.

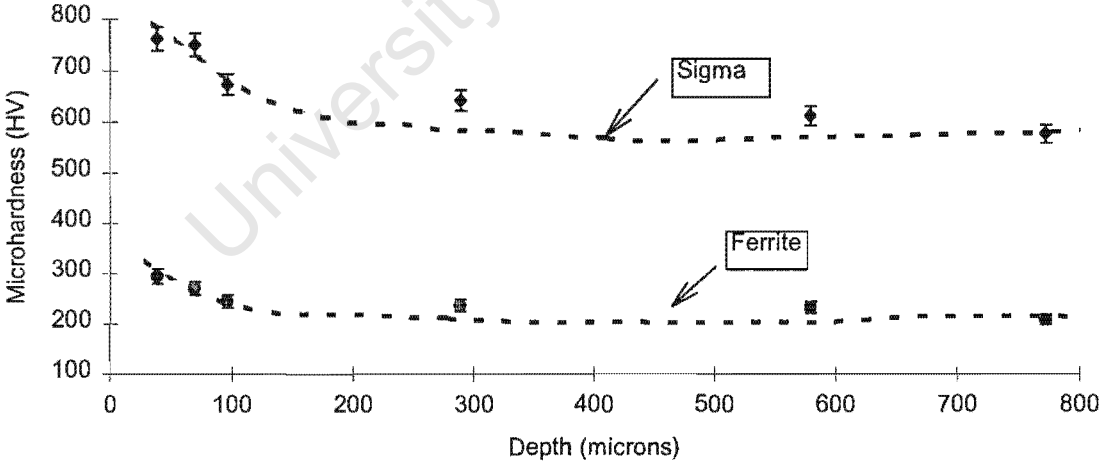

Figure 4.32. Microhardness vs depth graphs after abrasion for VF245 heat treated for 50 minutes at 600 °C.

After abrasion testing, the specimen surfaces were characterised using scanning electron microscopy. The abraded surfaces of ruthenium aluminide specimens were dominated by cracking, whereas all other specimens showed ductile modes of damage. Figures 4.33 and 4.34 are scanning electron micrographs of ruthenium aluminide after 18 meters of abrasion, showing that crack formation and propagation occurred as a result of the wear process. After the same length of abrasion, MCV in contrast showed evidence of material loss by ploughing and cutting, as shown in figures 4.35 and 4.36.

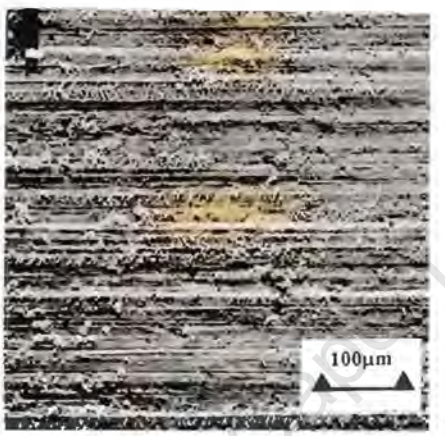

Figure 4.33. Scanning electron micrograph of the abraded surface of ruthenium aluminide, showing grooves and small multiple cracks.

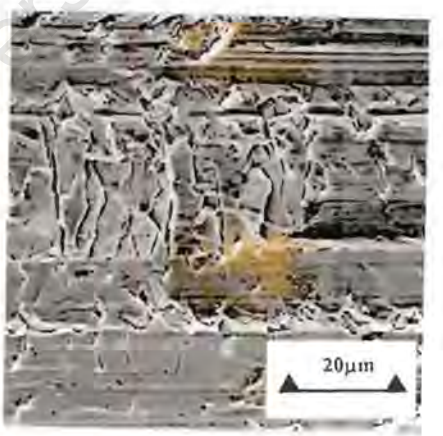

Figure 4. 34. Scanning electron micrograph of the abraded surface of ruthenium aluminide at high magnification, showing cracks that had formed on the surface after abrasion.

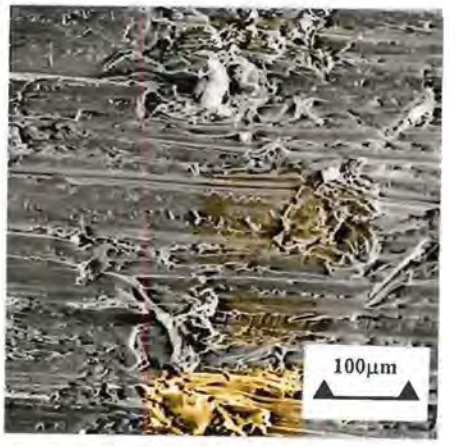

Figure 4. 35. Scanning electron micrograph of the abraded surface of MCV, showing wear grooves and debris.

Figure 4. 36. Scanning electron micrograph of the abraded surface of MCV at high magnification, showing a large debris particle lying across the wear grooves.

The surface response to abrasion of the VF660 specimens was similar in both the as-received and the heat treated specimens in spite of the presence of the hard sigma phase in the latter. The various percentage sigma volume in the heat treated specimens neither showed any difference in abrasion response between the specimens. Figure 4.37 is the scanning electron micrograph of the abraded surface of VF660 specimen in the as-received condition after 36 meters of abrasion, showing evidence of material loss by ploughing and cutting. Figures 4.38 and 4.39 are respectively the scanning electron micrographs of the abraded surfaces of the 30 minutes and 50 minutes heat treated specimens of VF660 after the same length of abrasion, showing similar features as in the as-received specimen of the same group.

Figure 4. 37. Scanning electron micrograph of the abraded surface of VF660 in the as-received condition, showing wear grooves and debris.

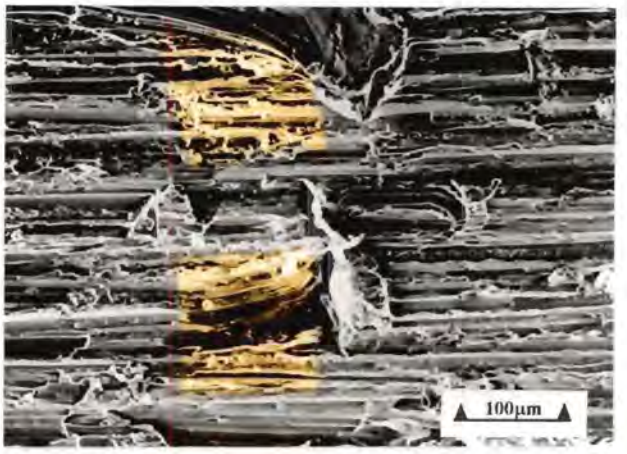

Figure 4. 38. Scanning electron micrograph of the abraded surface of VF660 specimen heat treated for 30 minutes, showing ductile shear lips, wear grooves and debris.

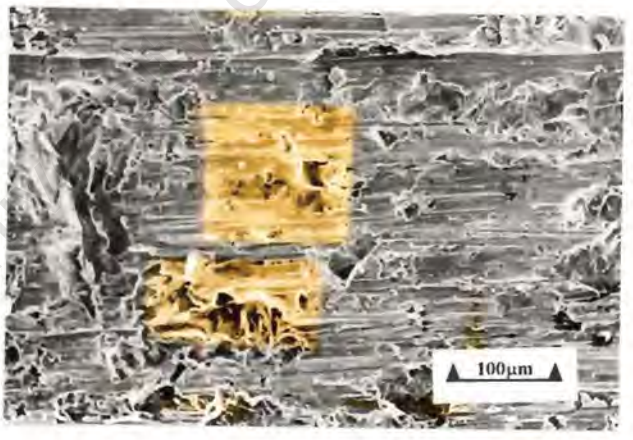

Figure 4.39. Scanning electron micrograph of the abraded surface of VF660 specimen heat treated for 50 minutes, showing debris covering the wear grooves.

The surface abrasion response of the VF245 specimens was similar to that shown by the VF660 specimens in both the as-received and heat treated conditions. The specimens were abraded for 36 meters and the material loss in these specimens was also by ploughing and cutting which is indicated by the ductile working of the surfaces. Figure 4.40 is the scanning electron micrograph of the abraded surface of the as-received specimen of VF245 after abrasion. Figures 4.41 and 4.42 are the scanning electron micrographs of the abraded surfaces of the 30 minutes and 50 minutes heat treated specimens after the same length of abrasion.

Figure 4.40. Scanning electron micrograph of the abraded surface of VF245 in the as-received condition, showing wear grooves and debris.

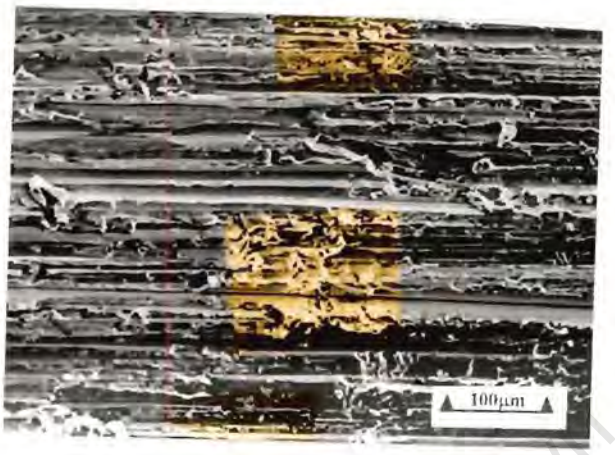

Figure 4. 41. Scanning electron micrograph of the abraded surface of VF245 specimen heat treated for 30 minutes, showing less ductile working than on an equivalent VF660 specimen.

Figure 4. 42. Scanning electron micrograph of the abraded surface of VF245 specimen heat treated for 50 minutes, showing wear grooves and comparatively less debris.

4.4 Mechanical Testing

Mechanical compression testing was conducted on the specimens in order to determine their rate of work-hardening. True-stress vs. true-strain curves were used to produce work-hardening rate vs. strain curves; the slopes of these curves, determined by linear regression analysis, were in turn used to determine the work-hardening coefficients. Figures 4.43 and 4.44 are the true-stress vs true-strain graphs for ruthenium aluminide and MCV respectively.

Figure 4.43. True stress vs. true strain curve for ruthenium aluminide, showing a yield point at approximately 500 MPa.

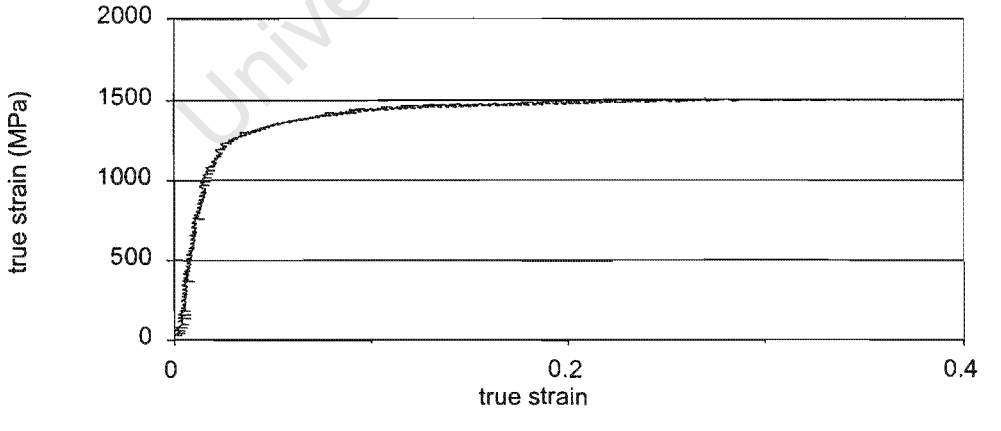

Figure 4. 44. True stress vs. true strain curve for MCV, showing a yield point at approximately 1250 MPa.

Figure 4.45 shows true-stress vs. true-strain curves for the VF 660 specimens in the as-received and heat treated conditions. The presence of sigma phase in the heat treated specimens is seen to have little effect on the yield point. Figure 4.46 similarly shows true-stress vs. true-strain curves for the as-received and heat treated VF245 specimens. The as received specimen shows a slightly higher yield point than the heat treated specimens in both groups.

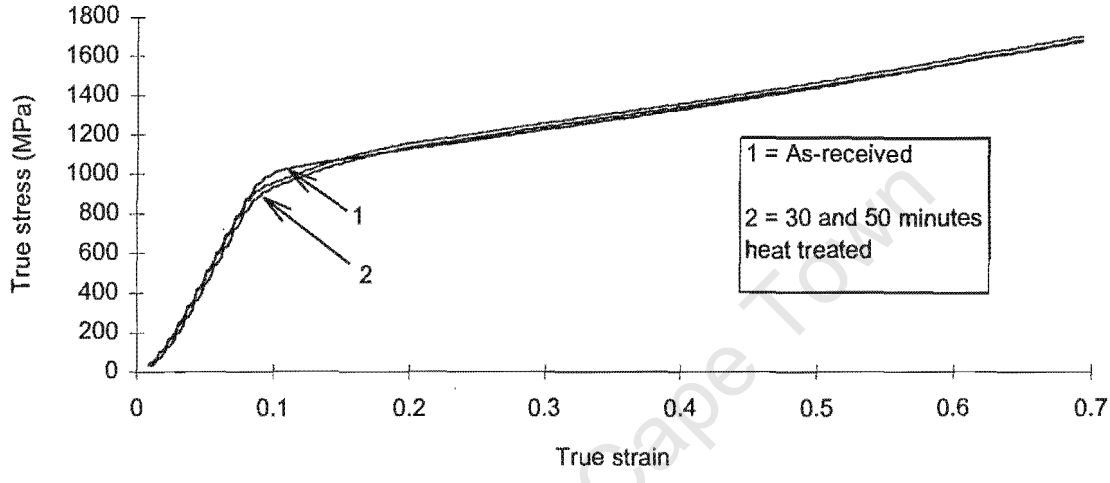

Figure 4. 45. True stress vs true strain curves for VF660 specimens on the same system of axes in the as-received and heat treated conditions, showing similar yield points.

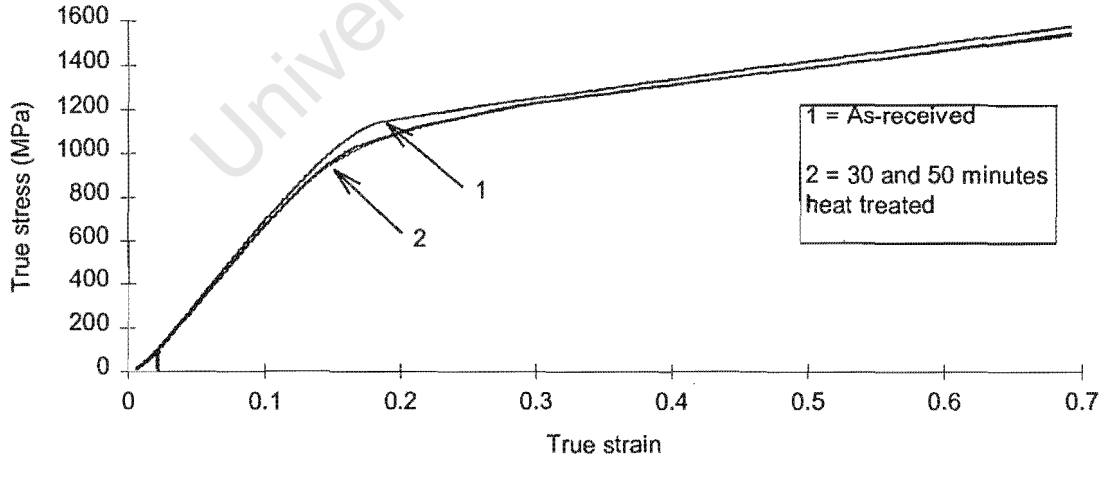

Figure 4. 46. True-stress vs true-strain curves for VF245 specimens on the same system of axes in the as-received and heat treated conditions, showing similar yield points.

Figure 4.47 is the work-hardening rate vs true strain graphs for ruthenium aluminide and MCV on the same system of axes, showing that the work hardening rate in ruthenium aluminide is superior than in MCV for the same amount of strain. The respective coefficients of work-hardening (or slopes values) of 4.34 x 10^{11} (Pa) and 3.15 x 10^{11}(Pa) confirmed the superiority of ruthenium aluminide.

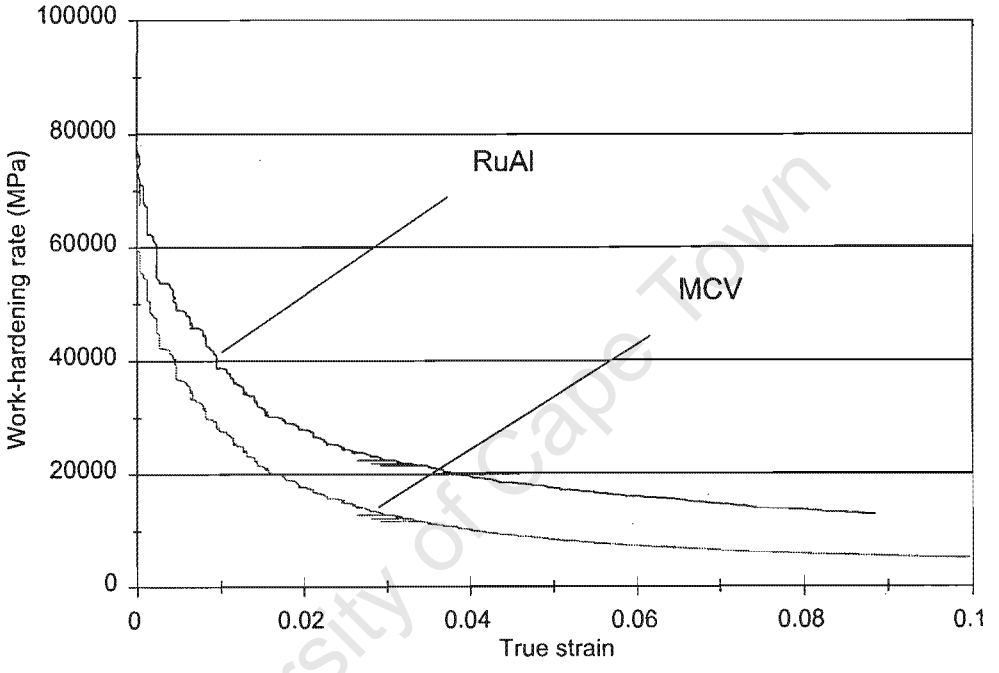

Figure 4.47. The work-hardening rate vs strain for ruthenium aluminide and MCV on the same system of axes.

Figures 4.48 and 4.49 are the work-hardening rates vs true-strain curves for VF660 and VF245 respectively. Figure 4.48 is the work-hardening rates of the as-received and heat treated specimens; the work-hardening rates of the two heat treated specimens are superimposed on one another as shown by curve 2. For the same amount of strain VF660 specimens show similar rates of work-hardening. The work-hardening coefficients for the specimens are: 9.5 x 10^3 (MPa) for the as-received specimen, 8.7 x 10^3 (MPa) for the 30 minutes heat treated specimen and 9.3 x 10^3 (MPa) for the 50 minutes heat treated. The rates of work-hardening in VF245 specimens show the as-received specimen with slightly higher rate than the heat treated specimens for lower strain values. The work-hardening coefficients in this group are: 3.7 x 10^4 (MPa) for the as- received specimen, 1.04 x 10^4 (MPa) for the 30 minutes heat treated specimen and 1.2 x 10^4 (MPa) for the 50 minutes heat treated specimen..

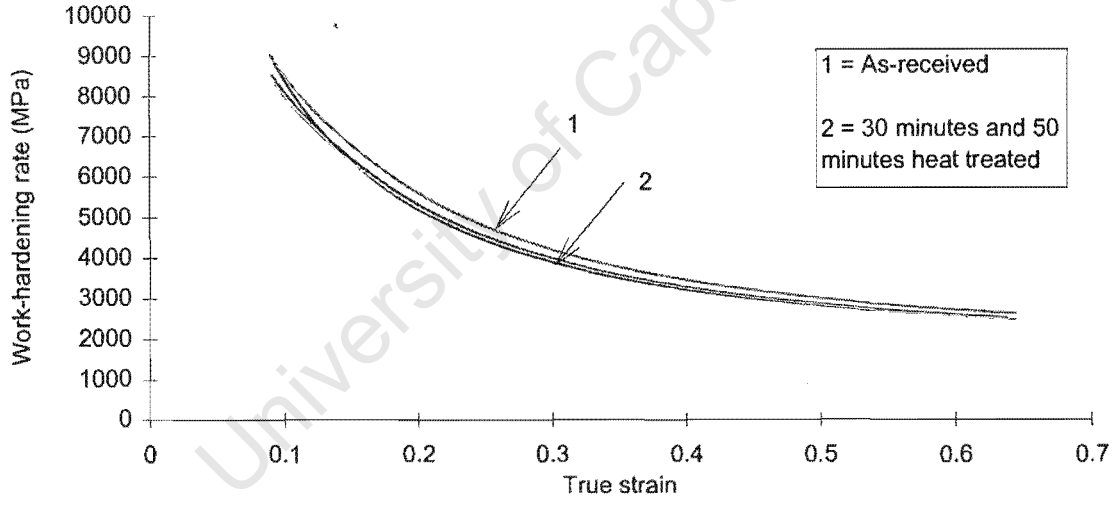

Figure 4. 48. The work-hardening rates for VF 660 specimens on the same system of axes.

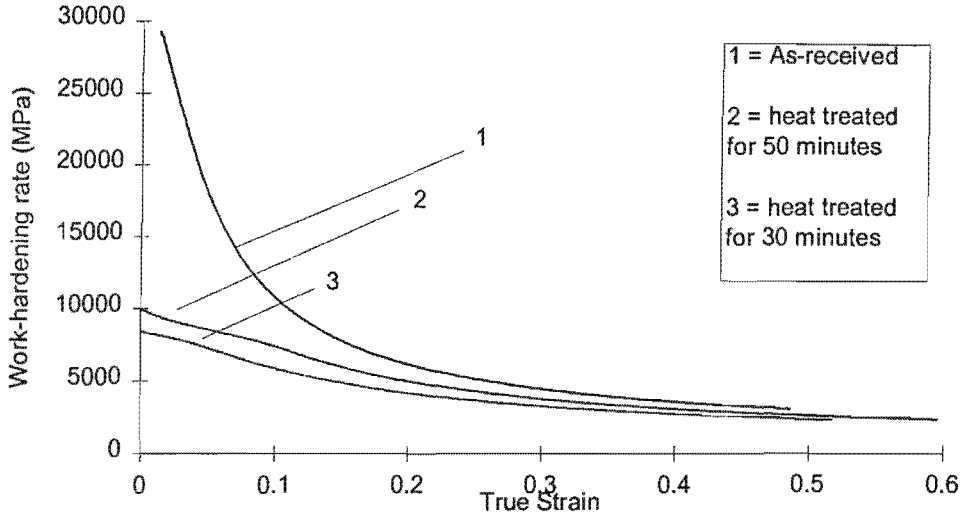

Figure 4. 49. The work-hardening rates for VF 245 specimens on the same system of axes.

CHAPTER 5: DISCUSSION

Under the same conditions of abrasive wear, the materials investigated showed different wear rates and different mechanisms by which material was lost from their operating surfaces. In Chapter Four, quantitative wear results for all specimens were presented in terms of the wear rate. In order to understand the results, in the present discussion the term wear resistance has been used to facilitate a comparison of the different types of materials tested. Wear resistance is by definition the inverse of the wear rate, so that the lower the wear rate in a material the higher will be its wear resistance and *vice versa*.

5.1 Abrasive Wear Of RuAl And MCV

Ruthenium aluminide and MCV have similar bulk hardness; however the results of this study have shown that the wear resistance of ruthenium aluminide is superior to that of MCV. It is clear from these results that the initial bulk hardness of these materials played a minimal role in their abrasive wear resistance. In addition to the difference in wear resistance, different mechanisms of wear were observed in ruthenium aluminide and MCV, as presented in the electron micrographs of the specimens after abrasion (Figures 4.33 and 4.35).

Contrary to bulk hardness, the hardness attained on the surface during abrasion showed a strong relationship with wear resistance. This was established from microhardness results obtained from tapered sections of specimens after abrasion. These results showed that ruthenium aluminide developed a high microhardness in the surface and subsurface region, to a depth of 100 microns, as a result of abrasion. The surface microhardness of MCV was comparatively lower. Indeed, a comparison of ruthenium aluminide with all other specimens investigated showed that it had the highest surface microhardness after abrasion. The surface work-hardening was accordingly the highest in ruthenium aluminide, which showed the greatest wear resistance. The role played by surface work-

hardening during the abrasion process has been supported by many workers [25, 28]. Compression tests were used to determine the rates at which work-hardening occurred in the individual specimens. The results of compression tests further showed ruthenium aluminide to have a superior work-hardening coefficient to MCV and ferritic steel specimens. This indicated that ruthenium aluminide had an exceptional rate of work-hardening in addition to the high surface microhardness after abrasion.

In spite of exceptional abrasive wear resistance qualities shown in ruthenium aluminide, its mechanism of wear is a source of concern because of the microcracks observed after abrasion (Figure 4.34). This may lead to rapid deterioration as material removal by abrasive wear may be enhanced by corrosion attack on the new surfaces exposed by the microcracks; fatigue failure may also be highly possible if cyclic stress are introduced. Electron micrographs of the surface after abrasion showed ruthenium aluminide to be characterised by little plastic deformation, indicating that it is a brittle material. The cracks observed in ruthenium aluminide are indicative of the brittle nature and response of this material to abrasive wear. The cracking during and after abrasion may be due to the high strain imposed by the abrasion process or coalition of pores inherent in ruthenium aluminide from the production process. A further source of cracking could be the mismatch strain that can arise between the work-hardened surface and the neighbouring less-deformed microstructure[98].

In order to optimise the wear resistance in ruthenium aluminide it may be necessary to reduce stress concentrators which initiate fracture such as porosity. This can be achieved by improving the production process of ruthenium aluminide to yield densities closer to the ideal.

The wear mechanism in MCV was dominated by both ploughing and cutting of the surface as shown in electron micrographs of the specimen after abrasion (Figure 4.35). The type of response shown by MCV, in which plastic deformation is dominant, is to be expected in ductile materials such as metals and steels.

Mulhearn and Sedriks[16] suggested that there is a transition between the cutting and ploughing modes of wear based on the attack angle. They maintained that if the attack angle (which is the angle between the surface and the front face of abrasive) is above a certain critical value, cutting occurs readily. If the angle is below this critical value of the attack angle ploughing will dominate. The fact that the two distinct modes of wear occurred together in MCV suggests that there were different angles at which the abrasive particles were oriented relative to the surface.

5.2 Abrasive Wear Of Ferritic Steels

Heat treatment procedures were identified and used to produce a dual phase microstructure consisting of the harder sigma phase in a ferrite matrix. The sigma-ferrite dual phase microstructure was aimed for because microstructures consisting of a harder phase and a relatively softer matrix (such as WC-Co) have been used successfully as wear resistant materials in numerous applications. It is known that sigma phase occurs in ferritic steel at certain temperatures, and the higher hardness of sigma in the relatively softer ferrite matrix appeared to present a similar system to WC-Co. An optical micrograph of the heat treated ferrite specimen containing sigma phase showed that cracks in the sigma phase characteristically terminated at the ferrite-sigma grain boundaries (Figure 4.10). Microhardness results of the dual phase specimens showed sigma to have a much greater hardness than ferrite. The heat-treated ferritic steels accordingly possessed the desirable combination of hardness and ductility; it was thus of interest to investigate whether these materials offer advantages similar to systems such as WC-Co in abrasive wear

Both phases in the microstructure of ferritic steels work-hardened during the abrasion process; sigma work-hardened more than ferrite as was shown in the microhardness measurements. The work-hardening coefficients in VF660 and VF245 specimens containing sigma phase were lower compared to the as-received specimens of the same

samples. However within each group (i.e. VF660 and VF245) the work-hardening coefficients were comparable between the heat treated specimens.

Abrasion wear resistance in ferritic steels was considered by comparing the as-received (ferritic phase) to the heat treated (dual phase) specimens. It was found that abrasion resistance initially showed a slight improvement when percentage of sigma phase in the microstructure is above approximately 10% in VF245. A similar trend was observed in VF660 when percentage sigma phase is above approximately 20%. A comparison between the two ferritic steels groups showed that the 50 minutes heat treated specimen in the VF245 group was overall the most wear resistant compared to other test specimens. It was also found that the abrasion resistance in this specimen was comparable to that of MCV.

It was expected that as percentage sigma phase increases in the microstructure its reinforcing strength as a hard phase will become more pronounced. On the contrary it was found that the relatively high concentration of sigma had little effect on the abrasion resistance in the ferritic steels. There are a number of possible factors which may have caused sigma to be ineffective. For example cracks on sigma suggested that it is a brittle phase with a possible low fracture toughness.

Work by Hutchings [35], Wayne *et al* [36] showed (through mathematical models) that fracture toughness in the abrasive wear of brittle material was a significant factor that needs serious consideration. According to the simplified models [35, 36] a brittle material with a relatively higher fracture toughness will result in a low wear rate and *vice versa* for a relatively low fracture toughness material. In the case of sigma, the introduction of a high percentage volume of this hard phase was accompanied by a reduction in the abrasion resistance (VF660) or resulted in a smaller gain than expected (VF245). The reason could possibly be that sigma is less tough and that this factor dominated over its potential reinforcing hardness.

Other factors that may have contributed to the ineffectiveness of sigma as a reinforcing phase in the ferritic microstructure although not easily evident include: The possible preferential removal of sigma phase during abrasion (a type of problem that is not uncommon in multiphase materials). Another cause could be the nature of coherency between the reinforcing phase and the matrix, that is, if the interface is weak it could have possibly contributed to the reduction in the abrasion resistance in the ferritic steels specimens.

Surface characterisation in all ferritic steel specimens after abrasion showed that the wear mechanism was dominated by cutting and ploughing. The wear mechanism was similar in spite of the amount of sigma present in the microstructure; confirming that sigma had a limited effect in the abrasion behaviour of ferritic steel specimens, and did not play the reinforcing role envisaged.

5.3 Wear Models

Wear models involving abrasive wear at a microscopic level were an important step in understanding the effects that often lead, for example, to replacement of worn parts, failure of engineering components etc. These models have also contributed to the notion of designing better wear resistant components. Archard's mathematical model was one of the first to quantify abrasive wear in materials such as metals [23]. His equation essentially suggested that, wear rate was directly proportional to the load applied during the process of wear and inversely proportional to the bulk hardness of the material as indicated in equation 5.1.

$$Q = \frac{KW}{H} \qquad \textbf{Equation 5. 1}$$

Where Q = Wear rate
K = Severity index constant
W = Total load
H = Hardness

Equation 5.1 encompasses processes such as ploughing, cutting and fracture mechanism of wear with their respective geometrical conditions [33, 16]. This model was used in abrasive system involving metals and was supported by Kruschov [38] who showed that the equation holds true for commercially pure metal elements. The model however fell short in predicting abrasive wear rates involving ruthenium aluminide, MCV and ferritic steel specimens in the present work. This was mainly because the equation predicts a linear relation between the wear rate and bulk hardness. Results obtained for ruthenium aluminide and MCV showed on the contrary that in spite of similar bulk hardness between these materials, their wear rates were different with the latter showing comparatively weaker wear resistance. In ferritic steels, results showed that wear rates were not significantly affected by the increased bulk hardness conferred by the presence of sigma. The results showed that the surface hardness obtained during the abrasion process conformed better with wear resistance than initial bulk hardness, that is, the higher the final surface hardness (work-hardened hardness) the better the wear resistance. These factors show that the relationship between wear rate and hardness is more complex than suggested in equation 5.1, as suggested by other workers [25, 28, 99].

5.4 Wear Of Inhomogeneous Materials

Research for wear resistant materials has lead to the designing of artificial microstructures in materials such as composites for application in various wear environments. Principles such as the linear law of mixture were introduced in order to explain wear behaviour of composites under certain load distribution conditions. For example, when the load in a composite or any material with an inhomogeneous microstructure is largely borne by the harder and reinforcing phase, wear resistance increases [37]. This is providing the reinforcing phase in the microstructure is harder than the abrasive medium. Another principle based on the load distribution during the abrasion process is the inverse rule of mixture that is described in equation 5.2 [38].

$$Q^{-1} = \sum fv_i Q_i^{-1}$$ **Equation 5. 2**

Where Q^{-1} = Wear resistance (inverse of wear rate) of the material

fv_i = volume fraction of the reinforcing components

Q_i^{-1} = Individual wear resistance of the reinforcing components

Equation 5.2 suggests that the total wear resistance of a composite or inhomogeneous material is the sum product of the volume fraction and wear resistance of the reinforcing constituents of the material. It also predicts that the total wear resistance in the composite increases with the volume fraction of the reinforcing constituents. In the work presented here, however, an increase in the volume fraction of sigma phase in ferritic steels does not significantly increase the total wear resistance. The load distribution models for composites in predicting wear resistance in multiphase materials such as ferritic steels containing a harder sigma phase may need further research before being evaluated. Such a research may be commenced by determining the individual wear resistance of the sigma phase. Using Archard's model the models for composites also emphasised a dependence of wear resistance on the bulk hardness, neglecting the hardness that the material attains during the process of abrasion; which the results in the present work have showed to be important. Shortcomings in the model could also be a result of overlooking other factors such as stress/strain effects of the interface between the reinforcing phase and the matrix, size of the microstructure and its behaviour during abrasion [40]. In spite of these shortcomings this model was successful in multiphase systems such as epoxy-CuAl and NiCrBSi-WC [40]. Failure of equation 5.2 to predict wear resistance in the sigma-ferrite system shows that this relation cannot be generalised to all multiphase systems, an argument supported by several workers [37, 39].

5.5 Overview.

Wear resistant materials commonly contain cobalt, chromium and magnesium because of the excellent physical and mechanical properties that they possess [100]. The increasing use of intermetallic materials, valued for their high strength and oxidation resistance properties at elevated temperatures, in structural engineering applications has led to an interest in their tribological behaviour. Aluminium based intermetallics are of particular interest for their weight saving properties. This has led to the use of intermetallic materials such as titanium aluminide and nickel aluminide in aircraft and aerospace industries. The tribological properties of ruthenium aluminide, however, have not been widely researched in spite of its excellent physical properties. Factors limiting research may include high production costs and a conservative approach to researching new materials. This trend is expected to change as more intermetallic systems are improved and applied in common engineering environments. Intermetallics, including ruthenium aluminide, may in future replace some of the dominant engineering materials. Understanding the tribology of these materials will become increasingly important in preventing possible catastrophic breakdowns and costly replacements of worn parts.

Ruthenium aluminide has relatively high density compared to other aluminium-based intermetallics, but it has high strength, high modulus, and excellent creep and oxidation resistance at elevated temperatures [46, 101]. Abrasive wear results in this project have shown that ruthenium aluminide also possesses potential as a wear resistant material, shown by its improved wear resistance compared to a commercial wear resistant steel (MCV), but ruthenium aluminide may need to be further compared with highly competent wear resistant material such as tungsten carbide, cobalt alloys etc. before being confidently accepted.

It has been reported that the abrasive wear of nickel aluminide is relatively low as a result of the aluminium oxide scale that forms on its surface [102]. A similar scale has been reported in ruthenium aluminide [103], but was not observed in the present study. The effect of the scale on wear resistance in nickel aluminide highlighted an important concept of considering surface microstructure in assessing wear resistance in materials. Other workers have also emphasised the importance of surface microstructure in wear resistance of materials[10, 22].

The presence of the intermetallic sigma phase in ferritic steels does not significantly enhance wear resistance. Nevertheless, these materials have potential as wear resistant materials if factors affecting sigma's ability to act as reinforcing phase can be understood and corrected. Properties such as work-hardening coefficient (work-hardening rate) and yield strength in ferritic steels showed a decline that accompanied the presence of sigma in the steel (Figures 4.45, 4.46,4.48 and 4.49). The wear resistance in VF660 specimens showed an increase with sigma volume when the percent sigma volume is above 30 % and also when sigma volume is below 20% ; for VF245 the increase was observed when the percent sigma volume was above 20 % (Figures 4.22 and 4.23). These factors in conjuction with others, such as, anisotropy in the matrix, reaction of the inherent cracks on sigma to high strains imposed by processes such a abrasive wear, effects of the chemical, thermomechanical and heat treatment on sigma-ferrite boundaries, if thoroughly understood can provide a basis upon which the sigma-ferrite microstructure can be further investigated for improving its wear resistance.

It is important to note that work-hardening in ruthenium aluminide, MCV and ferritic steel specimens occurred during abrasion. The degree of work-hardening and the rate of work-hardening differed amongst the different material types. The importance of work-hardening was illustrated in the evaluation of wear resistance in the test specimens. It was found that the material with higher work-hardening rate (i.e. ruthenium aluminide) showed better wear resistance compared to MCV and ferritic steel specimens with relatively lower work-hardening rates. This was significant since ruthenium aluminide

started with similar hardness to that of MCV. These results showed that work-hardening of the surface during the abrasive process corresponds better with wear resistance than does the intrinsic bulk hardness of the material. Surface characterisation of the specimens in this project showed that under high strains such as in abrasive wear, ruthenium aluminide is susceptible to cracking in spite of its superior wear resistance compared to other specimens.

Wear in the ductile materials investigated was dominated by cutting and ploughing as observed in MCV and the ferritic steel specimens. Mechanisms involved in the wear of material of interest are valuable in designing both components and environments under which such materials will perform optimally. It has been suggested that geometrical considerations are important in differentiating between cutting and ploughing [16]; another approach was presented by Moore and King [99]; who suggested an index parameter given by the ratio of fracture toughness of the material to its hardness. They maintained that the higher the index parameter the higher will be the plastic deformation mechanism of wear over the fracture mechanism; the opposite holds true for a lower index parameter. In the present study, although the materials have similar bulk hardness, ruthenium aluminide has a comparitively low fracture toughness, giving it a low index parameter which is consistent with the lack of plastic deformation observed. Moore and King's approach to mechanisms of wear is broader as it seeks to identify the wear mechanism dominant in any material irrespective of its ductility or brittleness. It also recognises that, as observed in the present work, tribosystems are complex and synergistic effects may occur between different mechanisms of wear.

CHAPTER 6: SUMMARY AND CONCLUDING REMARKS

The wear resistance of ruthenium aluminide, MCV and ferritic steel has illustrated the importance of work-hardening and its contribution to the wear resistance in abrasive wear. Ruthenium aluminide was the most wear resistant of the materials investigated. Although it did not have the highest hardness, the work-hardening rate in ruthenium aluminide was greater than that of the other materials.

The work-hardening rates which indicate the extent to which the surface work-hardens served as a better measure than bulk hardness for predicting relative abrasion resistance between the test specimens.

It was also clear that the microhardness measurements obtained after abrasion (i.e. "work-hardened" hardness) consistently correlated better with abrasion resistance than bulk hardness, except in the case of the dual phase ferritic specimens where sigma's presence introduced a slight deviation.

Microhardness measurements further showed that work-hardening was confined to a narrow region within approximately 100 microns from the abraded surface in the test specimens. This shows that a very narrow region of the surface determines the tribological behaviour of the materials studied.

VF245 ferritic steels are more sensitive to heat treatment temperature than VF660. Chemical and thermomechanical history in the ferritic samples played a role in influencing the precipitation of sigma phase at 600 °C. Sigma precipitation occurred at a temperature of 600°C in all the ferritic steel specimens after at least 20 minutes of heat treatment. In ferritic specimens, work-hardening rates in the as-received specimens were greater than work-hardening rates in specimens containing the sigma phase.

Abrasive wear involving ferritic steel specimens showed that sigma had limited effect in improving their wear resistance. Wear resistance in ferritic specimens was comparable to that of a wear resistant MCV steel. The presence of sigma in the ferritic specimens slightly reduced the yield strength; however both bulk hardness and final surface work-hardening were improved by the presence of sigma.

Wear models were unable to accurately predict wear resistance in the test specimens. The main shortcoming was that there was no provision for factors such as work-hardening.

Ruthenium aluminide and ferritic steel containing the sigma intermetallic phase have potential of being used as wear resistant materials if shortcomings in their mechanical behaviour are further investigated and corrected.

High final surface work-hardening in the specimens showed consistency with wear resistance (i.e. generally there is an increase in wear resistance the higher the surface work-hardening in the specimen and *vice versa*) as opposed to the work-hardening rate (work-hardening coefficient) which showed less consistency in relation to the wear resistance.

APPENDIX A

Table A1. Taper section values after abrasion for ruthenium aluminide.

RuAl		
Average linear distances (μm)	Calculated values of depth below surface (μm)	Average hardness (HV)
110	85	593
348	269	392
683	528	361
933	721	358
1192	1150	305

Table A2. Taper section values after abrasion for MCV.

MCV		
Average linear distances (μm)	Calculated values of depth below surface (μm)	Average hardness (HV)
13	10	462
13	170	318
443	343	301
708	547	302
1068	826	299

Table A3. Taper section values after abrasion for VF660 specimen in the as-received condition.

Average linear distances (μm)	Calculated values of depth below surface (μm)	Average hardness (HV)
75	58	300
136	105	241
245	189	237
347	268	233
562	434	233

Table A4. Taper section values after abrasion in VF660 specimens heat treated for 30 and 50 minutes.

Average linear distances (μm)		Calculated values of depth below surface (μm)		Average hardness (HV)			
30 minutes	50 minutes	30 minutes	50 minutes	30 minutes		50 minutes	
				FR	SG	FR	SG
85	85	66	**66**	271	689	**269**	**742**
125	125	97	**97**	253	683	**249**	**724**
250	375	193	**290**	223	620	**225**	**707**
500	625	386	**483**	213	572	**206**	**592**
663	875	512	**676**	210	566	**195**	**572**
788	1125	609	**875**	199	559	**192**	**544**

FR = ferrite

SG = Sigma

Table A5. Taper section values after abrasion for VF245 in the as-received condition.

Average linear distances (μm)	Calculated values of depth below surface (μm)	Average hardness (HV)
50	39	263
250	193	252
500	386	237
625	483	230
875	676	232

Table A6. Taper section values after abrasion in VF245 specimens heat treated for 30 and 50 minutes.

Average linear distances (μm)		Calculated values of depth below surface (μm)		Average hardness (HV)			
30 minutes	50 minutes	30 minutes	50 minutes	30 minutes		50 minutes	
				FR	SG	FR	SG
65	50	50	**39**	287	623	**294**	**762**
125	90	97	**70**	264	617	**270**	**750**
250	125	193	**97**	251	533	**243**	**673**
500	375	386	**290**	242	513	**236**	**641**
750	750	580	**580**	235	508	**232**	**612**
1000	1000	773	**773**	231	413	**208**	**578**
1413		1092		231	412		

FR = ferrite

SG = Sigma

APPENDIX B

Table B1 Presents physical properties of some of periodic table elements involved chemical systems prone to the formation of sigma phase. Table B2 lists some parameters and a few binary systems of the sigma phase (After Hall and Algie [81]).

TABLE B1. Elements Forming Sigma Phase

1st long period elements						
Element	V	Cr	Mn	Fe	Co	Ni
Atomic Number	23	24	25	26	27	28
Melting Point °C	1860	1850	1243	1534	1495	1453
Atomic Radius Å*	1.35	1.28	1.35	1.28	1.25	1.24
Structure	b.c.c	b.c.c	α -β-f.c.c-b.c.c	b.c.c-f.c.c-b.c.c	hcp-fcc	f.c.c
2nd long period elements						
Element	Nb	Mo	Tc	Ru	Rh	Pd
Atomic Number	41	42	43	44	45	46
Melting Point °C	2468	2620	2200	2450	1966	1552
Atomic Radius Å*	1.47	1.40	1.36	1.34	1.34	1.37
Structure	b.c.c	b.c.c	h.c.p	h.c.p	f.c.c	f.c.c
3rd long period elements						
Element	Ta	W	Re	Os	Ir	Pt
Atomic Number	73	74	75	76	77	78
Melting Point °C	2996	3380	3035	3060	2430	1769
Atomic Radius Å*	1.47	1.41	1.37	1.37	1.35	1.38
Structure	b.c.c	b.c.c	h.c.p	h.c.p	f.c.c	f.c.c

Notes

Å*= Goldschmidt atomic radius for co-ordiation number 12

Structural transformation and the corresponding transformation temperatures in Mn and Co

$$\text{Mn } \alpha \xrightarrow{727^{\circ}C} \beta \xrightarrow{1095^{\circ}C} \text{f.c.c} \xrightarrow{1133^{\circ}C} \text{b.c.c}$$

$$\text{Co hcp} \xrightarrow{400^{\circ}C} \text{fcc}$$

TABLE B2. Binary Sigma Phase Systems

System	Lattice Parameter			Composition range at % "A"	e/atom ratio	exchange factor	Notes
	a, Å	c, Å	c/a				
Group VA + 1st Long Period							
Mn-V	8.918	4.613 at 19%V	0.512	17-24%V at 600°C	6.52-6.66	0-0	Forms congruently from δ-Mn at 1050°C
Fe-V	8.956	4.627 at 50%V	0.518	36-60%V	6.20-6.92	5-2	Forms congruently from α-Fe at ~1200°C
Co-V	8.877	4.598 at 50.5%V	0.518	44-66%V at 1000°C	6.36-7.20	7.4	Forms by peritectic reaction at 1420°C
Ni-V	8.98	4.64 at 62%V	0.517	55-73%V at 1000°C	6.38-7.25	8.1	Forms by peritectic reaction at ~1270°C
Fe-Nb	-	-	-	45-49%Nb at 1000°C	6.53-6.65	12.9	Forms by peritectoid reaction at ~540°C
Group VI A + 1st Long Period							
Mn-Cr	8.885	4.587 at 20%Cr	0.517	16-24%Cr at 1030°C	6.76-6.84	-5.5	Forms by peritectic reaction at 1310°C
Fe-Cr	8.799	4.544 at 46.5%Cr	0.517	44-50%Cr at 700°C	7.00-7.12	0-0	Forms congruently from α-Fe at ~815°C
Co-Cr	8.80	4.56 at 56.4 %Cr	0.518	56-61% at 1000°C	7.17-7.32	2.3	Forms by peritectoid reaction at ~1500°C decomposes at ~540°C
Mn-Mo	9.10	4.74 at 37.3%Mo	0.52	Narrow ~36%Mo	6.64	3.6	diagram incomplete σ stable at high temperatures
Fe-Mo	9.188	4.812 at 50%Mo	0.5237	Triangular field-max 44-50 % Mo at 1480°C	7.00-7.12	8.6	Forms by peritectic reaction at 1540°C. Decomposes at 1180°C
Co-Mo	9.228	4.827 at 60%Mo	0.523	Triangular field ~1% wide at 1500°C	7.20	10.7	Forms by peritectic reaction at ~1585°C. Decomposes at ~1250°C

APPENDIX C

Some of the commonly used terminology in various tribological applications are presented in Table C1. Tables C2, C3 and C4 presents classification of tribological processes. Superscripts in Table 2 refer to: solid worn by another solid ; solid worn by gas; Solid worn by liquid; two surfaces in contact and worn by particles in a liquid trapped between them for the superscripts 2, 3, 4 and 5 respectively (After Peterson [7]).

TABLE C1. WEAR PROCESSES

Adhesion	Metal/Metal
Corrosion	Fretting
2-Body Abrasion	Cavitation
3-Body Abrasion	Fluid Erosion
Fatigue	Solid Erosion
Impact	Electrical Erosion
Low Stress Abrasion	Impingement
High Stress Abrasion	Particle Erosion
Gouging	Erosion Corrosion
Wire Drawing	Rain Erosion
Delamination	Deformation

TABLE C2. DESIGNATION OF WEAR PROCESSES

Contact	Particle	Motion	Common	Typical examples
Solid[2]	None	Sliding	Dry sliding wear	Bushing, breaks, seals
			metal/metal wear	
		Reciprocating	Fretting	Fasteners, clearance fits
		Impact	Impact wear	Rolling contact bearings, gears
		Rolling	Rolling wear	
Gas[3]/liquid[4]	None	Flow	Wire drawing	Water erosion, valve wear
		Impact	-	Pipe bends, deflectors
		Hammer	-	
	Hard			
Solid[2]	Rough	Wear surface	-	Tire wear
	Surface	Rolling		
	Hard			
Solid[2]	Rough	particle	Abrasion	Abrasive Papers, files
	Surface	sliding	2-body wear	
Liquid[5]	Solid	Wear surfaces	3-body wear	Dirt in machinery components
		Sliding	Dirt Abrasion	Lapping
		Wear surfaces	3-body wear	Dirt in lubricants
		Rolling	Dirt Abrasion	For rolling contacts, cams
		Wear surfaces	Erosion	Mixing , slurry pumping
		Sliding		blades
		Wear surfaces		
		Rolling		
Gas/liquid	Solid	Particle	Low angle	Pumping and Transporting
		Sliding	Particle erosion	Liquids or gases containing solid
				particles
		Particle	90°	Shot and sand blasting
		Impact	Particle erosion	
Gas	Solid	Wear surface	3-body wear	Soles of shoes
		Sliding		
		Wear surface	3-body wear	Rock crushing
		Rolling		
		Wear surface	2-body wear	Earth moving equipment
		Sliding	low stress abrasion	Digging
			Soil abrasion	
Liquid	Liquid	Particle		Slurry pumping
		Impact		
Gas	Liquid	Particle	Drop Erosion	
		Impact	Rain Erosion	
Liquid	Gas or	Particle	Cavitation	Valves, bearings, pipes
	Vapour	Impact		
	Particle	Particle	Wire drawing	Valves
		Flow	Erosion	

TABLE C3. DESIGN WEAR REGIMES

Description	Designation
Smooth solid sliding against an unlubricated smooth solid	Dry sliding wear
Smooth solid rolling against a lubricated smooth solid	lubricated sliding wear
Smooth solid rolling against an unlubricated smooth solid	Dry rolling wear
Smooth solid rolling against a lubricated smooth solid	Lubricated rolling wear
Smooth solid impacting smooth solid	Impact wear
Liquid or gas interacting with a solid surface or compacted solid particles	Fluid erosion
Solid rolling on a rough surface or compacted solid particles	Rolling abrasion
Solid sliding against a rough solid or compacted solid particles	Sliding abrasion (2-body abrasion)
Solid particles trapped between solid or rolling surfaces in a liquid or gas medium	3-body abrasion
Solid particles interacting with solid surfaces in liquid or gas medium	Particle erosion
Liquid particles interacting with solid surfaces in a liquid or gas medium	Drop erosion
Gas or Vapour particles interacting with a solid surface in a liquid medium	Cavitation

TABLE C4. WEAR PARTICLE REMOVAL PROCESSES

Adhesion and Transfer	Material weld at asperity tips, is transferred to the harder member possibly grows in subsequent encounters and eventually removed by fracture, fatigue or corrosion.
Corrosion film wear	A film formed by reaction with the environment or the lubricant is removed by sliding.
Cutting	A sharp particle or asperity cuts a chip.
Plastic deformation	The surface is worked plastically. Cracks from, grow and coalesce forming wear particles.
Surface fracture	If nominal stress exceeds the fracture stress of a brittle material, particles can be formed by fracture.
Surface reactions	One material dissolves or diffuses into another.
Tearing	Elastic material can be torn by a sharp indenter.
Melting	High temperature can cause wear by melting.
Electrochemical	The difference in potential on the surface due to a moving.
Fatigue	The surface is worked elastically. Microcracks form, grow and coalesce forming wear particles.

Some more wear terminology are to be found in the ASTM wear and erosion volume [104]

REFERENCES

[1]. Askeland D, *Elements of Material Science*, PWS-Kent, Boston, 805 (1991)

[2]. Burwell J T, *Survey Of Possible Wear Mechanisms*, Wear, **1**, 119 (1957/58).

[3]. Halling J, *Principles of Tribology*, The Macmillan Press, London, (1975).

[4]. Ko P L, Metallic, *Wear - A Review With Special References To Vibration Induced Wear In Power Plant Components,* Tribology International, **20**, April, No 2, 67 (1987).

[5]. Pugh, *Friction and Wear*, Butterworth, London, 141 (1973).

[6]. Eyre T S, *Wear Resistance of Metals*. In: Treatise On Material Science And Technology, (ed Scott D), Academic Press, New York, **13**, 363 (1979).

[7]. Peterson M B, *Classification Of Wear Processes*. In: Wear Control Handbook, (eds Peterson M B and Winer W O), American Society Of Mechanical Engineers, New York, 9 (1980).

[8]. Rigney D A, *Sliding Wear Of Metals*, Annual Review of Materials Science, **18,** 141 (1988).

[9]. Rigney D A and Glaeser W A, Source Book On Wear Control Technology, ASM, 1 (1978).

[10]. Dowson D, History of Tribology, Longman, London, 1979

[11]. Czichos H, *System Approach To Wear Problems*, Wear control hand book, (eds Peterson M B and Winer W O), American Society Of Mechanical Engineers, New York, 17 (1980).

[12]. Jones M H, *Wear*. In: Industrial Tribology, (eds Jones M H and Scott D), Elesevier Amsterdam, 1983.

[13]. Evans D C and Lancaster J K, *The Wear of Polymers*. In: Treatise On Materials Science And Technology, (ed Scott D), Academic Press, New York, **13**, 97 (1979).

[14]. Richardson R C D, *The Wear Of Metals By Relatively Soft Abrasive*, Wear, **11**, 245 (1968).

[15]. Kosel T H, Li S Z and Rao C M, *The Size Effect In Abrasion Of Dual-Phase Alloys*, ASLE Transactions, **28**, No 3, 343 (1984).

[16]. Mulhearn T O And Samuels L E, *The Abrasion Of Metals: A Model Of The Process*, Wear, **5**, 478 (1962).

[17]. Sedriks A J And Mulhearn T O, *Mechanics Of Cutting And Rubbing In Simulated Abrasive Processes*, Wear, **6**, 457 (1963).

[18]. Sedriks A J And Mulhearn T O, *The Effect Of Workhardening On The Mechanics Of Cutting In Simulated Abrasive Processes*, Wear, **7**, 451 (1964).

[19]. Moore M, *Abrasive Wear*. In: Treatise On Materials Science And Technology, (ed Scott D), Academic Press, New York, **13**, 217 (1979).

[20]. Swanson P A, Vetter A F, *The Measurement Of Abrasive Particle Shape And Its Effect On Wear*, ASLE Transactions, **28**, No2, 225.

[21]. Barwell F T, *Theories Of Wear And Their Significance*. In: Treatise On Materials Science And Technology, (ed Scott D), Academic Press, New York, **13**, 2 (1979).

[22]. Karl-Heinz Zum Gahr, *Microstructure And Wear Of Materials*, Elsevier, Amsterdam, 1987.

[23]. Archard J F And Hirst W, *The Wear Of Metals Under Unlubricated Conditions*, Proceeding Of The Royal Society, **236 A**, 396 (1956).

[24]. Summer-Smith D, *An Introduction To Tribology In Industry*, Machinery Publishing, Britain, 106 (1969).

[25]. Kruschov M M, *Resistance Of Metals To Wear By Abrasion As Related To Hardness*, Proceedings Of The Conference On Lubrication And Wear Institution Of Mechanical Engineers, London , 655 (1957).

[26]. Oberle T L, *Wear Of Metals*, Journal Of Metals, **June**, 438 (1951).

[27]. Borik F, *Metallurgy Of Ferrous Materials For Wear Applications*. In: Wear Control Handbook, (eds Peterson M B and Winer W O), American Society Of Mechanical Engineers, New York, 327 (1980).

[28]. Ball A, *On The Importance Of Work-hardening In The Design Of Wear-Resistant Materials*, Wear, **91**, 201 (1983).

[29]. Hornbogen E, *The Role Of Fracture Toughness In The Wear Of Metals*, Wear, **33**, 251 (1975).

[30]. Richardson R C D, *The Maximum Hardness Of Strained Surface And the Abrasive Wear Of Metals And Alloys*, Wear, **10**, 353(1967).

[31]. Bowden F P and Tabor D, *The Friction And Lubrication Of Solids*, **Part I**, Oxford University Press, London, 58 (1954).

[32]. Bowden F P and Tabor D, *The Friction And Lubrication Of Solids*, **Part II**, Oxford University Press, London, 350 (1964).

[33]. Lawn B and Wilshaw R, *Review Indentation Fracture: Principles and Applications*, Journal of Materials Science, **10**, 1049 (1975).

[34]. Lawn B R and Swain M V, *Microfracture Beneath Point Indentation In Brittle Solids*, *ibid*, 113-122.

[35]. Hutchings I M, *Tribology, friction and wear of engineering materials*, Edward Arnold, Great Britain, 1992.

[36]. Wayne S F, Buljan S T, Baldoni J G and Huckabee M L, *Microstructural Aspects Of Si_3N_4-TiC Composites Affecting Abrasion And Erosion Resistance*, Tribology Transactions, **34**, No 4, 553(1991).

[37]. Axèn N and Jacobson S, *A Model For The Abrasive Wear Resistance Of Multiphase Materials*, Wear, **174**, 187 (1994).

[38]. Kruschov M M, *Principles Of Abrasive Wear*, Wear, **28**, 69 (1974).

[39]. Garrison W M, *Kruschov `s Rule And The Abrasive Wear Resistance Of Multiphase Solids*, Wear, **82**, 213 (1982).

[40]. Simm W and Fretti S, *Abrasive Wear Of Multiphase Materials,* Wear, **129**, 105 (1989).

[41]. Yamada K, Kamiya N and Wada S, *Abrasive Wear Of Al_2O_3-SiC Composites*, Journal Of The Ceramic Society OF Japan, Int Edition, **99**, 797 (1991).

[42]. Rossiter P L, *The electrical Resistivity Of Metals And Alloys*, Cambridge University Press, London, (1987).

[43]. Cahn R W, *Load-Bearing Ordered Intermetallic Compounds A Historical View*, Materials Research Bulletin, **May**, 18 (1991).

[44]. Cahn R W, *Intermetallic Compounds As Structural Materials: History And Prospects*, Metals Materials And Processes, **1**, No1, 1 (1989).

[45]. Liu C T And Stiegler J O, *Ductile Ordered Intermetallic Alloys*, Science, **226**, November, No 9, 636 (1984).

[46]. Fleischer R L, Field R D And Briant C L, *Mechanical Properties Of High-Temperature Alloys Of AlRu*, Metallurgical Transactions, **22A**, February, 402 (1991).

[47]. Maupin H E, Wilson D And Hawk J A, *Wear Deformation of Ordered Fe-Al Intermetallic Alloys*, Wear, **162-163**, 432 (1993).

[48]. Varin R A And Winnicka M B, *Plasticity Of Structural Intermetallic Compounds*, Material Science And Engineering, **A137**, 93 (1991).

[49]. Hawk J A, Alman D E and Stollof N S, *Abrasive Wear Of MoSi-Nb Composites*, Scripta Metallurgical et Materialia, **31**, No 4, 473 (1994).

[50] Johnson M , Mikkola D E, March P A, Wright R N, *The Resistance Of Nickel And Iron Aluminides To Cavitation erosion And Abrasive Wear*, Wear, **140**, 279 (1990).

[51] Pope D P and Darolia R, *High-Temperature Application Of Intermetallic Compounds*, MRS Bulletin, **May**, 30(1996).

[52]. Khan T, Naka S, Veyssiere P And Costa P, *Intermetallics For Structural Applications*, Proceedings Of A Conference On High Temperature Materials For Power Engineering, Liege, Belgium, **24-27 September**, 1 (1990).

[53]. Schetky L.McD, *Miscellaneous Applications Of Intermetallic Compounds*, MRS Bulletin, **May**, 52 (1996).

[54]. R L Fleischer, *Effects Of Composition On the Mechanical Properties Of Tough High-Temperature Intermetallic Compounds*, ISIJ International, **31**, No 10, 1186 (1991).

[55]. Lin W, Xu Jian-Hua and Freeman A J, *Cohesive Properties, Electronic And Bonding Characteristics of RuAl- A comparison to NiAl,* Journal of Materials Research, **7**, No 3, 592 (1992).

[56]. Fleischer R L, *Substitutional Solutes In AlRu-I. Effects Of Solute On Moduli, Lattice Parameters And Vacancy Production,* Acta Metall Mater, **41**, No 3, 863 (1993).

[57]. Fleischer R L, *Substitutional Solutes In AlRu-II. Hardening And Correlations With Defect Structure*, Acta Metall Mater, **41**, No 4, 1197 (1993).

[58]. Fleischer R L and Zabala R J, *Mechanical Properties Of Diverse Binary High Temperature Intermetallic Compounds*, Metallurgical Transactions **21a**, 2709 (1990).

[59]. Dean M S and Plumbridge W J, *Prediction Of Sigma Phase Formation In Stainless Steels*, Nuclear Energy, **21**, April No 2, 119 (1982).

[60]. Shoemaker D P and Bergman B G, *The Crystal Structure Of A Sigma Phase*, Journal of Chemical Society, **72**, Sep-Dec, 5793 (1950).

[61]. Harries D R, *Physical Metallurgy of Fe-Cr-Ni Austenitic Steels*. In: Commission of the European Communities [Report] EUR 8055, EUR 1-14 (1982).

[62]. Sims C T, *Prediction Of Phase Composition*. In: Superalloys II, (eds Sims C T, Stoloff N S and Hagel E C), John Wiley and Sons, New York, 217 (1987).

[63]. Wernick J H, *Structure And Properties of Some Intermediate Phase*. In: Physical Metallurgy, (ed Cahn R W), North Holland, Amsterdam, 229 (1970).

[64]. Hendry A, Mazur Z F and Jack K H, *Influence Of Nitrogen On 475 °C Embrittlement Of High-Chromium Ferritic Steels*, Metal Science, **August**, 482 (1979).

[65]. Bain E C and Griffiths E W, *An Introduction To The Iron -Chromium -Nickel Alloys*, Transactions of the American Institute of Mining and Metallurgical Engineers, **75**, 166 (1992).

[66]. Novak C J, *Structure and Constitution Of Wrought Austenitic Stainless Steels*. In: Handbook Of Stainless Steels, (eds Peckner D and Bernstine I M), McGraw-Hill, New York, (4-3) 1977.

[67]. Fisher R M, Dulis E J and Carroll K G, *Identification Of The Precipitate Accompanying 885 °F Embrittlement In Chromium Steels*, Transactions of AIME, **May**, 690 (1953).

[68]. Williams R O and Paxton H W, *The Nature Of Ageing Binary Iron-Chromium Alloys Around 500 °C*, Journal Of The Iron And Steel Institute, **March**, 358 (1957).

[69]. Adcock F, *Alloys Of Iron Research*, Journal Of The Iron And Steel Institute, **No II**, 147 (1931).

[70]. Pickering F B, Met A and Met D, *The Metallurgical Evolution Of Stainless Steels*. In: The Metallurgical Evolution Of Stainless Steels, (ed Pickering F B), American Society For Metals, Ohio, 1 (1979).

[71]. Knight D S and McEwan J J, *A New Ferritic Stainless Steel For Highly Corrosive Environments*, Stainless Steel, **May/June**, 7 (1996).

[72]. Steigerwald R F, Dundas H J, Redmond J D and Davison R M, *The Physical Metallurgy Of Fe-Cr-Mo Ferritic Stainless Steels*. In: The Metallurgical Evolution Of Stainless Steels,(ed Pickering F B), American Society for Metals, Ohio, 284 (1979).

[73]. Semchysen M, Bond A P, Dundas H J, *Effect Of Composition On Ductility And Toughness of Ferritic Stainless Steels*. In: The Metallurgical Evolution Of Stainless Steels, (ed Pickering F B), American Society for Metals, New York, 260 (1979).

[74]. Biggs T and Knutsen R D, *The Effect Of Nitrogen On Martensite Formation in a Cr-Mn-Ni Stainless Steel*, Journal De Physique IV, **5**, December, C8-515 (1995).

[75]. Demo J J, *Structural and Constitution Of Wrought Ferritic Stainless Steels*. In: Handbook Of Stainless Steels, (eds Peckner D and Bernstine I M), McGraw-Hill, New York, (5-7) 1977.

[76]. Lagneborg R, *Metallography Of The 475 ℃ Embrittlement In An Iron -30% Chromium Alloy*, Transactions of ASM, **60**, 67 (1967).

[77]. Links H S and Marshall P W, *The Formation Of Sigma Phase In 13% to 16% Chromium Steels*, Transactions Of The A.S.M, **44**, 549 (1952).

[78]. Lena A J and Hawkes M F, *Embrittlement In Stainless Steels*, Journal Of Metals (Transactions AIME), **May**, 607 (1954).

[79]. Marcinkowski M J, Fisher R M, A Szirmae, *Effect of 500 ℃ Ageing On The Deformation Behaviour Of An Iron-Chromium Alloy*, The Transactions Of The Metallurgical Society Of AIME, **230**, June, 676 (1964).

[80]. Becket F M. A lecture: *On the Allotropy Of Stainless Steels*, Metals Technology (T.P), **131**, June, 16 (1938).

[81]. Hall E O and Algie S H, *The Sigma Phase*, Metallurgical Reviews, **11**, 61 (1961).

[82]. Bradley A J and Goldschmidt H J, *An X-ray Investigation Of Iron-Nickel-Chromium Alloys*, Journal Of The Iron And Steel Institute, **No II**, 273 (1941).

[83]. Lewis M H, *Precipitation Of (Fe,Cr) Sigma Phase From Austenite*, Acta Metallurgica, **14**, November, 1421 (1966).

[84]. Lena A J, *Sigma Phase-a Review*, Metal Progress, **July**, 86 (1954).

[85]. Franks R, Binder W O and Bishop C R, *The Effect Of Molybdenum And Columbium On The Structure, Physical Properties And Corrosion Resistance Of Austenitic Stainless Steel*, Transactions Of The A.S.M, **29**, March, 35 (1941).

[86]. Wolfe I M, *Ductility In High Chromium Super-Ferritic Alloys*, PhD Thesis University Of Cape Town, March 1989.

[87]. Premachandra K, *Sigma Phase In High Chromium Ferritic Stainless Steels*, MSc Thesis, Wits University Johannesburg, 1993.

[88]. Shortsleeve F J and Nicholson M E, *Transformation In Ferritic Chromium Steels Between 1100 and 1500°F (595 and 815°C)*, Transactions Of The A.S.M, Metal Park Ohio, **43**, 147 (1951).

[89]. Cook A J and Jones F W, *The Brittle Constituent Of The Iron-Chromium System (Sigma Phase)*, Journal Of The Iron And Steel Institute, **148**, 217 (1943).

[90]. Edmonds D V and Honeycombe R W K, *Precipitation In Iron-Base Alloys*. In: Precipitation Processes In Solids, (eds Russel K C and Aaronson H I), American Institute Of Mining, Metallurgical And Petroleum Engineers, New York, 121 (1978).

[91]. Gilman J J, *Hardening Of High-Chromium Steels By Sigma Phase Formation*, Transactions Of The A.S.M, **43**, 161 (1951).

[92]. Lena A J, *Effect of Sigma Phase On Properties Of Alloys*, Metal Progress, **August**, 94 (1954).

[93]. Cortie M B and Premachandra K P, *Microstructural Development And Abrasion-Resistance Of An Experimental Ferrite -Sigma Alloy*, Scripta Metallurgica et Materilia, **27**, 1847 (1992).

[94]. Burgess C O And Forgeng W D, *Constitution OF Iron-Manganese Alloys*, American Institute Of Mining And Metallurgic Engineers, **T.P No 911**, 227 (1938).

[95]. *ASTM, Annual Book Of Standards*, **Volume 03.01**, E9 (1993).

[96]. Ashby M F And Jones D R, *Engineering Materials: An introduction to their Properties and Applications,* Pergamon Press, Oxford, (1983).

[97]. Howard R L, *The Erosion Of Titanium Aluminide Intermetallic Alloys*, PhD Thesis UCT 1995.

[98]. Glaeser W.A, *Wear Experiment In The Scanning Electron Microscope*, Wear, **73**, 371 (1981).

[99]. Moore M A and King F S, *Abrasive Wear Of Brittle Solids*, Wear, **60**, 123 (1980).

[100]. Johnson M and Mikkola D E, *The Resistance Of Nickel And Iron Aluminides To Cavitation Erosion And Abrasive Wear*, Wear, **140**, 279 (1990).

[101]. Fleischer R L and Mckee D W, *Mechanical And Oxidation Properties Of AlRu-Based High-Temperature Alloys*, Metallurgical Transactions A, **24A**, March, 759 (1993).

[102]. Blau P J And DeVore C E, *Sliding Behaviour Of Alumina/Nickel And Alumina/Nickel aluminide Couples At Room And Elevated Temperature*, Journal Of Tribology, **110**, October, 646 (1988).

[103]. McKee D W and Fleischer R L, Oxidation Behaviour Of Advanced Intermetallc Compounds, Mat. Res. Soc. Symp. Proc., **213**, 970 (1991).

[104]. *ASTM, Annual Book Of Standards*, **Volume 03.02**, G40 (1993).